Advanced Analytical Treatment of Shapes and Shifts of Hydrogenic Spectral Lines in Plasmas and its Applications

by

Paul Sanders

A dissertation submitted to the Graduate Faculty of
Auburn University
in partial fulfillment of the
requirements for the Degree of
Doctor of Philosophy

Auburn, Alabama
May 5, 2018

Keywords: spectral line shapes, Stark broadening, electron density measurements, magnetized plasmas, relativistic electron beam, Langmuir waves

Approved by

Eugene Oks, Chair, Professor of Physics
Michael S. Pindzola, Professor of Physics
Joe D. Perez, Professor of Physics
Stuart D. Loch, Professor of Physics
Michel Smith, Professor of Mathematics

Publications

The results presented in this dissertation have been published in the following refereed journals.

1. Sanders, P, and Oks, E., "Allowance for More Realistic Trajectories of Plasma Electrons in the Stark Broadening of Hydrogenlike Spectral Lines", J. Phys. Communications, 2018, **2**, 035033, https://doi.org/10.1088/2399-6528/aab2d2.
2. Sanders, P. and Oks, E., "Estimate of the Stark Shift by Penetrating Ions within the Nearest Perturber Approximation for Hydrogenlike Spectral Lines in Plasmas", J. Phys. B: Atom. Mol. Opt. Phys., 2017, **50**, 245002.
3. Sanders, P. and Oks, E., "Lorentz–Doppler profiles of hydrogen/deuterium lines for magnetic fusion: analytical solution for any angle of observation and any magnetic field strength", J. Phys. Communications, 2017, **1**, 055011.
4. Oks, E., and Sanders, P., "Stark Broadening of Hydrogen/Deuterium Spectral Lines by a Relativistic Electron Beam: Analytical Results and Possible Applications to Magnetic Fusion Edge Plasmas", J. Phys. Communications, 2018, **2**, 015030, https://doi.org/10.1088/2399-6528/aa8f23.
5. Sanders, P., and Oks, E., "Improving the Method of Measuring the Electron Density via the Asymmetry of Hydrogenic Spectral Lines in Plasmas by Allowing for Penetrating Ions", Atoms, 2018, accepted.
6. Sanders, P, and Oks, E., "Role of Penetrating Ions in the Method of Measuring the Electron Density by the Asymmetry of Hydrogenic Spectral Lines in Plasmas", Intern. Review of Atomic and Molecular Phys. 2016, **7**, 81.
7. Sanders, P, and Oks, E., "On the Red Shift of Hydrogen-Like Spectral Lines in Plasmas", Intern. Review of Atomic and Molecular Phys. 2016, **7**, 1.
8. Sanders, P, and Oks, E., "Generalization of Analytical Results for Lorentz-Doppler Profiles of Hydrogen/Deuterium Lines", Intern. Review of Atomic and Molecular Phys. 2016, **7**, 21.
9. Sanders, P, and Oks, E., "Stark Broadening of Hydrogenlike Spectral Lines by Plasma Electrons: the Allowance for Non-Hyperbolic Trajectories", Intern. Review of Atomic and Molecular Phys. 2017, **8**, 53.

Abstract

This work presents a detailed analysis and improvement of various aspects of the theory of the Stark broadening of hydrogen and hydrogen-like ions for a broad range of dense plasma parameters, while looking at both the shape and shift of the spectral line. This was done in an effort to improve the fundamental understanding of Stark shapes and shifts of spectral lines in plasmas (by producing more accurate analytical results than previously existed) and to provide advanced diagnostic methods for determining the electron density. First, we introduced an additional source of the shift of hydrogen-like spectral lines arising from the configurations where the nearest perturbing ion is within the radiating atom/ion ("penetrating configurations") and in this way eliminated the existing discrepancy of a factor of two between the theory and experiments. Second, we improved the diagnostic method for measuring the electron density using the asymmetry of spectral lines in dense plasmas by taking into consideration these penetrating configurations. Third, we developed a more accurate theory of the broadening of hydrogen-like spectral lines by plasma electrons by using a more accurate description of the electron trajectories. Fourth, for plasmas of magnetic fusion machines, we obtained analytical results for the line shapes under two entangled broadening mechanisms: broadening by the Lorentz field and Doppler broadening – for an arbitrary angle of observation, in distinction to what had previously been done. Fifth, we developed an advanced analytical theory of the Stark broadening of hydrogen/deuterium spectral lines by a Relativistic Electron Beam (REB) and in this way suggested the diagnostic of the development of the REB in magnetic fusion machine,

allowing to timely mitigate such a development, which is disruptive for magnetic fusion machines.

Dedicated to my grandfather,
Paul Haddon Sanders, Jr.

Acknowledgements

First and foremost, I would like to thank my Lord and Savior, Jesus Christ. He has faithfully been with me along this difficult journey, even when my faith waivered. I would like to thank my gracious church, Grace Heritage Church, for being a support group I could lean on, as the encouragement and love and friendship provided to me during these tough times helped me to persevere. I would like to acknowledge my pastor, Paul Stith, who was the one I went to on countless occasions for advice, and who helped to shape me into so much more than a physicist, but a man of God.

Additionally, I would like to thank my outstanding advisor, Eugene Oks. I would not be in the position I am today without his guidance and patience, especially in the beginning stages as I was building my foundation on the topic. He is a truly remarkable individual, and I am truly thankful for the opportunity he provided to me.

During my time in graduate school, I have formed many relationships with those who hold a special place in my heart. I would like to thank my dear friend, Omar Eulogio Lopez Ortiz, for providing an example of dedication and hard work which motivated me to become a better physicist. Our many conversations on life and physics challenged me and taught me to examine the world in new and better ways. Additionally, I could not leave out Monika Kodrycka, whose smile and love towards other people I will not soon forget. I look back fondly when I remember our “amazing” trips and the great times we had. She always kept my spirits up, even through the hard times of my journey.

I would like to personally acknowledge Kevin and Ruth Ross, whose love they have shown to me goes beyond words. They brought me into their home to live with them and gave me an amazing example of what a godly marriage looks like - a true example of a God honoring man and woman. I can't help but vividly remember the conversations I had with Kevin on faith and life which occurred almost every morning. My faith and growth as a person are much stronger from knowing them and seeing their love.

Lastly, I would like to thank those who have been with me from the beginning, my parents. To my mother, Julie Sanders, who has shown me truly what it means to love someone, I hope to one day show the same amount of love to my children. I will always remember the love and care she poured out upon me at her expense, expecting nothing in return. To my father, Paul Sanders, who taught me the rigors of discipline and showered me with selfish love, I hope to give to my family the dedication with which he gave to me.

Table of Contents

List of Figures and Tables

List of Abbreviations

SL	Spectral lines
SB	Stark Broadening
HL	Hydrogen-like
QEF	Quasi-static Electric Fields
PPS	Plasma Polarization Shift
QS	Quadratic Stark
CT	Conventional Theory
HDSL	Hydrogen/deuterium Spectral Lines
FWHM	Full Width at Half Maximum
REB	Relativistic Electron Beam

Chapter 1. Introduction

The shape and shift of hydrogenic spectral lines (hereafter, SL) play an important role in providing insight into plasma processes – as discussed, e.g., in books [1.1-5]. The main source of the shape and shift of spectral lines is due to the various electric fields in plasmas caused by perturbing electrons or ions. This is known as the *Stark broadening* (hereafter called, SB) of spectral lines, which will constitute the majority of this dissertation in one way or another, with twists and wrinkles along the way. Trying to understand and describe the shape of the spectral lines in a high density plasma is a difficult task, but the result of this endeavor yields fruitful information about the plasma. Due to this difficulty, the physics of SB can best be understood for SL of one-electron systems: hydrogen atoms and hydrogen-like ions.

There are several practical reasons why SB of hydrogen lines (H-lines) and of hydrogen-like lines (HL-lines) are important, as presented in book [1.4]. First, hydrogen isotopes (deuterium, tritium) are employed as a fuel for the energy pursuit via controlled fusion. Thus, in magnetically-controlled fusion machines, SL of hydrogen isotopes are used for the experimental determination of various parameters of the edge plasmas. Second, in powerful Z-pinches with high-temperature discharges, HL-lines of multi-charged ions are employed for diagnostic purposes.

Third, hydrogen is the most abundant chemical element in the Universe. Thus, shapes and shifts of H-lines are used for deducing physical parameters of various astrophysical objects. In particular, red shifts of SL play an important role in astrophysics. For inferring the relativistic red shifts from the observed red shifts it is required to allow for the Stark shift of SL.

1.2 Brief Introduction to the Stark Broadening Theory

When a radiator is placed in a plasma, the width of the radiated spectral line becomes broader than the natural radiated width. This width is affected by the temperature and density of the plasma. The spectrum contains not only the quantum characteristics of a radiator, but the whole statistical information about the sequence of collisions for a whole ensemble of radiators. This distinguishes the problems of Stark broadening from the problems of atomic physics.

The physics of the spectral line broadening in plasmas containing quasi-static electric fields (QEF) is very rich and complex due to the interplay of a large number of characteristic times and frequencies. There are four following characteristic frequencies, which can be considered as "elementary" parameters:

1. $\Delta\omega$ – detuning from the unperturbed position of a given spectral line of the radiator. It affects the characteristic value of the argument τ of the correlation function of the plasma electric field (called the plasma microfield – to distinguish from the electrostatic plasma turbulence, if any, called macrofield). The spectral line shape is the Fourier transform of the correlation function.
2. $\omega_{pe}(N_e)$ – plasma electron frequency, which is also the inverse characteristic time of the formation of the screening by electrons (N_e is the electron density).
3. $\Omega_e(N_e, T_e) = v_{T_e}/\min(\rho_{Ne}, \rho_{We})$ – characteristic frequency of the variation of the electron microfield, which is responsible for the *homogeneous* broadening by electrons[*/]. Here T_e is the electron temperature, $v_{Te} = (T_e/m_e)^{1/2}$ is the electron thermal velocity,

[*/] The Stark broadening of a spectral line is *homogeneous* when it is the same for all radiators. A typical example is the Stark broadening by the electron microfield. In distinction, the Stark broadening by the quasi-static part F_{qs} of the ion microfield is *inhomogeneous* because different radiators are subjected to generally different values of F_{qs}.

$\rho_{Ne} \sim 1/{N_e}^{1/3}$ is the mean interelectronic distance, and $\rho_{We} \sim n^2\hbar/(m_e v_{Te})$ is the electron Weisskopf radius

(n is the principal quantum number of the radiator energy level involved in the radiative transition).

4. $\Omega_i(N_i, T_i) = v_{T_i}/\min(\rho_{Ni}, \rho_{W_i})$ – characteristic frequency of the variation of the *dynamic part* of the ion microfield, which is responsible for the *homogeneous* broadening by ions. Here T_i is the ion temperature, $v_{Ti} = (T_i/m_i)^{1/2}$ is the ion thermal velocity, $\rho_{Ni} \sim 1/{N_i}^{1/3}$ is the mean interionic distance, $\rho_{Wi} \sim n^2\hbar/(m_i v_{T_i})$ is the ion Weisskopf radius.

On the basis of the above four "elementary" frequencies, there occur three composite parameters that are various characteristic times as follows (*below the set of quantum numbers of the radiator is denoted by* k).

1. $\tau_e(k, N_e, T_e, \Delta\omega) \sim \min(1/\Omega_{\mathrm{e}}\,, 1/\omega_{\mathrm{pe}}\,, 1/\Delta\omega)$ – characteristic time of the formation of the homogeneous broadening by electrons.
2. $\tau_i(k, N_i, T_i, \Delta\omega) \sim \min(1/\Omega_{\mathrm{i}}\,, 1/\omega_{\mathrm{pe}}\,, 1/\Delta\omega)$ – characteristic time of the formation of the homogeneous broadening by dynamic part of ions.
3. $\tau_{life}(k, N_e, T_e, N_i, T_i, \Delta\omega)$ – the lifetime of the exited state of the radiator:

$$\tau_{life}(k, N_e, T_e, N_i, T_i, \Delta\omega) \sim 1/\Gamma, \tag{1.1}$$

$$\Gamma = \gamma_e(k, N_e, T_e, \Delta\omega) + \gamma_i(k, N_i, T_i, \Delta\omega). \tag{1.2}$$

In equation (1.2), Γ is the sum of the *homogeneous* Stark widths due to electrons and the dynamic part of ions.

In the theory of SB, two opposite approximations can be made, depending on the type of problem with which one may be interested.

The first approximation is to regard the perturbing particles as fixed with respect to the radiating particle. Because of the presence of the perturbers, the energy levels of the radiator are shifted, giving rise to a wavelength displacement of the spectral line. The line shape is then obtained by averaging over various possible perturbing configurations. This is inhomogeneous broadening is called the *quasi-static broadening*.

The Stark broadening of SL by plasma ions is quasi-static if any of the following two conditions are met. The first sufficient condition is that the number ν_{Wi} of perturbing ions in the sphere of the ion Weisskopf radius is greater than unity (see, e.g., [1.6]: $4\,\pi N_i {\rho_{W_i}}^3/3 > 1$). Under this condition, for the overwhelming majority of perturbing ions, the frequency of the variation of the ion microfield $\Omega_i(N_i, T_i)$ is smaller than the instantaneous Stark splitting in the ion microfield. Therefore the above requirement is called the modulation-type condition.

The second sufficient condition is $\Omega_i(N_i, T_i) < \gamma_e$. Under this condition the lifetime of the excited state of the radiator is smaller than the characteristic time of the variation of the ion microfield. This sufficient condition is called the damping-type condition.

The opposite (to the quasi-static) approximation is to consider the collisions of the radiator with perturbing charges as a sequence of single, discrete encounters, each of which upsets the phase of the emitted light by a certain amount. This is called the *impact broadening*. With respect to the electron microfield, this approximation is appropriate if the number ν_{We} of perturbing ions in the sphere of the electron Weisskopf radius is much smaller than unity (see, e.g., review [1.6]: $4\,\pi N_e {\rho_{W_e}}^3 \ll 1$). Under this condition, for the overwhelming majority of

perturbing ions, the frequency of the variation of the electron microfield $\Omega_e(N_i, T_i)$ is much greater than the instantaneous Stark splitting in the electron microfield.

In this work, we will make use of either one of these two approximations for various circumstances: for treating our new source of the shift of the spectral line by perturbing ions, we will make extensive use of the quasi-static approximation. Additionally, when determining the electron density from the contribution of perturbing ions to the asymmetry of the profile, again the quasi-static approximation will be used. When improving the Stark broadening theory for plasma electrons, we will make extensive use of the impact approximation.

Chapter 2. New Source of Shift of Hydrogenic Spectral Lines in Plasmas: Analytical Treatment of the Effect of Penetrating Ions

2.1 Introduction

Red shifts of spectral lines (hereafter, SL) play an important role in astrophysics. Indeed, the relativistic (cosmological and gravitational) red shifts (see, e.g. the book by Nussbaumer and Bieri [2.1]) are at the core of models of the Universe and of tests for the general relativity. However, for inferring the relativistic red shifts from the observed red shifts it is required to allow for the Stark shift of SL. Hydrogen and hydrogenlike (hereafter, H-like) SL in plasmas are usually shifted to the red by electric microfields – see, e.g., books by Griem [2.2] and by Oks [2.3] and references therein. Besides, in laboratory plasmas, measurements of the Stark shift can supplement measurements of the Stark width and thus enhance plasma diagnostics – specifically the determination of the electron density (see, e.g., paper by Parigger *et al*. [2.4]).

In the present paper we describe a new source of the Stark shift of H-like SL – in addition to the previously known sources of the shift (we call the latter "standard shifts"). As an example, we compare the results with the experimental shift of the Balmer-α SL of He II 1640 A measured in a laboratory plasma by Pittman and Fleurier [2.5]. We show that the allowance for this new additional red shift leads to a good agreement with the measured shift from [2.5] for the entire range of the electron density employed in that experiment, while without this new shift the standard shifts underestimated the measured shift by factors between two and five.

2.2 "Standard" shifts of hydrogenlike spectral lines

One of the most significant "standard" contributions to the shift of H-like SL is caused by quenching, non-zero Δn (Griem paper [2.6]), and elastic, zero Δn (Boercker and Iglesias paper [2.7]), collisions with plasma electrons – hereafter, the electronic shift (see also Griem paper [2.8]).

There is also a so-called plasma polarization shift (PPS), which plays an important role in explaining the observed shifts of the high-n H-like SL – see, e.g., books by Griem [2.2] and by Salzman [2.9] and the paper by Renner *et al* [2.10]. The PPS is less significant for the low-n H-like SL. Physically the PPS is caused by the redistribution of plasma electrons due to the attraction to the radiating ion. When only plasma electrons inside the orbit of the bound electron were taken into account, the resulting theoretical PPS was blue (such as, e.g., in paper by Berg *et al* [2.11]). Later it was found that after the allowance for redistributed plasma electrons both outside and inside the bound electron orbit, the resulting theoretical PPS becomes red. However, theoretical results for a red PPS by different authors differ by a factor of two – more details and the references will be provided below while comparing theoretical and experimental results.

Then there is a controversial issue of the "standard' shift caused by plasma ions – hereafter, the standard ionic shift. Various existing calculations were based on the multipole expansion with respect to the ratio r_{rms}/R (in the binary description of the ion microfield) or with respect to the analogous parameter $r_{rms}F^{1/2}$ (in the multi-particle description of the ion microfield F). Here r_{rms} is the root-mean-square value of the radius-vector of the atomic electron ($r_{rms} \sim n^2/Z_1$, where Z_1 is the nuclear charge), and R is the separation between the nucleus of the radiating atom/ion and the nearest perturbing ion. We use the atomic units here and below.

The dipole term of the expansion ($\sim 1/R^2$ *or* $\sim F$) does not lead to any shift of a hydrogenic SL. Indeed, each pair of the Stark components, characterized by the electric quantum numbers q and $-q$, is symmetric with respect to the unperturbed frequency ω_0 of the hydrogenic line – symmetric concerning both the displacement from ω_0 and the intensity. Here $q = n_1 - n_2$, where n_1 and n_2 are the first two of the three parabolic quantum numbers ($n_1 n_2 m$). The next, quadrupole term of the expansion ($\sim 1/R^3$ *or* $\sim F^{3/2}$) does not shift the center of gravity of hydrogenic lines. This was proven analytically in Oks paper [2.12]. Namely, after allowing for the quadrupole corrections to both the energies/frequencies and the intensities, and then summing up over all Stark components of a hydrogenic SL, the center of gravity shift becomes exactly zero at any fixed value of R or F.

Thus, within the approach based on the multipole expansion, the first non-vanishing ionic contribution to the shift of hydrogenic SL is supposed to originate from the next term of the multipole expansion: from the term $\sim 1/R^4$ or $\sim F^2$. In processing this term, many authors considered only the quadratic Stark (QS) effect – see papers by Griem [2.8] and by Könies and Günter [2.13, 2.14]:

$$\Delta E_{QS}{}^{(4)} = -\frac{{Z_2}^2 n^4}{16\,{Z_1}^4 R^4}\,(17n^2 - 3q^2 - 9m^2 + 19)\,. \qquad (1)$$

Here Z_2 is the charge of perturbing ions; the superscript (4) at ΔE_{QS} specifies that this term is of the 4th order with respect to the small parameter r_{rms}/R.

However, first, the corrections of this order to the energies are of the same order as the corrections to the intensities, as noted in the paper by Demura *et al* [2.15]. Therefore,

calculations in Könies and Günter papers [2.13, 2.14] were inconsistent because they took into account the QS corrections only to the energies. Second, there is an even more important flaw in the papers by Griem [2.8] and by Könies and Günter [2.13, 2.14], as follows.

The above Eq. (1) was obtained using the dipole term of the multipole expansion treated in the 2nd order of the perturbation theory. However, the quadrupole term, processed in the 2nd order of the perturbation theory, and the octupole term, processed in the 1st order of the perturbation theory, in fact also yield energy corrections $\sim 1/R^4$ – this was shown as early as in 1969 by Sholin [2.16]. The rigorous energy correction of the order $\sim 1/R^4$ can be obtained in the form (given in Sholin paper [2.16] and presented also in the book by Komarov *et al* [2.17]):

$$\Delta E^{(4)} = \frac{Z_2 n^3}{16\, {Z_1}^4 R^4}\left[Z_1 q(109q^2 - 39n^2 - 9m^2 + 59) - Z_2 n(17n^2 - 3q^2 - 9m^2 + 19)\right] \quad (2)$$

Apparently, it is inconsistent to allow for one term and to neglect two other terms of the same order of magnitude.

Nevertheless, from table III of Griem paper [2.8] it is clear the ionic shift $\Delta E^{(4)}$ due to the QS effect is by one or more orders of magnitude smaller than the corresponding electronic shift (and that while the latter is red, the former is blue). A more consistent calculation of the ionic shift $\Delta E^{(4)}$ does not change the fact it is just a very small correction to the corresponding electronic shift and is even a smaller correction to the sum of the corresponding electronic shift and the PPS. Therefore, the standard shift can be represented with the accuracy, sufficient for comparison with experiments, by the sum of the electronic shift and the PPS, while the standard ionic shift can be neglected.

2.3 New source of shift: analytical calculations and comparison with experiment

The standard approaches to calculating the ionic shift disregarded configurations where $r_{rms}/R > 1$, i.e., where the nearest perturbing ion is within the radiating atom/ion (below we call them "penetrating configurations"). In the standard approaches, all terms of the multipole expansion, starting from the quadrupole term, at the averaging over the distribution of the quantity R, resulted in integrals diverging at small R, which were evaluated one way or another, e.g., by introducing cutoffs. However, the fact of the divergence of these integrals should have been a warning the standard approach did not provide a consistent complete description of the ionic shift.

The contribution to the ionic shift from penetrating configurations is a product of two factors. The first fact is the statistical weight of penetrating configurations, which is relatively small. The second factor is the shift relevant to penetrating configurations is relatively large. We show below that the product of these two factors can exceed the total standard shift represented by the sum of the electronic shift and the PPS.

For penetrating configurations, we use the expansion in terms of the parameter $R/r_{rms} < 1$ in the basis of the spherical wave functions of the so-called "united atom", the latter being a hydrogenic ion of the nuclear charge $Z_1 + Z_2$, where Z_1 represents the radiator and Z_2 represents the perturbing ion. The unperturbed Hamiltonian of the united atom (ua) is:

$$H_{ua} = \frac{p^2}{2m} - \frac{Z_1 + Z_2}{r_{ua}}. \tag{3}$$

The expansion of the energy can be represented in the form (see, e.g., equations (5.10)–(5.12) from the book by Komarov *et al* [2.17]):

$$E = -\frac{(Z_1 + Z_2)^2}{2\,n^2} + \mathcal{O}\left(\frac{R^2}{{r_{rms}}^2}\right). \tag{4}$$

Thus, the first non-vanishing contribution $S(n)$ to the shift of the energy level is indeed relatively large:

$$S(n) = -\frac{(Z_1 + Z_2)^2}{2n^2} - \frac{{Z_1}^2}{2n^2} + \mathcal{O}\left(\frac{R^2}{{r_{rms}}^2}\right) = -\frac{2\,Z_1 Z_2\ + {Z_2}^2}{2n^2} + \mathcal{O}\left(\frac{R^2}{{r_{rms}}^2}\right). \tag{5}$$

Below in order to simplify formulas, while still getting the message across, we limit ourselves by the practically important case where $Z_1 = Z_2 = Z$. According to equations (5.11), (5.12) from book by Komarov *et al* [2.17], the perturbed energies E_{nlm} for $l > 0$ are given by:

$$E_{nlm} = -\frac{Z^2}{2n^2} - \frac{8[l(l+1) - 3m^2]}{nl(l+1)(2l-1)(2l+1)(2l+3)} Z^4 R^2\,. \tag{6}$$

For the case of $l = 0$, the relation simplifies to:

$$E_{n00} = -\frac{Z^2}{2n^2} + \frac{8\,Z^4 R^2}{3\,n^3}\,. \tag{7}$$

We note that according to the book by Komarov *et* al [2.17], the above result for $l = 0$ can be obtained from the result for $l > 0$, first by setting $m = 0$ in equation (6) and then, after canceling out $l(l+1)$ in the numerator and the denominator, by setting $l = 0$. At the last step of setting

$l = 0$, because of the term $(2l - 1)$ in the denominator, the 2nd term in equation (7) becomes positive (due to the typographic error, this 2nd term was printed as negative in equation (5.11) from [2.17]).

To avoid any confusion, it is very important to emphasize here that the primary, overwhelming part of the shift of any energy level by penetrating ions is controlled by the 1st term in equations (6), (7), and is given by the 1st term in the right side of equation (5). Namely, it is $-3Z^2/(2n^2)$, as yielded by equation (4) after setting $Z_1 = Z_2 = Z$. The shift of any energy level, caused by penetrating ions, is *negative for any value of* l.

Physically this is because the united atom of the nuclear charge $2Z$ represents a stronger, broader potential well for the atomic electron than the atom of the nuclear charge Z: the atomic electron becomes stronger bounded. Therefore, all energy levels shift down when the potential well broadens: this is a simple consequence of the variational principle—as shown in textbooks on quantum mechanics. Thus, the shift of any energy level, caused by penetrating ions, is to the *lower values of the energy or frequency*. Since the frequency and the wavelength relate to each other inversely, the shift to a lower frequency corresponds to the shift to a *higher wavelength*: the *red shift*.

Speaking about the shift of a spectral line, originating from the radiative transition between the upper and lower energy levels, we should emphasize the following. Both the upper and the lower energy levels shift to lower energies, but the upper level shifts more than the lower level. This is because for any level of the principal quantum number n, the negative shift (to lower energies) is actually the product of two factors: $S(n)$ from equation (5) and the statistical weight $I(n)$ of the corresponding penetrating configuration. While $S(n)$ scales $\sim 1/n^2$, the statistical weight $I(n)$ increases with growing n more rapidly than $\sim n^2$, as will be shown by examples below.

Therefore, the sign of the shift of the spectral line is determined by the sign of the shift of the upper level: it is negative in the frequency scale, so that it is positive in the wavelength scale—the red shift.

For sublevels of the energy levels of the principal quantum numbers $n = 1$, $n = 2$, and $n = 3$, respectively, we obtain the following results, up to (including) the terms $\sim R^2$ for the penetrating-ions-caused shifts (according to equation (5)):

$$\begin{aligned} S_{100} &= -\frac{3}{2}Z^2 + \frac{8}{3}Z^4R^2\,, & S_{200} &= -\frac{3}{8}Z^2 + \frac{1}{3}Z^4R^2, \\ S_{210} &= -\frac{3}{8}Z^2 - \frac{1}{15}Z^4R^2\,, & S_{21\pm1} &= -\frac{3}{8}Z^2 + \frac{1}{30}Z^4R^2\,, \\ S_{300} &= -\frac{1}{6}Z^2 + \frac{8}{81}Z^4R^2\,, & S_{310} &= -\frac{1}{6}Z^2 - \frac{8}{405}Z^4R^2\,, \\ S_{31\pm1} &= -\frac{1}{6}Z^2 + \frac{4}{405}Z^4R^2\,, & S_{320} &= -\frac{1}{6}Z^2 - \frac{8}{2835}Z^4R^2\,, \\ S_{32\pm1} &= -\frac{1}{6}Z^2 - \frac{4}{2835}Z^4R^2\,, & S_{32\pm1} &= -\frac{1}{6}Z^2 + \frac{8}{2835}Z^4R^2\,. \end{aligned} \tag{8}$$

Lyman-α Line

For any hydrogenic spectral line, the total intensity of σ-components is twice the intensity of all π-components. In particular, the Lyman-α line, the total intensity of the σ-components, which consists of the 21-1 and 211 sublevel, is twice the intensity of the single π-component, which consists of the 210 sublevel.

The total normalized shift of the Lyman-α line is given by:

$$S(R) = \frac{\sum_k I_k(S_k(n=2) - S_k(n=1))}{\sum_k I_k}\,, \tag{9}$$

where k represents the kth component to the total shift of the spectral line. The obtained result is:

$$S(R) = \frac{1}{3}\left(-\frac{3}{8}Z^2 - \frac{1}{15}Z^4R^2\right) + \frac{1}{3}\left(-\frac{3}{8}Z^2 + \frac{1}{3}Z^4R^2\right) + \frac{2}{3}\left(-\frac{3}{8}Z^2 + \frac{1}{30}Z^4R^2\right) - \left(-\frac{3}{2}Z^2 + \frac{8}{3}Z^4R^2\right), \quad (10)$$

which is left unsimplified here.

The next step is to average this shift over the appropriate distribution $P_u(u) = P_u(R/R_0)$ of the internuclear distances, scaled by the mean interionic distance

$$R_0 = \left(\frac{3Z}{4\pi N_e}\right)^{\frac{1}{3}}, \quad (11)$$

where N_e is the electron density. Since we consider here penetrating configurations, where the nearest neighbor ion is inside the electron cloud, then the distribution $P_u(R/R_0)$ can be obtained from the binary distribution $P_w(w) = P_w(F/F_0)$ of the ion microfield (where $F = Z_2/R^2$ and $F_0 = Z_2/{R_0}^2$, so that $u = \sqrt{1/w}$) presented in papers [2.18, 2.19], as follows. Since

$$P_u(u)\, du = -P_w(w)\, dw, \quad (12)$$

then for $P_u(u)$ we get

$$P_u(u) = \left(\frac{2}{u^3}\right) P_w\left(\frac{1}{u^2}\right). \quad (13)$$

Using the results from papers by Held [2.18] and by Held *et al* [2.19], for the case of $Z_1 = Z_2 \equiv Z$, the ion microfield distribution can be normalized analytically and brought to the form

$$P_w(w) = \frac{\left(\frac{3^{\frac{1}{2}}\pi}{w^{\frac{5}{2}}}\right) exp\left(-\frac{1}{w^{\frac{3}{2}}} - k\, w^{\frac{1}{2}}\right)}{\text{MeijerG}\left[\{\{\,\},\{\,\}\},\left\{\left\{0,\frac{1}{3},\frac{2}{3},1\right\},\{\,\}\right\},\frac{k^3}{27}\right]}, \tag{14}$$

where MeijerG[…] is the Meijer G-function (see appendix) and

$$k = \frac{T_e Z^{\frac{3}{2}} v^2}{2qT_i}\,, \qquad q = \frac{15}{4(2\,\pi)^{\frac{1}{2}}} = 1.496\,, \qquad v = \frac{R_0}{r_{De}}\,, \qquad r_{De} = \left(\frac{T_e}{4\pi e^2 N_e}\right)^{\frac{1}{2}}, \tag{15}$$

the latter being the Debye radius. A practical formula for the quantity v is

$$v\ = 8.98x10^{-2}[N_e(cm^{-3})]^{\frac{1}{6}}/[Te(K)]^{\frac{1}{2}}\,. \tag{16}$$

In equations (15) and (16), T_e and T_i are the electron and ion temperatures, respectively.

Then according to equation (13), for the distribution $P_u(u)$ we get

$$P_u(u) = \frac{2\pi\, 3^{\frac{1}{2}} u^2\, exp\left(-u^3 - \frac{k}{u}\right)}{\text{MeijerG}\left[\{\{\,\},\{\,\}\},\left\{\left\{0,\frac{1}{3},\frac{2}{3},1\right\},\{\,\}\right\},\frac{k^3}{27}\right]}. \tag{17}$$

The averages of various powers of $u = R/R_0$ can be also expressed via various Meijer$G$-functions as follows:

$$\int_0^\infty u^4\, P_u(u)\, du = \frac{k^{10}\text{MeijerG}\left[\{\{\},\{\}\},\left\{\left\{-\left(\frac{5}{3}\right),-\left(\frac{3}{2}\right),-\left(\frac{4}{3}\right),-\left(\frac{7}{6}\right),-1,-\left(\frac{5}{6}\right),0\right\},\{\}\right\},\frac{k^6}{46656}\right]}{80621568\,\sqrt{3}\,\pi^{\frac{5}{2}}\,C}, \quad (18)$$

$$\int_0^\infty u^5\, P_u(u)\, du = \frac{k^{12}\text{MeijerG}\left[\{\{\},\{\}\},\left\{\left\{-2,-\left(\frac{11}{6}\right),-\left(\frac{5}{3}\right),-\left(\frac{3}{2}\right),-\left(\frac{4}{3}\right),-\left(\frac{7}{6}\right),0\right\},\{\}\right\},\frac{k^6}{46656}\right]}{8707129344\,\sqrt{3}\,\pi^{\frac{5}{2}}\,C}, \quad (19)$$

$$\int_0^\infty u^6\, P_u(u)\, du = \frac{k^{14}\text{MeijerG}\left[\{\{\},\{\}\},\left\{\left\{-\left(\frac{7}{3}\right),-\left(\frac{13}{6}\right),-2,-\left(\frac{11}{6}\right),-\left(\frac{5}{3}\right),-\left(\frac{3}{2}\right),0\right\},\{\}\right\},\frac{k^6}{46656}\right]}{313456656384\,\sqrt{3}\,\pi^{\frac{5}{2}}\,C}, \quad (20)$$

where

$$\mathrm{C} = \frac{\sqrt{3}}{4\,\pi^{\frac{5}{2}}}\,\text{MeijerG}\left[\{\{\},\{\}\},\left\{\left\{0,\frac{1}{6},\frac{1}{3},\frac{1}{2},\frac{2}{3},\frac{5}{6},1\right\},\{\}\right\},\frac{\mathrm{k}^6}{46656}\right]. \quad (21)$$

However, from these general results it would be difficult to study asymptotics because Taylor expansions of Meijer$G$-functions are not available. More explicit results are possible to obtain for relatively low-density plasmas, where the distribution from equation (17) reduces to:

$$P(R) = 3\frac{R^2}{R_0^3} exp\left(-\frac{R^3}{R_0^3}\right). \quad (22)$$

(here we assumed again $Z_1 = Z_2 = Z$). More specifically, equation (17) reduces to equation (22) at relatively low N_e, such that the quantity v defined in equations (15), (16) is sufficiently small, so that in equation (15) $k \ll 1$ (no screening/correlation approximation).

Let us consider the limits of integration. We can approximate the upper limit of integration as the root mean square matrix element of the radial integral, which depends on the sublevel in consideration. This relation is:

$$r_{rms} = \sqrt{\frac{3n^2}{4Z^2}[5n^2 + 1 - 3\,l(l+1)]}\,. \quad (23)$$

After averaging over *l*, we obtain:

$$r_n = \left[\frac{n^2(7\,n^2 + 5)}{4\,Z^2}\right]^{\frac{1}{2}}. \quad (24)$$

(here and below we omit the subscript "rms")[1].

[1] We extend the integrations to the limit of validity of the expansions given by equations (5) and (6). Extending integrations to the limits of validity of various expansions is the standard practice in the area of spectral line shapes in plasmas. For example, in the standard theory of the Stark broadening of spectral lines in plasmas by Griem [2.20], the limit of the integration over the impact parameter ρ was chosen as the so-called Weisskopf radius ρ_W—even though the perturbation expansion used in that theory is valid, rigorously speaking, only for $\rho \ll \rho_W$. Another example: in the theory of the spectral lines shifts by

From Eq. (24), we find the upper limits of integration for the $n = 1$ and $n = 2$ levels, respectively, to be:

$$\mathrm{r}_1 = (3)^{\frac{1}{2}}\frac{1}{\mathrm{Z}}\,, \qquad \mathrm{r}_2 = (33)^{\frac{1}{2}}\frac{3}{\mathrm{Z}}\,. \tag{25}$$

Therefore, we can calculate the averaged shift due to penetrating ions (keeping terms up to $\sim R^5$) as follows:

$$\begin{aligned} S_{ave} = \int_0^{r_2} \Big\{ & \frac{1}{3}\left(-\frac{3}{8}Z^2 - \frac{1}{15}Z^4R^2\right) + \frac{1}{3}\left(-\frac{3}{8}Z^2 + \frac{1}{3}Z^4R^2\right) \\ & + \frac{2}{3}\left(-\frac{3}{8}Z^2 + \frac{1}{30}Z^4R^2\right)\Big\} 3\frac{R^2}{R_0^3} exp\left(-\frac{R^3}{R_0^3}\right) dR \\ & - \int_0^{r_1} \left(-\frac{3}{2}Z^2 + \frac{8}{3}Z^4R^2\right) 3\frac{R^2}{R_0^3} exp\left(-\frac{R^3}{R_0^3}\right) dR\,, \end{aligned} \tag{26}$$

where upon expansion of the distribution, S_{ave} is:

Boercker and Iglesias [2.7] and Griem [2.8], the upper limit of the integration over the wave number k was chosen at the value k_{max} corresponding to the limit of validity of the perturbation expansion used in that theory—even though the perturbation expansion used in that theory of the shifts is valid, rigorously speaking, only for $k \ll k_{max}$.

$$S_{ave} = \int_0^{(33)^{\frac{1}{2}}\frac{3}{Z}} \left\{ -\frac{9Z^2R^2}{8R_o^3} + \frac{9Z^2R^5}{8R_o^6} + \cdots \right\} dR$$

$$- \int_0^{(3)^{\frac{1}{2}}\frac{1}{Z}} \left\{ -\frac{9Z^2R^2}{2R_o^3} + \frac{8Z^4R^4}{R_o^3} + \frac{9Z^2R^5}{2\,R_o^6} + \cdots \right\} dR$$

$$\approx -\frac{88.2}{Z\,{R_0}^3}. \tag{27}$$

Then we substitute R_0 from equation (11), so that equation (27) reduces to the following:

$$S_{ave} = -\frac{370\,Ne}{Z^2}. \tag{28}$$

Lyman-β Line

Similarly to the above calculations for the Lyman-α line, by using the relative intensities of the line components and the perturbation to the energies, we obtain the following expression for the shift of the Lyman-β line:

$$S(R) = \frac{1}{3}\left[\left(-\frac{Z^2}{6} + \frac{8\,Z^4R^2}{81}\right) + \left(-\frac{Z^2}{6} - \frac{8\,Z^4R^2}{405}\right) + \left(-\frac{Z^2}{6} - \frac{8\,Z^4R^2}{2835}\right)\right]$$
$$+ \frac{2}{3}\left[\left(-\frac{Z^2}{6} + \frac{4\,Z^4R^2}{405}\right) + \left(-\frac{Z^2}{6} - \frac{4\,Z^4R^2}{2835}\right)\right] \tag{29}$$
$$-\left(\frac{3\,Z^2}{2} + \frac{8}{3}Z^4R^2\right).$$

Just as for the Lyman-α line, we average this shift over the same distribution $P(R)$ from equation (16) and use the same upper limit of integration for the $n = 1$ level. For the $n = 3$ level, according to equation (24), the upper limit of integration is:

$$r_3 = (17)^{\frac{1}{2}}\frac{3}{Z}\ . \tag{30}$$

Then the averaged shift of the Lyman-β line due to penetrating ions (keeping terms up to $\sim R^5$) is given by:

$$\begin{aligned} S_{ave} = & \int_0^{r_3}\left\{\frac{1}{3}\left[\left(-\frac{Z^2}{6}+\frac{8\,Z^4R^2}{81}\right)+\left(-\frac{Z^2}{6}-\frac{8\,Z^4R^2}{405}\right)+\left(-\frac{Z^2}{6}-\frac{8\,Z^4R^2}{2835}\right)\right]\right. \\ & \left.+\frac{2}{3}\left[\left(-\frac{Z^2}{6}+\frac{4\,Z^4R^2}{405}\right)+\left(-\frac{Z^2}{6}-\frac{4\,Z^4R^2}{2835}\right)\right]\right\}\frac{3\,R^2}{R_0^3}exp\left(-\frac{R^3}{R_0^3}\right)\,dR \\ & -\int_0^{r_1}\left(-\frac{3}{2}Z^2+\frac{8}{3}Z^4R^2\right)3\frac{R^2}{R_0^3}exp\left(-\frac{R^3}{R_0^3}\right)\,dR\ , \end{aligned} \tag{31}$$

where upon expansion of the distribution, S_{ave} is:

$$\begin{aligned} S_{ave} = & \int_0^{(17)^{\frac{1}{2}}\frac{3}{Z}}\left\{-\frac{Z^2R^2}{2R_o^3}+\frac{Z^2R^5}{2R_o^6}+\cdots\right\}dR \\ & -\int_0^{(3)^{\frac{1}{2}}\frac{1}{Z}}\left\{-\frac{9Z^2R^2}{2R_o^3}+\frac{8Z^4R^4}{R_o^3}+\frac{9Z^2R^5}{2\,R_o^6}+\cdots\right\}dR \\ \approx & -\frac{333}{Z\,{R_0}^3}. \end{aligned} \tag{32}$$

Then we substitute R_0 from equation (11), so equation (33) reduces to the following:

$$S_{ave} = -\frac{1.39x10^3\ N_e}{Z^2}. \tag{33}$$

Balmer-α Line

The calculation for the Balmer-α line is similar to the above calculations for the Lyman-α and Lyman-β lines, though it is more involved. It yields

$$S(R) = \left(-\frac{Z^2}{6} + \frac{40\ Z^4R^2}{25461} + \frac{128\ Z^6R^4}{89667}\right)_3 - \left(-\frac{3Z^2}{8} + \frac{160\ Z^4R^2}{2829} + \frac{101\ Z^6R^4}{9430}\right)_2, \tag{34}$$

where the subscripts refer to the levels $n = 3$ and $n = 2$, respectively. It is important to separate the results between levels for averaging over R since the limits of integration differ between the levels. Then the averaged shift of the Balmer-α line due to penetrating ions is given by:

$$\begin{aligned} S_{ave} = \int_0^{r_3} &\left(-\frac{Z^2}{6} + \frac{40\ Z^4R^2}{25461} + \frac{128\ Z^6R^4}{89667}\right)\frac{3\ R^2}{R_0^3}\,exp\left(-\frac{R^3}{R_0^3}\right)\,dR \\ &- \int_0^{r_2} \left(-\frac{3Z^2}{8} + \frac{160\ Z^4R^2}{2829} + \frac{101\ Z^6R^4}{9430}\right)\frac{3\ R^2}{R_0^3}\,exp\left(-\frac{R^3}{R_0^3}\right), \end{aligned} \tag{35}$$

where upon expansion of the distribution, S_{ave} is:

$$S_{ave} = \int_0^{(17)^{\frac{1}{2}}\frac{3}{Z}} \left\{ -\frac{Z^2R^2}{2R_o^3} + \frac{40\,Z^4R^4}{8487R_o^3} + \frac{Z^2R^5}{2\,R_o^6} + \cdots \right\} dR$$

$$- \int_0^{(33)^{\frac{1}{2}}\frac{3}{Z}} \left\{ -\frac{9Z^2R^2}{8R_o^3} + \frac{160Z^4R^4}{943\,R_o^3} + \frac{9Z^2R^5}{8\,R_o^6} + \cdots \right\} dR$$

$$\approx -\frac{184}{Z\,{R_0}^3}. \qquad (36)$$

Then we substitute R_0 from equation (11), so that equation (33) reduces to the following:

$$S_{ave} = -\frac{769\,Ne}{Z^2}. \qquad (37)$$

As an example, we compare various theoretical sources of the shift (including our result) for the He II Balmer-α line with the experimental shift of this line obtained by Pittman and Fleurier [2.5] for the electron densities in the range of $N_e = (0.3 - 2.3) \times 10^{17}$ cm^{-3}. In figure 1, the experimental shifts $\Delta\lambda_{exp}$ are shown by circles. The theoretical shift by Griem [2.6, 2.8] $\Delta\lambda_{Griem}$, with which Pittman and Fleurier [2.5] compared their experimental results, is shown by the dashed blue line.

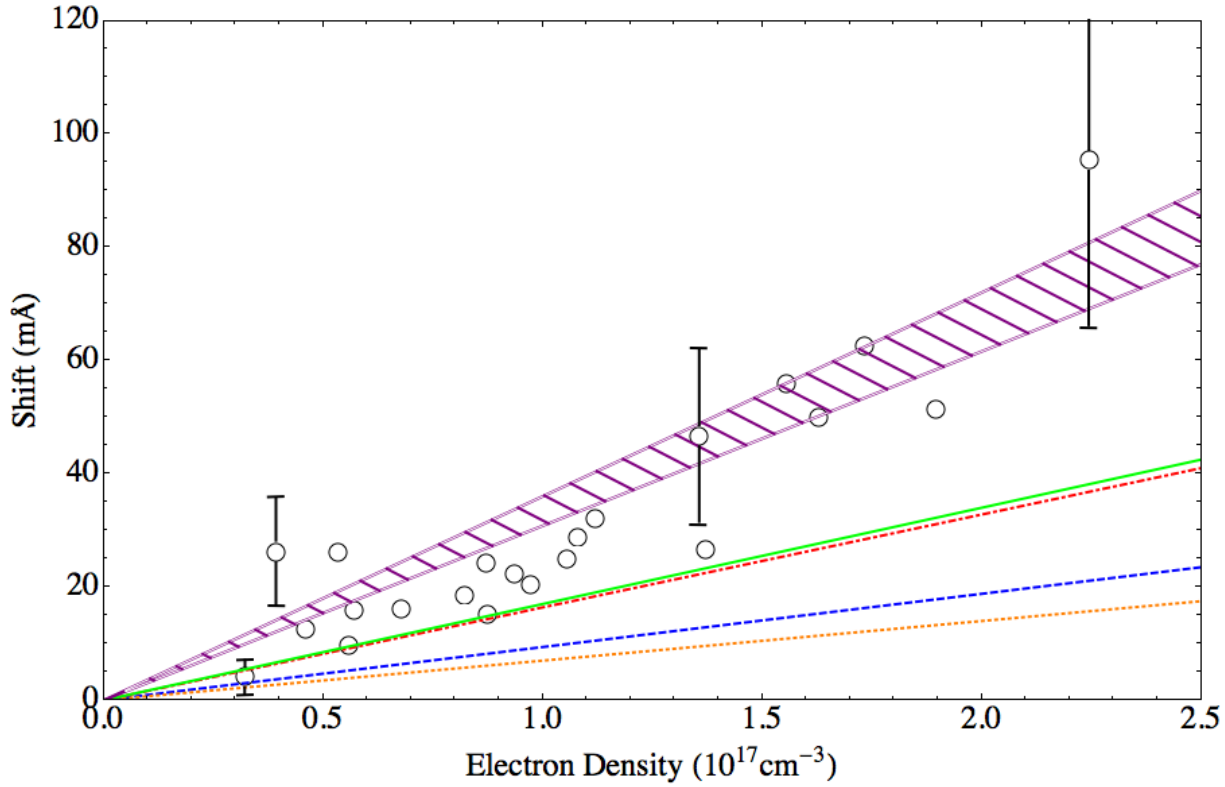

Fig. 2.1. Comparison of the experimental shift of the He II Balmer-α line 1640 A measured by Pittman and Fleurier [2.5], shown by circles, with the following theoretical shifts: Griem's shift [2.6, 2.8] – dashed blue line; plasma polarization shift – dotted orange line; the sum of the latter two theoretical shifts – dashed-dotted red line; shift due to penetrating ions (introduced in the present paper) – solid green line; the sum of all three theoretical shifts – purple band, the width of which reflects the theoretical error. The experimental error bars are shown only for few electron densities in order to avoid making the figure too "busy" and difficult to understand.

It is seen that there was a huge discrepancy between the experimental red shift $\Delta\lambda_{exp}$ and the theoretical red shift by Griem

$$\Delta\lambda_{Griem}(mA) = 9.4\, N_e(cm^{-3})/10^{17}\,. \tag{38}$$

The discrepancy is by a factor of 2.6 at $N_e = 10^{17}$ cm^{-3} and increasing to almost a factor of five at $N_e = 2.2 \times 10^{17}$ cm^{-3}.

Griem's shift [2.6, 2.8] is a well-established part of the "standard shifts". The other part – plasma polarization shift (PPS) – has a factor of two difference in calculations by different authors. For example, from the results of the paper Benredjem *et al* [2.20], the PPS of the three components of the He II Balmer-α line at $T = 4\ eV$ can be deduced to be as follows.

For 3d-2p: $\Delta\lambda_{PPS}(mA) = 8.5\ N_e(cm^{-3})/10^{17}$. (Relative intensity 0.814422)

For 3p-2s: $\Delta\lambda_{PPS}(mA) = 11.8\ N_e(cm^{-3})/10^{17}$. (Relative intensity 0.169671)

For 3s-2p: $\Delta\lambda_{PPS}(mA) = 14.8\ N_e(cm^{-3})/10^{17}$. (Relative intensity 0.0159067)

The average is: $\Delta\lambda_{PPS}(mA) = 9.2\ N_e(cm^{-3})/10^{17}$.

On the other hand, there are PPS calculations by Blaha and Davis [2.22] for He II 1640 A, quoted by Marangos *et al* [2.23]. For Blaha-Davis' case B, which is the more realistic than case A, at $N_e = 2 \times 10^{18}$ cm^{-3} and $T = 3.3\ eV$, it yielded $\Delta\lambda_{PPS} = 100\ mA$, thus corresponding to $\Delta\lambda_{PPS}(mA) = 5\ N_e(cm^{-3})/10^{17}$. At the temperature $T = 4\ eV$, relevant to Pittman-Fleurier experiment [2.5], the PPS would be slightly less than $5\ N_e(cm^{-3})/10^{17}$ because it decreases as the temperature increases.

So, for the comparison with Pittman-Fleurier experiment [2.5] we adopt the theoretical PPS averaged over the above two sets of theoretical calculations, namely:

$$\Delta\lambda_{\mathrm{PPS}}(\mathrm{mA}) = 7\ \mathrm{N_e}(\mathrm{cm^{-3}})/10^{17}\ . \tag{39}$$

In figure 1, it is shown by the dotted red line[2].

[2] We mention also paper by Junkel *et al* [2.24], where by using the relaxation model, the authors calculated the shift of spectral lines of highly-charged ions (such as Ar XVII) in super-high density plasmas (such as at $N_e = 10^{24}\ cm^{-3}$) caused by penetrating electrons. This shift is relatively insignificant for He II at $N_e = 10^{17}\ cm^{-3}$).

The sum $\Delta\lambda_{Griem} + \Delta\lambda_{PPS}$ is shown by the dash-dotted red line. It is seen that even after adding the PPS to Griem's shift, their sum still underestimates the experimental shift at least by a factor of two.

As for the new source of shift presented in our paper – the shift due to penetrating ions $\Delta\lambda_{PI}$ – for the He II Balmer-α line it is given by:

$$\Delta\lambda_{PI}(mA) = 17\, N_e(cm^{-3})/10^{17}\,. \tag{40}$$

In figure 1 it is shown by the solid green line. The sum $\Delta\lambda_{Griem} + \Delta\lambda_{PPS} + \Delta\lambda_{PI}$ is presented in figure 1 by the dashed purple band. (The width of the band reflects the theoretical error of this sum, originated from the relative inaccuracy of our relatively simple model and from the theoretical uncertainty of the PPS.) It is seen that adding the shift due to the penetrating ions brings the total shift into a good agreement with the experimental shift.

For checking the accuracy of the application of our relatively simple model to the experimental shifts by Pittman and Fleurier [2.5], we performed more rigorous calculations by taking into account the following. For the spectral lines of hydrogenic helium (He II) emitted from helium plasmas, the would-be molecular ion He_2^{3+} does not exist—there is no bonding molecular orbitals (that otherwise would significantly affect and invalidate our relatively simple model). So, we checked the effect of antibonding molecular orbitals. For this purpose we employed the code developed by Salin [2.25], based on the well-known analytical results by Power [2.26]. The obtained electronic terms $E(R)$ were then used to modify the ion microfield distribution from paper [2.18, 2.19]. It turned out that the combined effect of the allowance for the antibonding molecular orbitals for the quasimolecule $\alpha e \alpha$ (where α stands for the alpha-particle—the nucleus

of He) and of using equations (17)–(21) instead of the approximate equation (22), diminished the contribution to the shift from penetrating configurations by only 10%–15%. The effect of this correction on the total theoretical shift was only 5%–10%, which is well within the previously estimated theoretical error of about 30% (originated from the relative inaccuracy of our relatively simple model and from the theoretical uncertainty of the PPS). Thus, it is legitimate to use our relatively simple model—to get the message across concerning the new contribution to the shift.

2.4 Conclusions

We introduced an additional source of the shift of H-like spectral lines arising from the configurations where the nearest perturbing ion is within the radiating atom/ion ("penetrating configurations"). We demonstrated, as an example, that for the He II Balmer-α line it makes the primary contribution to the total red shift and brings the total theoretical shift in a good agreement with the experimental shift measured by Pittman and Fleurier [2.5], while without the allowance for penetrating configurations the discrepancy between theoretical and experimental shifts was by factors between two and five.

It is important to emphasize that our relatively simple model does not apply to some radiator-perturber combinations. Let us consider, e.g, hydrogen or deuterium spectral lines. At low principal quantum numbers, such as, e.g., $n = 1 - 3$, the penetrating configuration – a proton inside the hydrogen or deuterium atom – corresponds to the proton-proton or proton-deuteron separation of the same order of magnitude as in the molecules H_2^+ or HD^+ (if hydrogen/deuterium lines are emitted from hydrogen/deuterium plasmas), or in the molecules HeH^{++} and HeD^{++} (if hydrogen/deuterium lines are emitted from helium plasmas). Therefore, in this case the presence of the bonding molecular orbital has to be taken into account, which is beyond our relatively simple model[3].

However, for the spectral lines of hydrogenic helium (He II) emitted from helium plasmas, our simple model applies because the corresponding would-be molecule He_2 and its ions, such as,

[3] We note that for highly-excited hydrogen spectral lines from hydrogen plasmas, the shift due to penetrating ions can be calculated within a similar simple model (adjusted for high n) because highly-excited states do not form bonding molecular orbitals of H_2^+—see paper [2.27], where the allowance for this shift removed a large discrepancy between the shifts of high-n Balmer lines observed from the atmosphere of Sirius and the theoretical shifts, as well as very significantly diminished a large discrepancy between the shifts of these lines observed in a laboratory plasma and the theoretical shifts.

e.g., He_2^{3+}, do not exist. Similarly, for the lines of hydrogenic beryllium (Be IV) emitted from beryllium plasmas, our simple model applies because the corresponding would-be molecule Be_2 and its ions, such as, e.g., Be_2^{7+}, do not exist. In fact, our relatively simple model applies to most pairs consisting of a heavy hydrogenic ion and a heavy perturbing, fully-stripped ion – because for the overwhelming majority of such combinations the bonding molecular orbitals do not exist.

2.5 Appendix. Meijer$G$ function

A general definition of the Meijer G-function is given by the following line integral in the complex plane:

$$\text{Meijer}G\left["a_1,\dots,a_n,'a_{n+1},\dots,a_p,"b_1,\dots,b_m,'b_{m+1},\dots,b_q,x\right] = G_{p,q}^{m,n}\left(x\left|\begin{matrix}a_1 & ,\dots, & a_p\\ b_1 & ,\dots, & b_q\end{matrix}\right.\right)$$
$$= \frac{1}{2\,\pi\,i}\int_{\gamma L}\frac{\prod_{j=1}^{m}\Gamma\left(b_j-s\right)\prod_{j=1}^{m}\Gamma\left(1-a_j+s\right)}{\prod_{j=n+1}^{p}\Gamma\left(a_j-s\right)\prod_{j=m+1}^{q}\Gamma\left(1-b_j+s\right)}x^s\,ds\,,$$

where Γ denotes the gamma function. This integral is of the so-called Mellin–Barnes type, and may be viewed as an inverse Mellin transform. The definition holds under the following assumptions:

- $0 \le m \le q$ and $0 \le n \le p$, where m, n, p and q are integer numbers
- $a_k - b_j \neq 1,2,3,\dots$ for $k = 1,2,\dots,n$ and $j = 1,2,\dots,m$, which implies no pole of any $\Gamma\left(b_j - s\right), j = 1,2,\dots,m$, coincides with any pole of any $\Gamma(1 - a_k + s), k = 1,2,\dots,n$

The contour of the integration γL runs from $-i\infty$ to $+i\infty$ such that all poles of $\Gamma\left(b_j - s\right), j = 1,2,\dots,m$, are on the right of the path, while all poles of $\Gamma(1 - a_k + s), k = 1,2,\dots,n$, are on the left.

The G-function satisfies the following linear differential equation of order $\max(p, q)$:

$$\left\{(-1)^{p-m-n}x\sum_{j=1}^{P}\left[x\left(\frac{d}{dx}\right)-a_j+1\right]-\sum_{j=1}^{P}\left[x\left(\frac{d}{dx}\right)-b_j\right]\right\}G(x)=0\,.$$

Chapter 3. Revision of the Method for Measuring the Electron Density based on the Asymmetry of Hydrogenic Spectral Lines in Dense Plasmas

3.1 Introduction

In medium density plasmas, profiles of hydrogenic spectral lines look symmetric, but in high density plasmas they become asymmetric. This asymmetry is caused primarily by the nonuniformity of the ion microfield, as noted by Sholin and his co-workers in papers [3.1-3] (for the latest advances in the theory of the asymmetry we refer to papers [3.4, 3.5] and references therein). Often the blue maximum of the spectral line is higher than the red maximum, and the positions of the intensity maxima are asymmetrical with respect to the unperturbed line center.

A new diagnostic method for measuring the electron density using the asymmetry of hydrogenic spectral lines in dense plasmas was proposed and implemented in paper [3.6]. In that paper, in particular, from the experimental asymmetry of the C VI Lyman-delta line emitted by a vacuum spark discharge, the electron density was deduced to be $N_e = 3x10^{20}$ cm^{-3}. This value of N_e was in a good agreement with the electron density determined from the experimental widths of C VI Lyman-beta and Lyman-delta lines.

Later this diagnostic method was employed also in the experiment presented in paper [3.7]. In that laser-induced breakdown spectroscopy experiment, the electron density $N_e \sim 3x10^{17}$ cm^{-3} was determined from the experimental asymmetry of the H I Balmer-beta (H-beta) line.

This new diagnostic method has the following advantages compared to the method of deducing N_e from the experimental widths of spectral lines. First, the latter, traditional method requires measuring widths of at least two spectral lines – because the widths are affected not only by the Stark broadening, but also by competing broadening mechanisms, such as, e.g., the Doppler broadening. In distinction, for using the new diagnostic method it is sufficient to obtain the

experimental profile of just one spectral line – because the Doppler broadening does not cause the asymmetry.

Second, the traditional method based on the experimental widths would be difficult to implement if the center of the spectral lines is optically thick. In distinction, the new diagnostic method can still be used even if the spectral line is optically thick in its central part. This is because the overwhelming contribution to the asymmetry originates from the wings of the spectral line, the wings being usually optically thin. More details can be found in Sect. 1.6 of book [3.8][*/].

In the theory underlying this new diagnostic method, the contribution of plasma ions to the spectral line asymmetry was calculated only for configurations where the perturbing ions are outside the "atomic sphere", i.e., outside the bound electron cloud of the radiating atom/ion (non-penetrating configurations). In the present paper we take into the contribution to the spectral line asymmetry from *penetrating configurations*, i.e., from the configurations where the perturbing ion is inside the bound electron cloud of the radiating atom/ion (hereafter, radiator). We show that in high density plasmas, the allowance for penetrating ions can result in significant corrections to the electron density deduced from the spectral line asymmetry.

[*/]We note that Ref. [40] from Ch. 1 of [3.8] on the paper referred here as [3.6] has typographic errors. The correct one is our Ref. [3.6] here.

3.2 Allowance for penetrating ions

Let us first present a brief overview of the underlying theory for non-penetrating configurations. The dipole interaction of the radiator with perturbing ions outside the bound electron cloud splits the spectral line into Stark components symmetrically with respect to the unperturbed frequency or wavelength – in terms of both positions and intensities of the Stark components. The quadrupole interactions of the radiator with perturbing ions outside the bound electron cloud causes the asymmetry of the Stark splitting – in terms of both positions and intensities of the Stark components.

However, in paper [3.9] it was shown that the quadrupole interaction, despite casing the asymmetric splitting of the spectral line into Stark components, does not shift the center of gravity of the line profile. Therefore, in the new diagnostic method presented in paper [3.6], first the center of gravity of the experimental profile was determined and then it was taken as the reference point. Then with respect to this point, the integrated intensities of the blue (I_B) and red (I_R) wings of the experimental profile were found. After that, the experimental degree of asymmetry, defined as

$$\rho_{quad} = \frac{I_B - I_R}{0.5[I_B + I_R]}, \tag{1}$$

was determined and then compared with the corresponding theoretical value given below.

The theoretical intensities of the blue and red wings, resulting from dipole and quadrupole interactions of the radiator with perturbing ions outside the bound electron cloud, can be expressed as follows (see paper [3.6]):

$$I_B = \sum_{k>0} I_k^{(0)} \left(1 + \frac{Z_p\, a_o}{{Z_r}^2 R_o} \epsilon_k^{(1)} \langle R_0/\mathrm{R} \rangle\right), \tag{2}$$

and

$$I_R = \sum_{k<0} I_k^{(0)} \left(1 + \frac{Z_p\, a_o}{{Z_r}^2 R_o} \epsilon_k^{(1)} \langle R_0/\mathrm{R} \rangle\right), \tag{3}$$

where Z_p is the charge of perturbing ions, Z_r is the nuclear charge of the radiator, a_o is the Bohr radius, and $R_o = [(4\pi/3)N_p]^{-1/3}$ is the mean interionic distance, $N_p = N_e/Z_p$ being the perturbing ion density. Here $I_k^{(0)}$ and $\epsilon_k^{(1)}$ are the unperturbed intensity and the quadrupole correction to the intensity, respectively, the subscript *k* being the label of Stark components of the spectral line: $k > 0$ and $k < 0$ correspond to the blue-shifted and red-shifted components, respectively (the values of $I_k^{(0)}$ and $\epsilon_k^{(1)}$ for several Lyman and Balmer lines were tabulated in paper [3.2]). The quantity $\langle R_0/\mathrm{R} \rangle$ is the scaled inverse distance between the perturbing ion and the radiator averaged over the distribution of such distances.

Finally, the theoretical degree of asymmetry was presented in paper [3.6] in the form:

$$\rho_{quad} = 0.46204 \left(\frac{N_e\,[cm^{-3}]}{10^{21}}\right)^{\frac{1}{3}} \frac{Z_p^{\frac{2}{3}}}{Z_r^2} \sum_{k>0} I_k^{(0)} \epsilon_k^{(1)}\,, \tag{4}$$

Then the electron density N_e was determined in paper [3.6] by substituting the experimental degree of asymmetry into the left side of Eq. (4).

In the present paper we consider the contribution of penetrating ions to the spectral line asymmetry – in order to refine this diagnostic method. To get the message across in a simple form, we limit ourselves below to the practically important case $Z_p = Z_r = Z$. The energy shifts due to penetrating ions can be calculated by the perturbation theory in the basis of the spherical wave functions of the so-called "united atom" of the nuclear charge $2Z$.

The perturbed energy shifts (counted from the unperturbed energies) for the orbital quantum number $l > 0$ are given by (see, e.g., Eqs. (6) and (7) from paper [3.10] or Eqs. (5.11), (5.12) from book [3.11]):

$$E_{nlm} = -\frac{8\,[\mathrm{l(l+1)} - 3\mathrm{m}^2]\; Z^4 R^2\; e^2}{\mathrm{a_o}^3\; \mathrm{n}^3 \mathrm{l(l+1)(2l-1)(2l+1)(2l+3)}}. \tag{5}$$

For the case of $l = 0$, the calculated energy shift is:

$$E_{n00} = \frac{8\; Z^4 R^2 e^2}{3\; \mathrm{a_o}^3 n^3}. \tag{6}$$

We note that Eq. (6) can be also obtained from Eq. (5), first by setting m = 0, and then by cancelling out $l(l + 1)$ in the numerator and denominator, and by setting $l = 0$. (This was mentioned in book [3.11], but in Eq. (5.11) from [3.11] corresponding to our Eq. (6), there was a typographic error in the sign.)

The frequency change of an individual Stark component is thus given by

$$\Delta\omega_k = -\frac{Z^2 e^2 \Delta_k^1}{2\,\hbar\,{a_o}^3} R^2\,, \tag{7}$$

where

$$\Delta_k^1 = 16\,Z^2\left[\frac{l(l+1)-3\,m^2}{n^3 l(l+1)(2l-1)(2l+1)(2l+3)} - \frac{l'(l'+1)-3\,m'^2}{n'^3 l'(l'+1)(2l'-1)(2l'+1)(2l'+3)}\right]. \tag{8}$$

For the specific case where either $l = 0$ or $l' = 0$, Eq. (8) reduces to

$$\Delta_k^1 = \begin{cases} 16\,Z^2\left[\dfrac{1}{3\,n^3} - \dfrac{l'(l'+1)-3\,m'^2}{n'^3 l'(l'+1)(2l'-1)(2l'+1)(2l'+3)}\right], & l = 0;\, l' \neq 0 \\ 16\,Z^2\left[\dfrac{l(l+1)-3\,m^2}{n^3 l(l+1)(2l-1)(2l+1)(2l+3)} - \dfrac{1}{3\,n'^3}\right], & l' = 0;\, l \neq 0 \end{cases}. \tag{9}$$

Then the quasi-static profile of each Stark component can be represented in the form:

$$S_k(\Delta\lambda) = \int_0^{u_{max}} W(u)\left[I_k^{(0)} + I_k^{(1)}\right]\delta\left(\Delta\lambda - \frac{Z^2 e^2 \Delta_k^1\,{\lambda_0}^2}{4\,\pi\,c\,\hbar\,{a_o}^3}u\right)du\,. \tag{10}$$

Here, $u \equiv R^2$, and the probability of finding the perturbing ion a distance u away from the radiating atom is taken to be the binary distribution. For simplifying the integration, we use the expansion of the distribution in powers u/R_0^2 and keep the terms up to ~u^2:

$$W(u)du = \frac{3\sqrt{u}}{2\,R_o^3}\exp\left(-\frac{\sqrt{u}^3}{R_o^3}\right)du \;\approx \frac{3\sqrt{u}}{2\,R_o^3} - \frac{3\,u^2}{2\,R_o^6}\,du. \tag{11}$$

For the case of a hydrogenic radiator under the presence of a penetrating ion, the relative intensities of each line component can be best calculated analytically using the robust perturbation theory developed by Oks and Uzer [3.12]. A more detailed explanation of this procedure is outlined in Appendix A. The relative intensities of each component can be written as

$$I_k = \Delta_{Ik}^0 + Z^2\Delta_{Ik}^1 u^2\,, \tag{12}$$

where Δ_{Ik}^0 and Δ_{Ik}^1 are tabulated in Appendix B for each component of the spectral line Balmer-alpha, considered here as an example.

The upper limit u_{max} of the integration in Eq. (10) should be the smallest of the following two "candidates". One candidate for u_{max} is the root mean square size of the bound electron cloud, which depends on the sublevel in consideration:

$$\mathrm{r_{rms}} = \sqrt{\frac{n^2}{2\,Z^2}\left[5\,n^2 + 1 - 3\,l\,(l+1)\right]}\,. \tag{13}$$

The other candidate for u_{max} is defined by the limit of the applicability of the perturbation theory. Of course, this would ensure that formally calculated corrections to the energy and intensities of the spectral line would remain relatively small.

The allowance for penetrating ions shifts the center of gravity of the spectral line, as shown in paper [3.13]. (This is the only contribution to the shift of the center of gravity since the dipole and quadrupole interactions of the radiator with perturbing ions outside the bound electron cloud do not shift the center of gravity, as shown in paper [3.9] and mentioned above). For the He II Balmer-alpha line, which we use as an example, the center of gravity shift due to penetrating ions was calculated analytically in paper [3.13] to be

$$\Delta\lambda_{PI}\ (mA) = \ 17\ N_e(cm^{-3})/10^{17}. \tag{14}$$

The shift by this amount center of gravity serves as the reference point for calculating the integrated intensities of the blue and red wings with the allowance for penetrating ions.

After carrying out the integration in Eq. (10), the profile reduces to

$$S_k(\Delta\lambda) = \left(\frac{Z^2 e^2 \Delta_k^1\ {\lambda_0}^2}{4\,\pi\,c\,\hbar\,{a_o}^3}\right)^{-1} I_k(u_0)\left(\frac{3{u_0}^{\frac{1}{2}}}{2\,R_o^3} - \frac{3{u_0}^2}{2\,R_o^6}\right)\Theta\left[u_{max}\frac{Z^2 e^2 \Delta_k^1\ {\lambda_0}^2}{4\,\pi\,c\,\hbar\,{a_o}^3} - |\Delta\lambda|\right], \tag{15}$$

where $\Theta[...]$ is the Heaviside step function and u_0 is the root of the delta function, given by

$$u_0 = \frac{4\,\pi\,c\,\hbar\,{a_o}^3}{Z^2 e^2 \Delta_k^1\ {\lambda_0}^2}\Delta\lambda\,. \tag{16}$$

Thus, for the contributions of the penetrating ions to the integrated intensities of the blue and red parts of the line profile we get

$$\mathrm{I_{PI,B}} = \sum_{k<0} \int_{-\Delta\lambda_{max}}^{\Delta\lambda_{PI}} S_k(\Delta\lambda)\, d\Delta\lambda \tag{17}$$

and

$$\mathrm{I_{PI,R}} = \sum_{k>0} \int_{\Delta\lambda_{PI}}^{\Delta\lambda_{max}} S_k(\Delta\lambda)\, d\Delta\lambda, \tag{18}$$

respectively. Here

$$\Delta\lambda_{max} = u_{max} \frac{Z^2 e^2 \Delta_k^1 \, {\lambda_0}^2}{4\,\pi\, c\, \hbar\, {a_o}^3}, \tag{19}$$

which is obtained by equating to zero the argument of the Heaviside step function. Additionally, what is meant in Eqs. (17) and (18) by k < 0 (or k > 0) is the inclusion of only those components which involve corrections to the energy which are positive (or negative), implying a blue-shifted (or red-shifted) components of the spectral line.

By combining the above result with the contribution of the quadrupole interaction (the interaction of the radiator with perturbing ions outside the bound electron cloud) to the integrated intensities of the blue and red parts of the profile, we obtain our final result for the degree of asymmetry

$$\rho_{act} = \frac{I_B + \mathrm{I_{PI,B}} - I_R - \mathrm{I_{PI,R}}}{0.5\left[I_B + \mathrm{I_{PI,B}} + I_R + \mathrm{I_{PI,R}}\right]}, \tag{19}$$

where the subscript *act* stands for *actual* – in distinction to ρ_{quad}.

The combination of Eqs. (4) and (19) connects the degree of asymmetry with the electron density N_e and thus allows a more accurate determination of the electron density from the experimental asymmetry. We illustrate this below by the example of the He II Balmer-alpha line.

Table 1 presents the following quantities for the He II Balmer-alpha line at five different values of the actual electron density:

- the theoretical degree of asymmetry ρ_{act} calculated with the allowance for penetrating ions,
- the theoretical degree of asymmetry ρ_{quad} calculated without the allowance for penetrating ions,
- the electron density $N_{e,quad}$ that would be deduced from the experimental asymmetry degree while disregarding the contribution of the penetrating ions,
- the relative error $|N_{e,quad}–N_{e,act}|/N_{e,act}$ in determining the electron density from the experimental asymmetry degree while disregarding the contribution of the penetrating ions.

$N_{e,act}/(10^{18}cm^{-3})$	ρ_{act}	ρ_{quad}	$N_{e,quad}/(10^{18}cm^{-3})$	$\lvert N_{e,quad}–N_{e,act}\rvert/N_{e,act}$
2	0.0925	0.0955	1.82	9.03%
4	0.114	0.120	3.42	14.5%
6	0.128	0.138	4.86	19.1%
8	0.139	0.152	6.16	23.1%
10	0.147	0.163	7.33	26.7%

Table 3.1. The relative error in determining the electron density N_e from the experimental asymmetry degree while disregarding the contribution of the penetrating ions for the He II Balmer-alpha line. The physical quantities in Table 3.1 are explained in the text directly above Table 3.1.

It is seen that in high density plasmas, the allowance for penetrating ions can indeed result in significant corrections to the electron density deduced from the spectral line asymmetry.

3.3 Conclusions

For improving the diagnostic method for measuring the electron density using the asymmetry of spectral lines in dense plasmas, we took into the contribution to the spectral line asymmetry from *penetrating configurations*, i.e., from the configurations where the perturbing ion is inside the bound electron cloud of the radiating atom/ion. After performing the corresponding analytical calculations we demonstrated that in high density plasmas the allowance for penetrating ions can result in significant corrections to the electron density deduced from the spectral line asymmetry.

It is worth clarifying why we took into account the shift of the line *as the whole* due to penetrating ions, but do not take into account other mechanisms shifting the line *as the whole*, such as, e.g., plasma polarization shift and the shift by plasma electrons. The experimental integrated intensities of the blue (I_B) and red (I_R) parts of the profile are calculated with respect to the experimental center of gravity of the profile. The latter shifts of the line *as the whole* do not contribute to the asymmetry and thus should not affect the experimental values of I_B and I_R. The reason we took into account the shift of the line *as the whole* by penetrating ions is that penetrating ions contribute simultaneously to both the asymmetry and the shift of the line as the whole. Since these two effect of penetrating ions are two sides of the same coin, both of them should be taken into account.

Finally we note that the electron densities $N_e \sim (10^{18} – 10^{19})$ cm^{-3}, which we used in the illustrative example of the He II Balmer-alpha line, are achievable in plasma spectroscopy. Examples are experiment [3.14] with a hydrogen plasma and experiment [3.15] with a helium plasma.

3.4 Appendix A. Details of Calculating Perturbed Matrix Elements

The redistribution of intensities of Stark components, along with wavelength shifts due to the presence of perturbing ions, play a crucial role in determining the degree of asymmetry of the spectral line. These values have been tabulated according to the robust perturbation theory developed by Oks and Uzer [3.12] based on using the super-generalized Runge-Lenz vector derived by Kryukov and Oks [3.16]. Since the unperturbed system has an additional constant of the motion (namely the Runge-Lenz vector), then the task of calculating the corrections to the state is simplified. The reason for this beneficial result is as follows: the correction to the Runge-Lenz vector is non-degenerate with respect to the same states that are degenerate in the correction to the Hamiltonian. The mixing of the states is elucidated by the Runge-Lenz vector correction under the influence of the perturbing ion. Here are some details, formulas being presented in atomic units.

According to paper [3.16], for the problem of an electron in the field of two Coulomb centers of charges Z_1 and Z_2, the additional conserved quantity is the following projection of the super-generalized Runge-Lenz vector on the internuclear axis

$$A_z = \mathbf{p} \times \mathbf{L} \cdot \mathbf{e_z} - \frac{L^2}{R} - Z_1 \frac{z}{r} - Z_2 \frac{R - z}{|\mathbf{R} - \mathbf{r}|} + Z_2 , \qquad \text{(A.1)}$$

where **p**, **L**, and **r** are the linear momentum, the angular momentum, and the radius-vector of the electron, respectively; **R** is the vector directed from charge Z_1 to charge Z_2. For the case where R << r, the unperturbed part A_{z0} of the operator A_z can be chosen as

$$A_{z0} = -\frac{L^2}{R}, \tag{A.2}$$

corresponding to the unperturbed Hamiltonian of the so-called "united atom" of the nuclear charge $Z_1 + Z_2$:

$$\mathrm{H}_0 = \frac{\mathrm{p}^2}{2} - \frac{\mathrm{Z}_1 + \mathrm{Z}_2}{\mathrm{r}}, \tag{A.3}$$

Operators H_0 and A_{z0} have common eigenfunctions (the spherical eigenfunctions of the Coulomb problem). The spectrum of eigenvalues of the operator H_0 is degenerate. Therefore, calculating corrections to the eigenfunctions of the operator H_0 using the standard perturbation theory would require going to the 2nd order of the *degenerate* perturbation theory, thus involving generally infinite summations (see, e.g., the textbook [3.17]).

In distinction, the spectrum of eigenvalues of the operator A_{z0} is nondegenerate (the eigenvalues being $-l(l+1)/R$). Therefore, the corrections to the eigenfunctions can be easily calculated in the 1st order of the standard *nondegenerate* perturbation theory. The coefficients of the corresponding linear combinations of the unperturbed eigenfunctions are

$$< nl'm|A_z - A_{z0}|nlm > = \frac{l'(l'+1) - l(l+1)}{R} \tag{A.4}$$

and do not involve infinite summations. This example is another illustration of the advantages of the robust perturbation theory developed in paper [3.12] over the standard perturbation theory.

In this way we obtained the following expression for the 1st order corrections to the eigenfunctions for the specific case of $Z_1 = Z_2 = Z$

$$\Psi_{nlm}^{(1)} = \frac{5\left[\frac{(l_>^2 - m^2)(n^2 - l_>^2)}{(2\,l_> + 1)(2\,l_> - 1)}\right]^{\frac{1}{2}}}{n\,[l(l+1) - l'(l'-1)]} Z\,R\,\Psi_{nl'm'}^{(0)}\,, \tag{A.5}$$

where $l_>$ denotes the greater value between l and l'. The selection rules are $l' = l \pm 1$ and $m' = m$.

We note that in the opposite case, where R >> r, the unperturbed part $A_{z1,0}$ of the operator A_z can be chosen in the usual way

$$A_{z1,0} \;=\; z\,p^2 - p_z(\boldsymbol{rp}) - Z_1\frac{z}{r}\,, \tag{A.6}$$

where the notation (**rp**) stands for the scalar product (also known as the dot-product) of the operators **r** and **p**. The corresponding unperturbed Hamiltonian is

$$H_{1,0} \;= \frac{p^2}{2} - \frac{Z_1}{r}\,, \tag{A.7}$$

The operator $A_{z1,0}$ has a nondegenerate spectrum of eigenvalues equal to q/n, where $q = (n1 - n2)$ is the difference of the parabolic quantum numbers. Therefore, the first nonvanishing corrections to the common eigenfunctions of the operators $H_{1,0}$ and $A_{z1,0}$ can be easily calculated

in the 1st order of the standard *nondegenerate* perturbation theory. The coefficients of the corresponding linear combinations of the unperturbed eigenfunctions are

$$< nl'm|L^2|nlm > = \frac{\frac{q'}{n} - \frac{q}{n}}{R}, \tag{A.8}$$

where $|q' - q| = 2$, as follows from the selection rules.

In distinction, for obtaining the same corrections to the eigenfunctions using the operator $H_{1,0}$, whose spectrum of eigenvalues is degenerate, it would require going to the 2nd order of the *degenerate* perturbation theory and dealing with its complications, as Sholin did in his paper [3.2].

3.5 Appendix B. Table of Intensities and Energy Level Corrections for the He II Balmer-α line

The perturbed intensity and frequency corrections for He II Balmer-alpha line are presented below. The quantum numbers of the upper and lower sublevels are in the spherical quantization.

Upper sublevel	Lower sublevel	Δ_{Ik}^{0}	Δ_{Ik}^{1}	Δ_{k}^{1}
322	211	$\frac{768}{4715}$	0	$\frac{173}{5670}$
321	211	$\frac{384}{4715}$	$-\frac{32}{14145}$	$\frac{197}{5670}$
321	210	$\frac{384}{4715}$	$-\frac{64}{2829}$	$-\frac{37}{567}$
321	200	0	$\frac{2792}{127305}$	$\frac{949}{2835}$
320	211	$\frac{128}{4715}$	$-\frac{128}{127305}$	$\frac{41}{1134}$
320	210	$\frac{512}{4715}$	$-\frac{3968}{127305}$	$-\frac{181}{2835}$
320	200	0	$\frac{11168}{381915}$	$\frac{953}{2835}$
311	211	0	$\frac{32}{14145}$	$\frac{19}{810}$
311	210	0	$\frac{232}{14145}$	$-\frac{31}{405}$
311	200	$\frac{160}{2829}$	$-\frac{400}{25461}$	$\frac{131}{405}$
310	211	0	$\frac{8}{3105}$	$\frac{43}{810}$
310	210	0	$\frac{2512}{127305}$	$-\frac{19}{405}$
310	200	$\frac{160}{2829}$	$-\frac{280}{8487}$	$\frac{143}{405}$
300	211	$\frac{5}{943}$	$-\frac{40}{25461}$	$-\frac{53}{810}$
300	210	$\frac{5}{943}$	$-\frac{295}{101844}$	$-\frac{67}{405}$
300	200	0	$\frac{5525}{305532}$	$\frac{19}{81}$

Chapter 4. Advanced Analytical Treatment of the Stark Broadening of Hydrogenic Spectral Lines by Plasma Electrons

4.1 Introduction

The theory of the Stark broadening of hydrogenlike spectral lines by plasma electrons, developed by Griem and Shen [4.1] and later presented also in books [4.2, 4.3], is usually referred to as the Conventional Theory, hereafter CT, also known as the standard theory. (Further advances in the theory of the Stark broadening of hydrogenlike spectral lines by plasma electrons can be found, e.g., in books [4.4, 4.5] and references therein.) In the CT, the perturbing electrons are considered moving along hyperbolic trajectories in the Coulomb field of the effective charge $Z - 1$ (in atomic units), where Z is the nuclear charge of the radiating ion. In other words, in the CT there was made a simplifying assumption that the motion of the perturbing electron can be described in frames of a two-body problem, one particle being the perturbing electron and the other "particle" being the charge $Z - 1$.

However, in reality one have to deal with a three-body problem: the perturbing electron, the nucleus, and the bound electron. Therefore, trajectories of the perturbing electrons should be more complicated.

In the present paper we take this into account by using the standard analytical method of separating rapid and slow subsystems – see, e.g., book [4.6]. The characteristic frequency of the motion of the bound electron around the nucleus is much higher than the characteristic frequency of the motion of the perturbing electron around the radiating ion. Therefore the former represents the rapid subsystem and the latter represents the slow subsystem. This approximate analytical method allows a sufficiently accurate treatment in situations where the perturbation theory fails – see, e.g., book [4.6].

By applying this method we obtain more accurate analytical results for the electron broadening operator than in the CT. We show by examples of the electron broadening of the Lyman lines of He II that the allowance for this effect increases with the electron density N_e, becomes significant already at $N_e \sim 10^{17}$ cm^{-3} and very significant at higher densities.

4.2 Analytical results

In the CT the electron broadening operator is expressed in the form (see, e.g., paper [4.1])

$$\Phi_{ab} \equiv 2\,\pi\,v\,N_e \int d\rho\,\rho\,\{S_a S_b{}^{*} - 1\}\,, \tag{1}$$

where N_e, v, and ρ are the electron density, velocity, and impact parameter, respectively; $S_a(0)$ and $S_b(0)$ are the S matrices for the upper (a) and lower (b) states involved in the radiative transition, respectively; $\{\ldots\}$ stands for the averaging over angular variables of vectors **v** and **ρ**. Further in the CT, the collisions are subdivided into weak and strong. The weak collisions are treated by the time-dependent perturbation theory. The impact parameter, at which the formally calculated expression $\{S_a S_b^* - 1\}$ for a weak collision starts violating the unitarity of the S-matrices, serves as the boundary between the weak and strong collisions and is called Weisskopf radius ρ_{We}.

So, in the CT the integral over the impact parameter diverges at small ρ. Therefore in the CT this integral is broken down in two parts: from 0 to ρ_{We} (strong collisions) and from ρ_{We} to ρ_{max} for weak collisions. The upper cutoff ρ_{max} (typically chosen to be the Debye radius $\rho_D = [T/(4\pi e^2 N_e)]^{1/2}$, where T is the electron temperature) is necessary because this integral diverges also at large ρ.

In the CT, after calculating the S matrices for weak collisions, the electron broadening operator becomes (*in atomic units*)

$$\Phi_{ab}{}^{weak} \equiv C \int_{\rho_{we}}^{\rho_{max}} d\rho\,\rho \sin^2\frac{\Theta(\rho)}{2} = \frac{C}{2}\int_{\Theta_{min}}^{\Theta_{max}} d\Theta\,\frac{d\rho^2}{d\Theta}\sin^2\frac{\Theta}{2}\,, \tag{2}$$

where Θ is the scattering angle for the collision between the perturbing electron and the radiating ion (the dependence between Θ and ρ being discussed below) and the plasma electron and the operator C is

$$C = -\frac{4\pi}{3} N_e \left[\int_0^\infty dv\, v^3 f(v) \right] \frac{m^2}{(Z-1)^2} (\boldsymbol{r}_a - \boldsymbol{r}_b{}^*)^2 \,. \tag{3}$$

Here $f(v)$ is the velocity distribution of the perturbing electrons, $\boldsymbol{r}$ is the radius-vector operator of the bound electron (which scales with Z as 1/Z), and m is the reduced mass of the system "perturbing electron – radiating ion".

In the CT the scattering occurs in the effective Coulomb potential, so that the trajectory of the perturbing electron is hyperbolic and the relation between the impact parameter and the scattering angle is given by

$$\rho^{(0)} = \frac{Z-1}{m\, v^2} \cot\frac{\Theta}{2} \,. \tag{4}$$

In the present paper we consider the realistic situation where trajectories of the perturbing electrons are more complicated because the perturbing electron, the nucleus, and the bound electron should be more accurately treated as the three-body problem. We use the standard analytical method of separating rapid and slow subsystems – see, e.g., book [4.6]. It is applicable here because the characteristic frequency $\nu_{\mathrm{Te}}/\rho_{\mathrm{We}}$ of the variation the electric field of the perturbing electrons at the location of the radiating ion is much smaller than the frequency Ω_{ab} of

the spectral line (the latter, e.g., in case of the radiative transition between the Rydberg states would be the Keppler frequency or its harmonics) – more details are presented in Appendix.

The first step in this method is to "freeze" the slow subsystem (perturbing electron) and to find the analytical solution for the energy of the rapid subsystem (the radiating ion) that would depend on the frozen coordinates of the slow subsystem (in our case it will be the dependence on the distance R of the perturbing electron from the radiating ion). To the first non-vanishing order of the R-dependence, the corresponding energy in the parabolic quantization is given by

$$E_{nq}(R) = -\frac{Z^2}{n^2} + \frac{3\,n\,q}{2\,Z\,R^2}\,, \tag{5}$$

where n and $q = n_1 - n_2$ are the principal and electric quantum numbers, respectively; n_1 and n_2 are the parabolic quantum numbers.

The next step in this method is to consider the motion of the slow subsystem (perturbing electron) in the "effective potential" $V_{\text{eff}}(\text{R})$ consisting of the actual potential plus $E_{\text{nq}}(\text{R})$. Since the constant term in equation (5) does not affect the motion, the effective potential for the motion of the perturbing electron can be represented in the form

$$V_{eff}(R) = -\frac{\alpha}{R} + \frac{\beta}{R^2}\,, \qquad \alpha = Z - 1\,. \tag{6}$$

For the spectral lines of the Lyman series, since the lower (ground) state b of the radiating ion remains unperturbed (up to/including the order ~$1/\text{R}^2$), the coefficient β is

$$\beta = \frac{3\, n_a q_a}{2\, Z}. \tag{7}$$

For other hydrogenic spectral lines, for taking into account both the upper and lower states of the radiating ion, the coefficient β can be expressed as

$$\beta = \frac{3\, (n_a q_a - n_b q_b)}{2\, Z}\ . \tag{8}$$

The motion in the potential from equation (6) allows an exact analytical solution. In particular, the relation between the scattering angle and the impact parameter is no longer given by Equation (4), but rather becomes (see, e.g., book [4.7])

$$\Theta = \pi - \frac{2}{\sqrt{1 + \frac{2\, m\, \beta}{M^2}}} \arctan \sqrt{\frac{4\, E}{\alpha^2}\left(\beta + \frac{M^2}{2m}\right)}\ . \tag{9}$$

Here E and M are the energy and the angular momentum of the perturbing electron, respectively. We can rewrite the angular momentum in terms of the impact parameter ρ as

$$M = m\, v\, \rho \tag{10}$$

Then a slight rearrangement of equation (9) yields

$$\tan\left(\frac{\pi-\Theta}{2}\sqrt{1+\frac{2\,\beta}{m\,v^2\rho^2}}\right)=\frac{v}{\alpha}\sqrt{m^2v^2\rho^2+2\,m\,\beta}\,. \tag{11}$$

After solving equation (11) for ρ and substituting the outcome in equation (2), a more accurate expression for the electron broadening operator can be obtained. However, equation (11) does not have an exact analytic solution for ρ so that this could be done only numerically.

In the present paper, to get the message across in the simplest form, we will provide an approximate analytical solution of equation (11) by expanding it in powers of β. This yields (keeping up to the first power of β)

$$\tan\left(\frac{\pi-\Theta}{2}\right)+\left(\frac{\pi-\Theta}{2}\right)\left[1+\tan^2\left(\frac{\pi-\Theta}{2}\right)\right]\frac{\beta}{m\,v^2\rho^2}\approx\frac{m\,v^2\rho}{\alpha}+\frac{\beta}{\alpha\,\rho}\,. \tag{12}$$

We seek the analytical solution for ρ in the form $\rho\approx\rho^{(0)}+\rho^{(1)}$, where $\rho^{(0)}$ corresponds to $\beta=0$ (and was given by equation (4)) and $\rho^{(1)}\ll\rho^{(0)}$. Substitution of $\rho\approx\rho^{(0)}+\rho^{(1)}$ into equation (12) yields the expression

$$\frac{(\pi-\Theta)\,\beta}{2\,m\,v^2{\rho^{(0)}}^2\sin^2\frac{\Theta}{2}}-\frac{\beta}{\alpha\,\rho^{(0)}}\approx\frac{m\,v^2\rho^{(1)}}{\alpha}\,. \tag{13}$$

After solving equation (13) for $\rho^{(1)}$, we get the expression for ρ:

$$\rho \approx \frac{\alpha}{m\,v^2}\cot\frac{\Theta}{2} + \frac{\beta}{\alpha}\left(\frac{\pi - \Theta}{2\cos^2\frac{\Theta}{2}} - \tan\frac{\Theta}{2}\right). \tag{14}$$

As a reminder, our goal is to perform the integration in equation (1) for obtaining a more accurate analytical result for the electron broadening operator. This can be more easily accomplished by performing the integration over Θ instead of ρ. For this purpose, first we square equation (14)

$$\rho^2 \approx \frac{\alpha^2}{m^2\,v^4}\cot^2\frac{\Theta}{2} + \frac{\beta}{m\,v^2}\left(\frac{\pi - \Theta}{\sin\frac{\Theta}{2}\,\cos\frac{\Theta}{2}} - 1\right), \tag{15}$$

where only the first order terms in β have been kept for consistency. To make formulas simpler, we denote $\phi = \Theta/2$. After differentiating equation (15) with respect to ϕ, we obtain

$$\frac{d\rho^2}{d\phi} \approx -\frac{\alpha^2}{m^2\,v^4}\frac{2\cot\phi}{\sin^2\phi} - \frac{2\,\beta}{m\,v^2}\left[\left(\frac{1}{\sin\phi\cos\phi}\right) + \left(\frac{\pi}{2} - \phi\right)\left(\frac{1}{\sin^2\phi} - \frac{1}{\cos^2\phi}\right)\right] \tag{16}$$

After substituting in the utmost right side of equation (2) first $\Theta = 2\phi$ and then $\frac{d\rho^2}{d\phi}$ from equation (16), the contribution of the weak collisions to the electron broadening operator becomes

$$\Phi_{ab}{}^{weak} = -C\left[\frac{\alpha^2}{m^2 v^4}\int_{\phi_{min}}^{\phi_{max}} \cot\phi\, d\phi + \frac{\beta}{m\, v^2}\int_0^{\frac{\pi}{2}} \tan\phi\, d\phi + \frac{\beta}{m\, v^2}\int_0^{\frac{\pi}{2}} \left(\frac{\pi}{2} - \phi\right)(1 - \tan^2\phi)\, d\phi\right]. \tag{17}$$

In equation (17), in the two correction terms proportional to β, we extended the integration over the full range of the variation of the angle ϕ. The corresponding minor inaccuracy would not contribute significantly to the electron broadening operator, since the terms involving β are considered to be a relatively small correction to the first term in equation (17).

Performing the integrations in equation (17) we obtain:

$$\Phi_{ab}{}^{weak} = -\frac{4\,\pi}{3} N_e (\boldsymbol{r}_a - \boldsymbol{r}_b{}^*)^2 \left[\int_0^\infty dv\, \frac{f(v)}{v}\right]\left[\log\frac{\sin\phi_{max}}{\sin\phi_{min}} + \frac{m v^2 \beta}{(Z-1)^2}\left(\frac{\pi^2}{4} - 1\right)\right]. \tag{18}$$

Here and below the expression $(\boldsymbol{r}_a - \boldsymbol{r}_b{}^*)^2$ stands for the scalar product (also known as the dot-product) of the operator $(\boldsymbol{r}_a - \boldsymbol{r}_b{}^*)$ with itself. In the theory of the dynamical Stark broadening of spectral lines in plasmas by electrons, the corresponding matrix elements are calculated with respect to the unperturbed wave functions.

Now we add the CT estimate for the contribution of strong collisions

$$\Phi_{ab}{}^{strong} \approx \pi\, v\, N_e\, \rho_{We}{}^2\,, \tag{19}$$

where ρ_{We} corresponds to ϕ_{max}. Expressions for ϕ_{max} and ϕ_{min} are given in paper [4.1] (in equations (9) and (10a)) as follows

$$\sin\phi_{max} = \sqrt{\frac{3}{2}}\frac{Z(Z-1)}{(n_a^2 - n_b^2)m\,v}, \tag{20}$$

$$\sin\phi_{min} = \frac{\dfrac{Z-1}{m\,v^2\rho_D}}{\sqrt{1+\dfrac{(Z-1)^2}{m^2v^4\rho_D^2}}} \tag{21}$$

It should be emphasized that the factor $(n_a^2 - n_b^2)$ in the denominator of the right side of equation (20) was an approximate allowance by the authors of paper [4.1] for the contribution of the lower level *b* while estimating the operator $(\boldsymbol{r}_a - \boldsymbol{r}_b{}^*)$ for hydrogenic lines of spectral series other than the Lyman lines. However, for the Lyman lines the lower (ground) level does not contribute to electron broadening operator, so that for the Lyman lines equation (20) should be simplified as follows:

$$\sin\phi_{max} = \sqrt{\frac{3}{2}}\frac{Z(Z-1)}{n_a^2 m\,v}. \tag{22}$$

We also note that at relatively small velocities of perturbing electrons, the right side of equation (20) or equation (22) could exceed unity. In this case one should set $\sin\phi_{max} = 1$, which corresponds to $\rho_{\min} = 0$, so that there would be no contribution from strong collisions.

Typically, the range of such small velocities has a very low statistical weight in the electron velocity distribution.

After substituting the above formulas for $\sin\phi_{max}$ and $\sin\phi_{min}$ into equation (17), and combining the contributions from weak and strong collisions, we obtain the final results for the electron broadening operator:

$$\Phi_{ab}(\beta) = -\frac{4\pi}{3} N_e (\boldsymbol{r}_a - \boldsymbol{r}_b{}^*)^2 \left[\int_0^\infty dv\ \frac{f(v)}{v}\right] \left\{ \frac{1}{2}\left[1 - \frac{3}{2}\frac{Z^2(Z-1)^2}{(n_a^2 - n_b^2)^2 m^2\ v^2}\right] + \log\left[\sqrt{\frac{3}{2}}\frac{Z\ v\ \rho_D}{(n_a^2 - n_b^2)}\sqrt{1 + \left(\frac{Z-1}{m\ v^2 \rho_D}\right)^2}\right] + \frac{m v^2 \beta}{(Z-1)^2}\left(\frac{\pi^2}{4} - 1\right)\right\} \tag{23}$$

for the non-Lyman lines and

$$\Phi_{ab}(\beta) = -\frac{4\pi}{3} N_e (\boldsymbol{r}_a - \boldsymbol{r}_b{}^*)^2 \left[\int_0^\infty dv\ \frac{f(v)}{v}\right] \left\{ \frac{1}{2}\left[1 - \frac{3}{2}\frac{Z^2(Z-1)^2}{n_a^4 m^2\ v^2}\right] + \log\left[\sqrt{\frac{3}{2}}\frac{Z\ v\ \rho_D}{n_a^2}\sqrt{1 + \left(\frac{Z-1}{m\ v^2 \rho_D}\right)^2}\right] + \frac{m v^2 \beta}{(Z-1)^2}\left(\frac{\pi^2}{4} - 1\right)\right\} \tag{24}$$

for the Lyman lines. Here and below log[…] stands for the natural logarithm.

4.3 Significance of the effect

In order to determine the significance of this effect, it is necessary then to evaluate the ratio

$$ratio = \frac{\frac{3}{2}\frac{mv^2(n_a q_a - n_b q_b)}{(Z-1)^2}\left(\frac{\pi^2}{4}-1\right)}{\frac{1}{2}\left[1-\frac{3}{2}\frac{Z^2(Z-1)^2}{(n_a^2-n_b^2)^2 m^2\, v^2}\right] + \log\left[\sqrt{\frac{3}{2}}\frac{Z\, v\, \rho_D}{(n_a^2-n_b^2)}\sqrt{1+\left(\frac{Z-1}{m\, v^2 \rho_D}\right)^2}\right]} \tag{25}$$

for the non-Lyman lines or the ratio

$$ratio = \frac{\frac{3}{2}\frac{mv^2 n_a q_a}{(Z-1)^2}\left(\frac{\pi^2}{4}-1\right)}{\frac{1}{2}\left[1-\frac{3}{2}\frac{Z^2(Z-1)^2}{n_a^4 m^2\, v^2}\right] + \log\left[\sqrt{\frac{3}{2}}\frac{Z\, v\, \rho_D}{n_a^2}\sqrt{1+\left(\frac{Z-1}{m\, v^2 \rho_D}\right)^2}\right]} \tag{26}$$

for the Lyman lines.

Below we present numerical examples for several Lyman lines. As it is customary in the Stark broadening theory, instead of the integration over velocities, for the numerical examples we use the mean thermal velocity v_T of the perturbing electrons. In atomic units, the mean thermal velocity v_T, the Debye radius ρ_D, and the reduced mass can be expressed as follows

$$v_T = 0.1917\sqrt{\frac{T(eV)}{m}} \quad \rho_D = 1.404\times 10^{11}\sqrt{\frac{T(eV)}{N_e(cm^{-3})}} \quad m = \frac{1+\frac{m_e}{A\, m_p}}{1+\frac{2\, m_e}{A\, m_p}}\,, \tag{27}$$

where m_e is the electron mass, m_p is the proton mass, and A is the atomic number of the radiating ion ($A \approx 2Z$).

Table 1 presents the values of the ratio from Equation (26) for several Lyman lines of He II at the temperature T = 8 eV and the electron density $N_e = 2x10^{17}$ cm^{-3}.

N	|q|	$ratio$
2	1	0.326
3	1	0.375
3	2	0.750
4	1	0.516
4	2	1.03
4	3	1.55

Table 4.1. Ratio from Equation (26) for the Stark components of several Lyman lines of He II at the temperature T = 8 eV and the electron density $N_e = 2 \times 10^{17}$ cm^{-3}.

Figure 1 shows the ratio from Equation (26) versus the electron density N_e for the Stark components of the electric quantum number |q| = 1 of Lyman-alpha (n = 2), Lyman-beta (n = 3), and Lyman-gamma (n = 4) lines of He II at the temperature T = 8 eV.

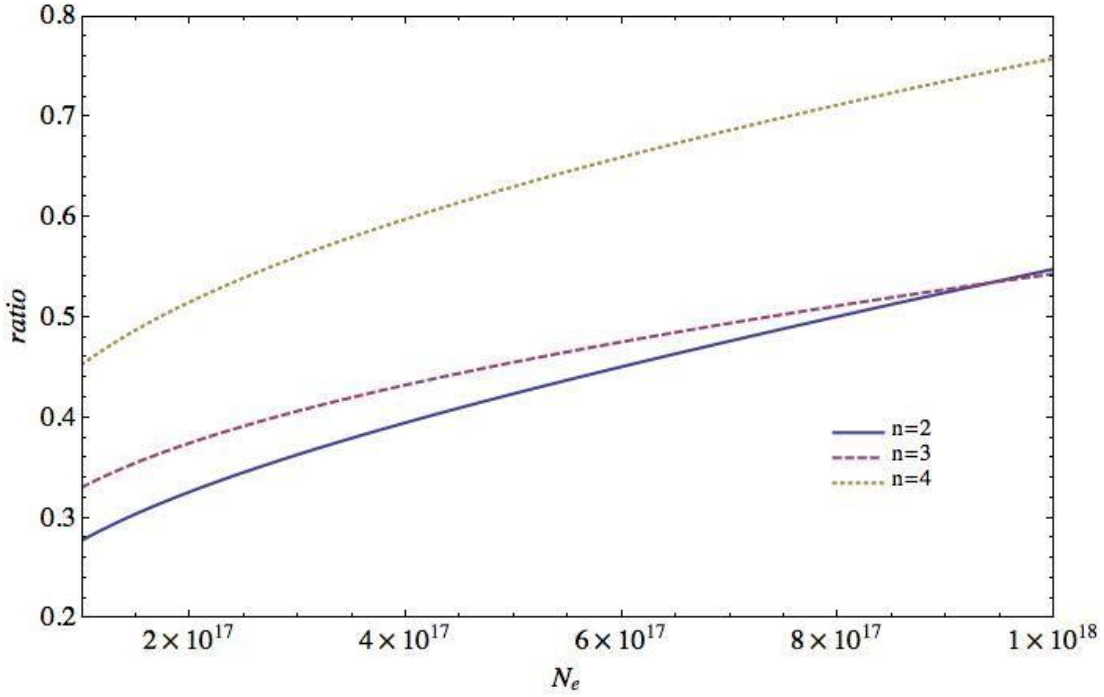

Figure 4.1. Ratio from Equation (26) versus the electron density N_e for the Stark components of the electric quantum number |q| = 1 of Lyman-alpha (n = 2), Lyman-beta (n = 3), and Lyman-gamma (n = 4) lines of He II at the temperature T = 8 eV.

It is seen that for the electron broadening of the Lyman lines of He II, the allowance for the effect under consideration indeed becomes significant already at electron densities $N_e \sim 10^{17}$ cm^{-3} and increases with the growth of the electron density. It should be noted that when the ratio, formally calculated by Equation (26), becomes comparable to unity, this is the indication that the approximate analytical treatment based on expanding Equation (11) up to the first order of parameter β, is no longer valid. In this case the calculations should be based on solving Equation (11) with respect to ρ without such approximation.

4.4 Conclusions

In this paper we considered the electron broadening of hydrogenlike spectral lines in plasmas more accurately than in the CT. In distinction to the CT, we treated it as a three-body problem involving the perturbing electron, the nucleus, and the bound electron. We employed the standard analytical method of separating rapid and slow subsystems by using the fact that the characteristic frequency of the motion of the bound electron around the nucleus is much higher than the characteristic frequency of the motion of the perturbing electron around the radiating ion.

With the help of this method we obtained more accurate analytical results for the electron broadening operator compared to the CT. By examples of the electron broadening of the Lyman lines of He II, we demonstrated that the allowance for this effect becomes significant at electron densities $N_e \sim 10^{17}$ cm^{-3} and very significant at higher densities.

It is important to emphasize that we were able to obtain the above analytical results primarily due to the underlying fundamental symmetry of the class of potentials $V(R) = -A/R + B/R^2$, where A and B are constants. Namely, this class of potentials possesses an additional conserved quantity ${M_{eff}}^2 = M^2 + 2mB$, where M is the angular momentum and m is the mass of a particle, so that M_{eff} is the effective angular momentum. As for the impact approximation, it was not crucial to our work – we used it only for the following two purposes: first, to get the message across in a simple form, and second, for the comparison with the CT (in which the impact approximation was crucial), so that we would compare "apples to apples" rather than "apples to oranges". A brief outline of the impact approximation is presented in Appendix B.

We also mention that in 1981, Baryshnikov and Lisitsa [4.8] published very interesting results for the electron broadening of hydrogenlike spectral lines in plasmas (also presented later in

book [4.9]) in frames of the quantum theory of the dynamical Stark broadening, while we obtained our results in frames of the semiclassical theory of the dynamical Stark broadening, just as in the CT. (For clarity: in the semiclassical theory, the radiating atom/ion is treated quantally, while perturbing electrons classically; in the quantum theory both the radiating atom/ion and perturbing electrons are treated quantally.) Both in paper [4.8] and in our paper, there was used the underlying symmetry of the class of potentials $V(R) = -A/R + B/R^2$, for obtaining analytical solutions.

A specific result for the line width Baryshnikov and Lisitsa [4.8] obtained for Lyman lines in the classical limit using the impact approximation, as presented in their equations (4.5) and (4.6). We compared their results from equations (4.5) and (4.6) with the CT [4.1] for He II Lyman lines. It turned out that for $N_e \sim (10^{17} - 10^{18})$ cm^{-3}, i.e. for the range of electron densities, in which the overwhelming majority of measurements of the width of He II lines were performed, Baryshnikov-Lisitsa's line width exceeds the CT line width by two orders of magnitude or more. In view of the fact that the width of He II lines, measured by various authors in benchmark experiments (i.e., experiments where plasma parameters were measured independently of the line widths), never exceeded the CT width by more than a factor of two (see, e.g., benchmark experiments [4.10-12]), this seems to indicate that something might be incorrect in equations (4.5) and (4.6) from paper [4.8] (though methodologically it was a very interesting paper). In distinction, the corrections to the CT that we introduced in the present paper, do not exceed the factor of two for He II lines in the range of $N_e \sim (10^{17} - 10^{18})$ cm^{-3}.

4.5 Appendix A. Validity of using the analytical method based on separating rapid and slow subsystems

The characteristic frequency of the motion of the perturbing electron around the radiating ion in the process of the Stark broadening of spectral lines is the so-called Weisskopf frequency

$$\omega_{We} = \frac{v_T}{\rho_{We}} \sim \frac{Z\, m\, v_T^2}{(n_a^2 - n_b^2)\hbar} \sim \frac{Z\, T}{(n_a^2 - n_b^2)\hbar}. \quad \text{(A.1)}$$

The characteristic frequency of the motion of the bound electron around the nucleus is the frequency of the spectral line

$$\Omega = \frac{Z^2 U_H}{\hbar}\left(\frac{1}{n_b^2} - \frac{1}{n_a^2}\right), \quad \text{(A.2)}$$

where U_H is the ionization potential of hydrogen. The ratio of these two frequencies is

$$\frac{\omega_{We}}{\Omega} \sim \left(\frac{T}{Z\, U_H}\right)\left[\frac{n_a^2 n_b^2}{(n_a^2 - n_b^2)^2}\right]. \quad \text{(A.3)}$$

For the simplicity of estimating this ratio, let us consider $n_a >> n_b$, so that

$$\frac{\omega_{We}}{\Omega} \sim \left(\frac{T}{Z\, n_a^2 U_H}\right) \ll 1 \quad \text{(A.4)}$$

as long as

$$\mathrm{T(eV)} \ll (13.6\ \mathrm{eV})\ \mathrm{Z}\ \mathrm{n_a^2}\ . \tag{A.5}$$

For example, for $Z = 2$ the above validity condition becomes

$$\mathrm{T(eV)} \ll (27.2\ \mathrm{eV})\ \mathrm{n_a^2} \tag{A.6}$$

and is satisfied for a broad range of temperatures, at which He II spectral lines are observed in plasmas.

Appendix B. Brief Outline of the Impact Approximation in the Conventional Theory (CT) of the Stark broadening of Spectral Lines in Plasmas

The dynamical broadening of spectral lines in plasmas by electrons is effective if the number ν_{We} of perturbing electrons in the sphere of the electron Weisskopf radius ρ_{We} is much smaller than unity (see, e.g., review by Lisitsa [4.13]): $\nu_{We} = 4\pi N_e \rho_{We}^3/3 << 1$, where $\rho_{We} \sim n^2 \hbar/(m_e v_{Te})$, n is the principal quantum number of the radiator energy level involved in the radiative transition, and v_{Te} is the mean thermal velocity of plasma electrons. Under this condition, for the overwhelming majority of perturbing electrons, the characteristic frequency of the variation of the electron microfield $\Omega_e \sim v_{Te}/\rho_{We}$ is much greater than the instantaneous Stark splitting in the electron microfield. Physically the electron Weisskopf radius is related to the impact parameters $\rho \sim \rho_{We}$ that contribute most effectively to the dynamical Stark broadening of spectral lines by electrons in plasmas [4.13].

The gist of dynamical effects in the Stark broadening of spectral lines in plasmas by electrons is the following. Collisions with plasma electrons cause *virtual transitions* mostly within the upper (n) and lower (n′) multiplets during the radiative transition $n \leftrightarrow n'$. The primary outcome is a *decrease of the lifetime* of the states n′ and/or n of the radiator, thus leading to the broadening of the corresponding spectral line.

The fact that virtual transitions occur mostly within the upper and lower multiplets conventionally leads to so-called *no-quenching approximation*, in which virtual transitions between states of different principal quantum numbers are totally disregarded. This approximation allows to introduce a *line space*: a direct product of the Hilbert space, spanned on the basis vectors of the n-shell, with the Hilbert space, spanned on the (complex-conjugated) basis vectors of the n′-shell.

Both the impact formalism (developed by Baranger [4.14] and then by Kolb and Griem [4.15]) and the key features of the unified formalism (developed by Vidal, Cooper, and Smith [4.16]) can originate from the same sequence of mathematical operations – see, e.g., review by Sahal-Brechot [4.17]. The primary difference between them is the following. The *impact* formalism considers only *completed collisions*, while the *unified* formalism allows also for *incomplete collisions*. (Another distinction is that the unified formalism allows in principle a transition to the nearest-neighbor quasistatic result in the wings of the spectral line – this is a less important distinction because numerically the unified theory does not always yield such transition correctly.)

The most important step toward the impact formalism is the introduction of a *coarse-grained time scale* Δt, chosen such that

$$\rho/v_e \ll \Delta t \ll \left[max\left(\gamma, \Delta\omega, \omega_{pe}\right)\right]^{-1}. \tag{B.1}$$

Here γ is the inversed lifetime of the radiator (the impact width of the spectral line is of the order of γ), $\Delta\omega$ is the detuning from the unperturbed frequency ω_0 of the spectral line, $\omega_{pe} = (4\pi N_e e^2/m_e)^{1/2}$ is the plasma electron frequency. Physically, the coarse-grained time scale means that one gives up details of the evolution of the radiator during the time ~ ρ/v_e (which is the characteristic time of the individual collision). Instead, the focus is at the evolution of the radiator during the time intervals ~ Δt defined by equation (B.1). The possibility of introducing the coarse-grained time scale controls the limits of validity of the impact formalism. We note that in the unified formalism, the left strong inequality of equation (B.1) is relaxed to: $\frac{\rho}{v_e} \approx \Delta t$.

The electron broadening operator Φ_{ab} is defined via the time evolution operators U_a and U_b for the upper (a) and lower (b) multiplets in the line space, respectively, as follows (see, e.g., review [4.13]):

$$\Phi_{ab} = [U_a(t, t + \Delta t) U_b{}^*(t, t + \Delta t) - 1]/\Delta t \,. \tag{B.2}$$

Under the impact approximation $\rho/v_e \gg \Delta t$, within the interval $(\mathrm{t}, \mathrm{t} + \Delta\mathrm{t})$ the time evolution operators in equation (B.2) are replaced by the corresponding scattering matrices S_a and S_b, leading to equation (1) of the main text. We note that the terminology of having not one, but two scattering matrices S_a and S_b is related to the concept of the line space and is used in the entire extensive scope of literature on the impact broadening of spectral lines in plasmas.

Finally we note that the dynamical Stark broadening of *any* hydrogenic spectral lines (whether Lyman or non-Lyman) in plasmas by electrons occurs in the overlapping regime: the Stark components of any hydrogenic spectral line become overlapping. This is true even for the simplest hydrogenic line Lyman-alpha, as shown in detail, e.g., by Strekalov and Burshtein [4.18].

Chapter 5. Lorentz-Doppler Profiles of Hydrogen/Deuterium Spectral Lines for Magnetic Fusion: Analytical Solution for any Angle of Observation and any Magnetic Field Strength

5.1 Introduction

Strongly-magnetized plasmas are encountered both in astrophysics (e.g., in Sun spots, in the vicinity of white dwarfs etc.) and in laboratory plasmas (e.g., in magnetic fusion devices). In such plasmas, as hydrogen/deuterium atoms move across the magnetic field $\boldsymbol{B}$ with the velocity $\boldsymbol{v}$, they experience a Lorentz electric field $\boldsymbol{E}_L = \boldsymbol{v} \times \boldsymbol{B}/c$ in addition to other electric fields. The Lorenz field has a distribution because the atomic velocity **v** has a distribution. So, for radiating hydrogen/deuterium atoms this becomes an additional source of the *broadening* of spectral lines.

In paper [5.1] were described situations where the Lorentz broadening serves as the primary broadening mechanism of Highly-excited Hydrogen/deuterium Spectral Lines (HHSL). One example discussed in paper [5.1] was HHSL emitted from edge plasmas of tokamaks. In laboratory plasmas, HHSL are used for measuring the electron density at the edge plasmas of tokamaks (see, e.g., papers [5.2, 5.3] and Sect. 4.3 of review [5.4]) and in radiofrequency discharges (see, e.g., paper [5.5] and book [5.6]).

Another example discussed in paper [5.1] was HHSL emitted from the solar chromosphere. They are observed and used for measuring the electron density in the solar chromosphere (see, e.g., paper [5.7]).

One of the most interesting features of these situations is that the combination of Lorentz and Doppler broadenings cannot be taken into account simply as a convolution of these two broadening mechasnisms, as it was pointed out for the first time in paper [5.8]. The Lorentz and Doppler broadening intertwine in a more complicated way. Indeed, let us consider a Stark component of HHSL. Its Lorentz-Doppler profile in the frequency scale is proportional (in the

laboratory reference frame) to $\delta[\Delta\omega - (\omega_0 v/c)\cos\alpha - (kX_{\alpha\beta}Bv/c)\sin\theta]$, where in the argument of this δ-function the quantity α is the angle between the direction of observation and the atomic velocity $\boldsymbol{v}$, and ϑ is the angle between vectors $\boldsymbol{v}$ and $\boldsymbol{B}$.

In paper [5.1] was derived a general expression for the Lorentz-Doppler profiles of HHSL for the arbitrary strength of the magnetic field $\boldsymbol{B}$ and for the arbitrary angle of the observation ψ with respect to $\boldsymbol{B}$. However, more *specific* analytical results were obtained in paper [5.1] only for $\psi = 0$ and $\psi = 90°$. It was shown that a relatively strong magnetic field causes a significant *suppression of π-components* compared to σ-components for the observation at $\psi = 90°$, which was a counterintuitive result.[*/]

In the present paper we obtain *specific* analytical results for the Lorentz-Doppler profiles of HHSL for the arbitrary strength of the magnetic field $\boldsymbol{B}$ and for an *arbitrary angle of the observation* ψ. In particular, we show that the effect of the suppression of π-components at a relatively strong magnetic field rapidly diminishes as the angle of observation ψ decreases from 90 degrees.

[*/] We note in passing that in paper [5.1] there were minor typographic errors in Eqs. (31), and (32). In Equation (31), the factor in front of the integral should be $\pi^{-1}|2w|^{-½}$. In Equation (32), the factor in front of the last brackets should be $[\Gamma(1/4)\Gamma(-1/4)]^{-1}|w|^{-1/2}$. Also, in Figs. 9 and 10 from paper [5.1], the profiles of π-components were not to scale. The corrected Figs. 9 and 10 are presented in Appendix.

5.2 Analytical Results

For an arbitrary angle ψ between the direction of observation and the magnetic field, the relative configuration of the vectors $\boldsymbol{B}$, $\boldsymbol{E}_L$, and $\boldsymbol{v}$, as well as the choice of the reference frame is shown in Figure 5.1.

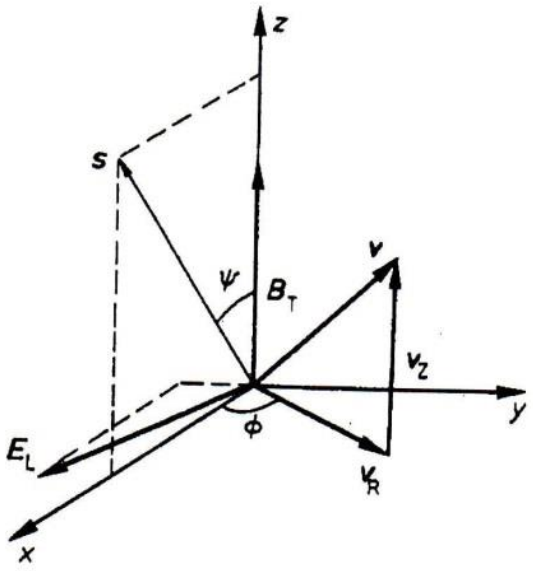

Figure 5.1. Relative configuration of the magnetic $\boldsymbol{B}$ and Lorentz $\boldsymbol{E}_L$ fields and of the direction of the observation **s** ("s" stands for "spectrometer"). The z axis is along $\boldsymbol{B}$. The direction of the observation **s** constitutes a non-zero angle ψ with **B**. The xz plane is spanned on vectors $\boldsymbol{B}$ and **s**. The atomic velocity $\boldsymbol{v}$ has a component v_z along **B** and a component $\mathbf{v}_R$ perpendicular to $\boldsymbol{B}$. The component $\boldsymbol{v}_R$ constitutes an angle φ with the x axis.

In paper [5.1] for obtaining universal analytical results the following dimensionless notations were introduced:

$$w = c\,\Delta\omega/v_T\omega_0 = c\,\Delta\lambda/v_T\lambda_0\,, \quad \mathbf{b} = kX_{\alpha\beta}\mathbf{B}/\omega_0\,, \quad \mathbf{u} = \mathbf{v}/v_T\,, \tag{1}$$

Here w is the scaled detuning from the unperturbed frequency ω_0 or from the unperturbed wavelength λ_0 of a hydrogen spectral line, **b** is the scaled magnetic field, and **u** is the atomic velocity scaled with respect to the atomic thermal velocity v_T. The quantities k and $X_{\alpha\beta}$ in Equation (1) are

$$k = 3\hbar/(2m_e e)\,, \quad X_{\alpha\beta} = n_\alpha(n_1 - n_2)_\alpha - n_\beta(n_1 - n_2)_\beta\,, \tag{2}$$

where n_1 , n_2 are the parabolic quantum numbers, and n is the principal quantum numbers of the upper (subscript α) and lower (subscript β) Stark sublevels involved in the radiative transition.

A general expression for the Lorentz-Doppler profiles of components of HHSL for the arbitrary strength of the magnetic field **B** and for the arbitrary angle of the observation ψ with respect **B** was derived in paper [5.1] in the form of the following triple integral

$$I(w, b, \psi)= \int_0^\infty du_z\, f_z(u_z) \int_0^\infty du_R f_R(u_R) \int_0^\pi (d\phi/\pi)\, g(\psi, \phi)\, \delta[w-u_z\cos\psi-u_R(b+\sin\psi\cos\phi)]\,, \tag{3}$$

where

$$f_z(u_z)=\frac{1}{\sqrt{\pi}} e^{-u_z^2},\ f_R(u_R)= 2\, u_R e^{-u_R^2},\ 0<\psi<\frac{\pi}{2}\,, \tag{4}$$

and $g(\psi, \phi)$ are factors which are different for π- and σ- components:

$$g_\pi(\psi)=1-\sin^2\psi\sin^2\phi\,,\ g_\sigma(\psi)=\frac{1}{2}(1+\sin^2\psi\sin^2\phi)\,. \tag{5}$$

We note that the functions $f_z(u_z)$ and $f_R(u_R)$ are, respectively the one-dimensional and the two-dimensional Maxwell distributions of the scaled atomic velocity $\mathbf{u} = \mathbf{v}/v_T$.

For the particular cases of $\psi = 0$ and $\psi = 90$ degrees, the triple integral from Equation (3) immediately reduces to double integrals (still having the δ-function in the integrand), as given by Eqs. (9) and (21) from paper [5.1], respectively. Then the properties of the δ-function were used for performing the angular integration in paper [5.1], leading to the specific analytical results $\psi = 0$ and $\psi = 90$ degrees in the form of a single integral.

In the present paper we consider the angle ψ to be arbitrary, so that we have to start from the triple integral given by Eq. (3). In distinction to paper [5.1], instead of using the δ-function in the integrand for performing the angular integration, we use it for integrating over u_z. The root of the argument of the delta function is given by:

$$u_z = \frac{w - u_r(b + \sin\psi\cos\phi)}{\cos\psi}. \tag{6}$$

Employing the properties of the δ-function, we get:

$$I(w, b, \psi) = \frac{2}{\pi^{\frac{3}{2}}\cos\psi}\int_0^\infty du_R u_R e^{-u_R^2}\int_0^\pi d\phi\, e^{-\frac{[w-u_R(b+\sin\psi\cos\phi)]^2}{\cos^2\psi}}\, g(\psi, \phi)$$

$$= \frac{2\, e^{-\frac{w^2}{\cos^2\psi}}}{\pi^{\frac{3}{2}}\cos\psi}\int_0^\infty du_R u_R e^{-u_R^2}\int_0^\pi d\phi\, e^{-\frac{u_R^2(b+\sin\psi\cos\phi)^2 - 2\,w\,u_R\,(b+\sin\psi\cos\phi)}{\cos^2\psi}}\, g(\psi, \phi) \tag{7}$$

$$= \frac{2\, e^{-\frac{w^2}{\cos^2\psi}}}{\pi^{\frac{3}{2}}\cos\psi}\int_0^\pi d\phi\int_0^\infty du_R u_R e^{-u_R^2\left[1+\frac{(b+\sin\psi\cos\phi)^2}{\cos^2\psi}\right]+2\,w\,u_R\,\frac{b+\sin\psi\cos\phi}{\cos^2\psi}}\, g(\psi, \phi)\,.$$

Then we perform the integration over u_R to obtain:

$$I(w, b, \psi)=\frac{e^{-\frac{w^2}{\cos^2\psi}}}{\pi^{\frac{3}{2}}\cos\psi}\int_0^{\pi}\frac{g(\psi,\phi)}{[a(b,\psi,\phi)]^{\frac{3}{2}}}\left\{\sqrt{a(b,\psi,\phi)}+\sqrt{\pi}\,c(w,b,\psi,\phi)\,e^{\frac{c(w,b,\psi,\phi)^2}{a(b,\psi,\phi)}}\left[1+\mathrm{Erf}\frac{c(w,b,\psi,\phi)}{\sqrt{a(b,\psi,\phi)}}\right]\right\}d\phi \quad (8)$$

where

$$a(b,\psi,\phi)=1+\frac{(b+\sin\psi\cos\phi)^2}{\cos^2\psi}\ ,\ \ c(w,b,\psi,\phi)=w\frac{b+\sin\psi\cos\phi}{\cos^2\psi}\ . \quad (9)$$

Thus, even for the general case of an arbitrary angle of the observation ψ, we managed to perform analytically two integrations and to reduce the result to just a single integral.

Figures 5.2–6 present Lorentz-Doppler profiles of π-components of HHSL calculated by equations (8), (9). Each figure shows profiles for five values of the angle ψ (in degrees): 0, 20, 45, 70, and 90. We note that, for example, 20 degrees is the actual angle of observation for the spectroscopic diagnostics at the tokamak EAST in China (other tokamaks around the world have different angles of observation). Figures 5.2-6 differ from each other by the value of the scaled magnetic field b (defined in Eq. (1)): b = 0.2, 0.5, 1, 2, and 5.

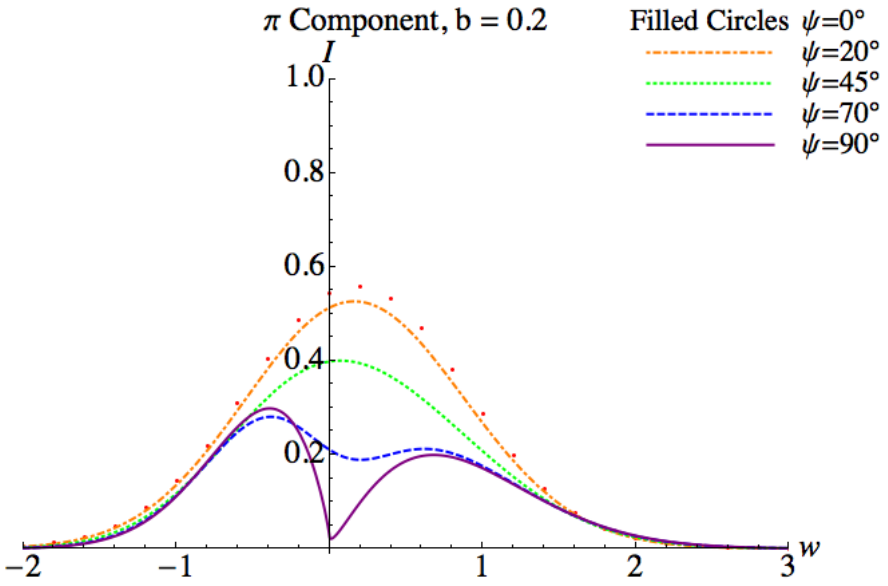

Figure 5.2. Lorentz-Doppler profiles of π-components of highly-excited hydrogen/deuterium spectral lines calculated by equations (8), (9), for the scaled magnetic field b = 0.2 (defined in equation (1)) at five different values of the angle of observation ψ with respect to the magnetic field.

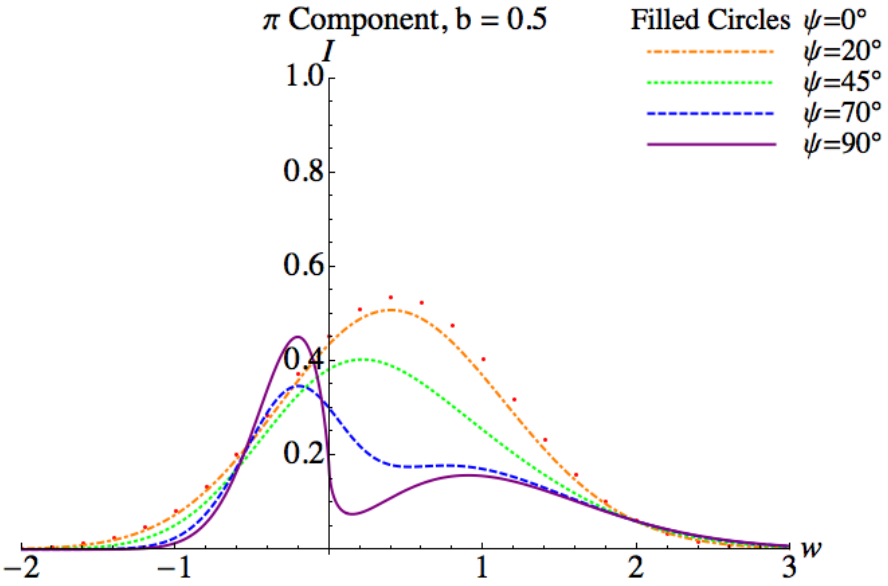

Figure 5.3. Same as in Fig. 2, but for b = 0.5.

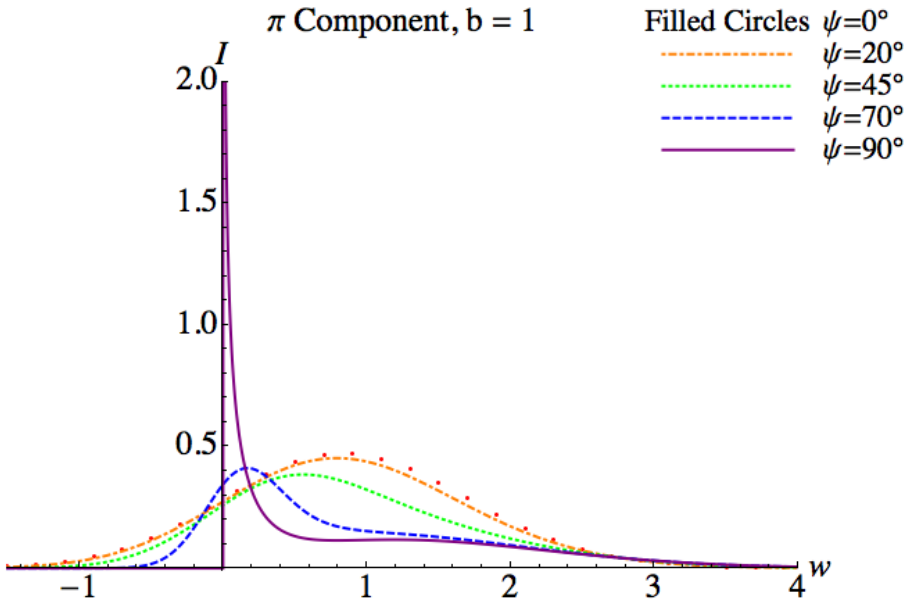

Figure 5.4. Same as in Figure 5.2, but for b = 1.

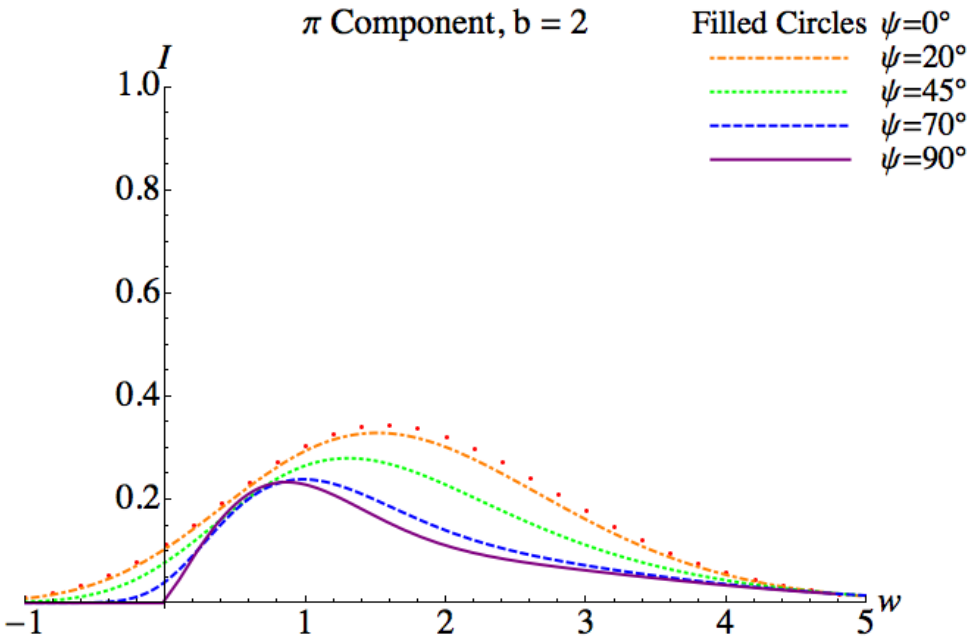

Figure 5.5. Same as in Figure 5.2, but for b = 2.

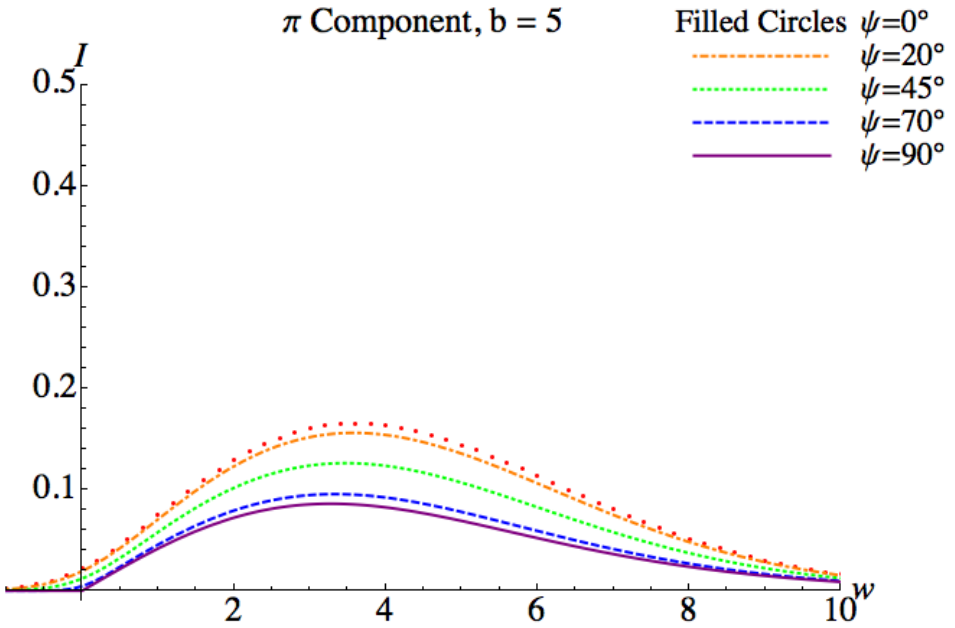

Figure 5.6. Same as in Figure 5.2, but for b = 5.

Figures 5.7–11 present the analogous set of Lorentz-Doppler profiles, but for σ-components of HHSL.

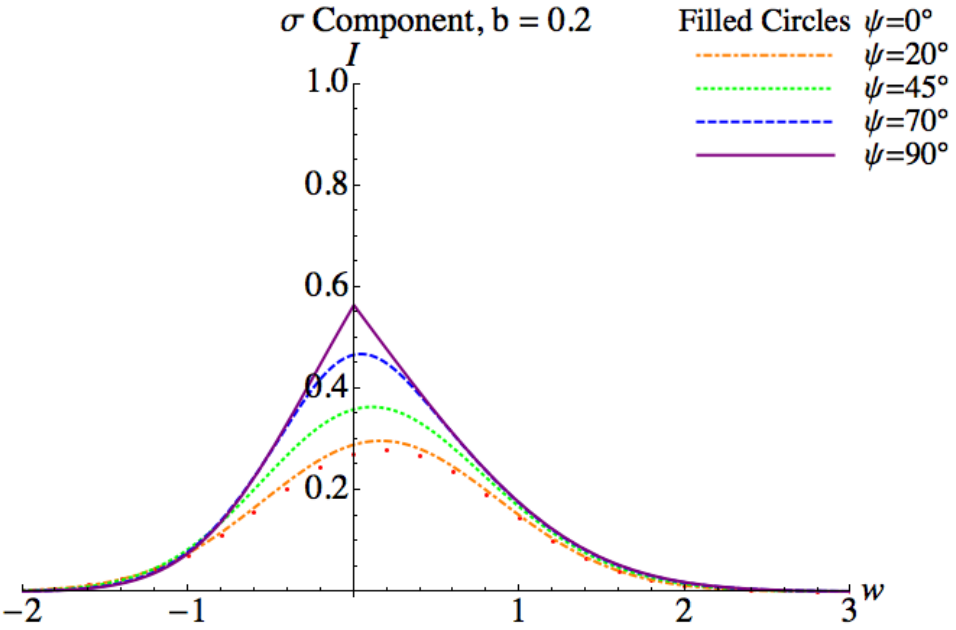

Figure 5.7. Lorentz-Doppler profiles of σ-components of highly-excited hydrogen/deuterium spectral lines calculated by equations (8), (9), for the scaled magnetic field b = 0.2 (defined in equation (1)) at five different values of the angle of observation ψ with respect to the magnetic field.

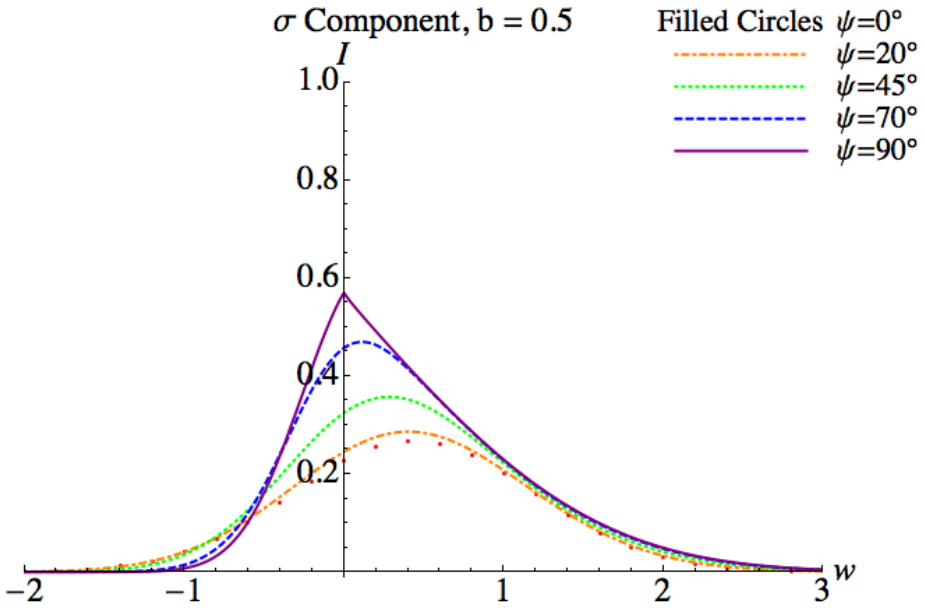

Figure 5.8. Same as in Figure 5.7, but for b = 0.5.

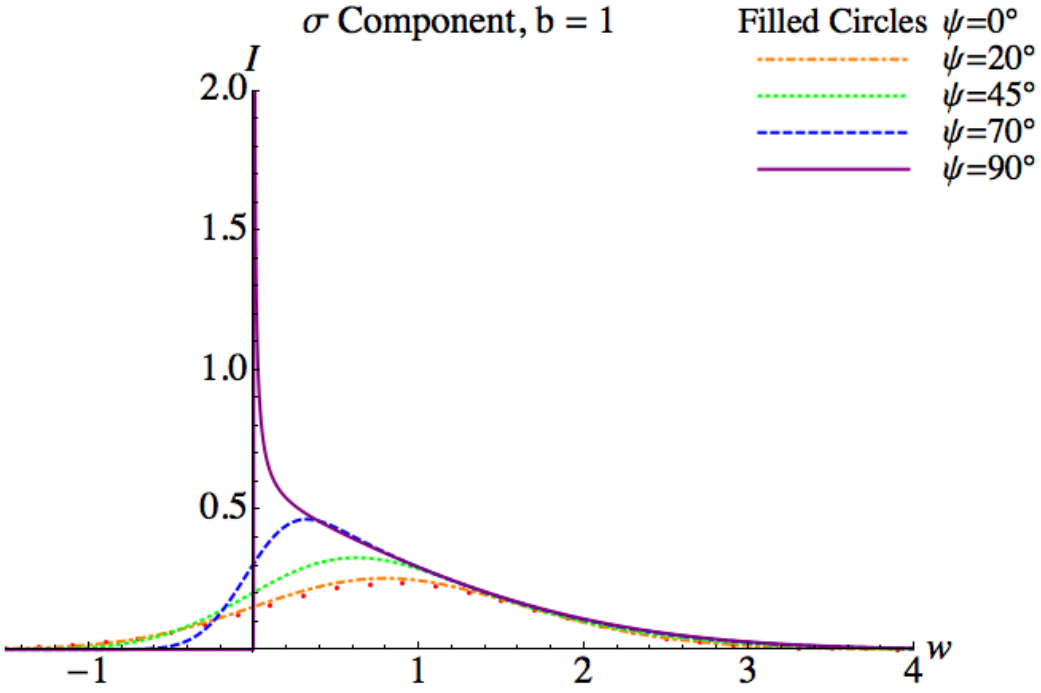

Figure 5.9. Same as in Figure 5.7, but for b = 1.

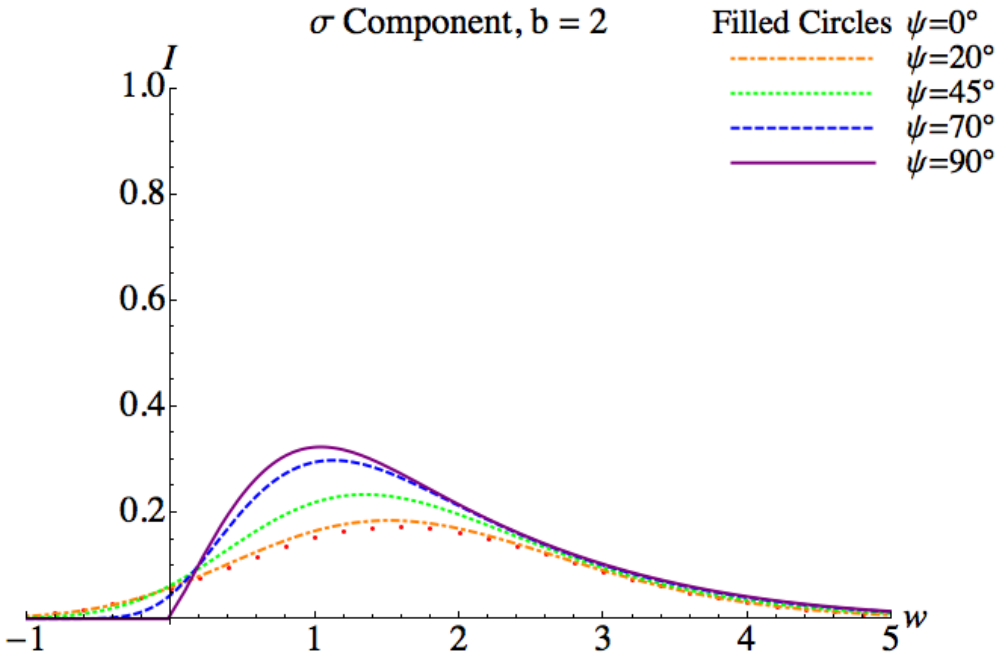

Figure 5.10. Same as in Figure 5.7, but for b = 2.

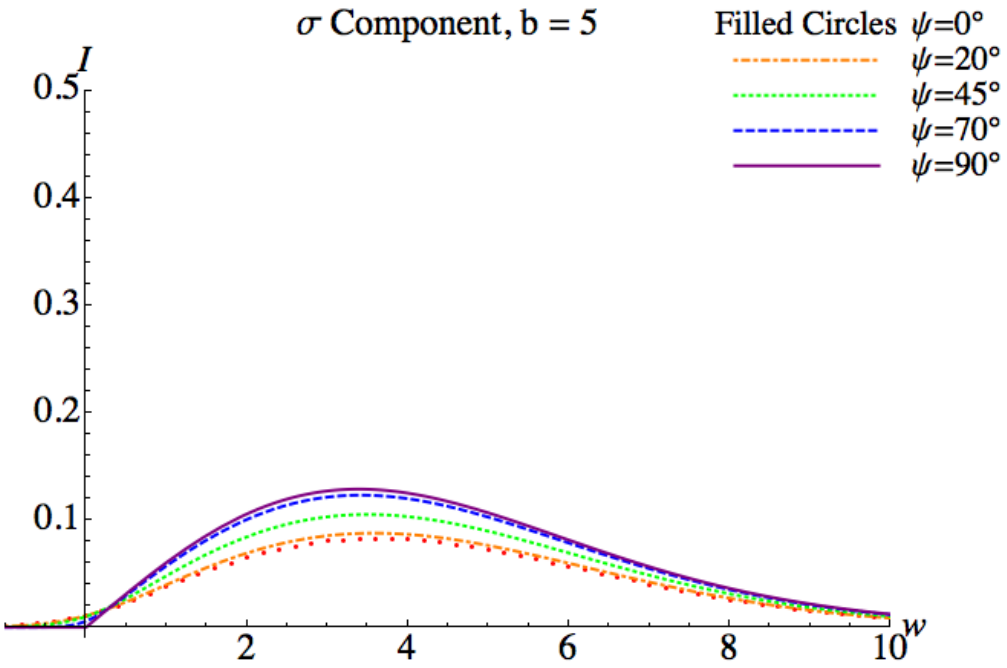

Figure 5.11. Same as in Figure 5.5, but for b = 5.

One of the purposes of the present study was to see the evolution of the effect of the suppression of the π- components (compared to the σ-components) as the angle of the observation ψ decreases from 90 degrees, i.e., as ψ decreases from the value, at which this effect was discovered in paper [5.1]. By comparing Fig. 4 and Fig. 7 (both of which correspond to b = 5, i.e., to the relatively strong magnetic field) we can deduce the following. As ψ decrease from 90 to 70 degrees, the effect of suppression, while diminishing, is still present. However, already at ψ = 45 degrees, the effect of the suppression is absent. Thus, we arrive to the conclusion that the suppression of the π- components (compared to the σ-components) occurs at the perpendicular or close to the perpendicular direction of observation (with respect to the magnetic field **B**), but disappears at lower values of the angle of the observation.

Another interesting result is the following. The width of the Lorentz-Doppler profiles is a non-monotonic function of the scaled magnetic field b for observations perpendicular to **B**. As |b| increases from zero, the width first decreases, then reaches a minimum at |b| = 1 (i.e., when the shift in the Lorentz field is equal to the Doppler shift), and then increases – as presented in Fig. 12 using the Ly-beta line as an example. This is a counterintuitive result.

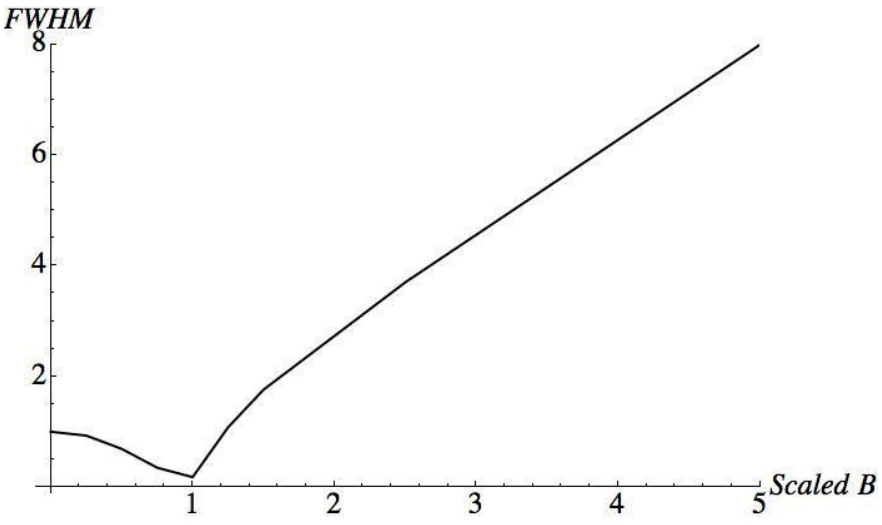

Figure 5.12. The Full Width at Half Maximum (FWHM) of the hydrogen/deuterium Ly-beta line observed perpendicular to the magnetic field **B** with a polarizer along **B**. The scaled magnetic field is the ratio of the Lorentz-field shift to the Doppler shift. The FWHM is in units of the Doppler half width at half maximum. The narrowing effect is the most pronounced when the Lorentz-field shift is equal to the Doppler shift.

The decreasing part of the FWHM dependence on the magnetic field corresponds to relatively small magnetic fields: $|b| < 1$. In this range of $|b|$, the line profile has the bell shape. In this range of $|b|$, the complicated entanglement of the Doppler and Lorentz-filed mechanisms (that cannot be described as their convolution) causes the FWHM to decrease as $|b|$ increases. This narrowing effect has a limited analogy with the well-known Dicke narrowing. Namely, in the Dicke case, the correlations between the Doppler mechanism and collisions cause the narrowing, while in our case the correlations (the complicated entanglement) between the Doppler mechanism and Lorentz-field mechanisms cause the narrowing. At relatively large magnetic fields, where $|b| > 1$, the line profile has the two-peak shape (one in the red part of the symmetric profile, another in the blue part of the symmetric profile). In this range of $|b|$, the Lorentz-field mechanism dominates over the Doppler mechanism. Therefore, as $|b|$ increases in this range, the two peaks of the profile move further apart and the FWHM increases.

5.3 Conclusions

We studied the evolution of the effect of the suppression of the π-components (compared to the σ-components) as the angle of the observation ψ decreases from 90 degrees, i.e., as ψ decreases from the value, at which this effect was discovered in paper [5.1]. We found that the suppression of the π- components (compared to the σ-components) occurs at the perpendicular or close to the perpendicular direction of observation (with respect to the magnetic field **B**), but rapidly disappears at lower values of the angle of the observation.

We also found that the width of the Lorentz-Doppler profiles is a non-monotonic function of the magnetic field for observations perpendicular to **B**. This is a counterintuitive result.

The results of the present paper should be important, e.g., for spectroscopic diagnostics of edge plasmas of various magnetic fusion devices around the world – see, e.g., review [5.9] and references therein.

Chapter 6. Stark Broadening of Hydrogen/Deuterium Spectral Lines by a Relativistic Electron Beam: Analytical Results and Applications to Magnetic Fusion

6.1 Introduction

The interaction of a Relativistic Electron Beam (REB) with plasmas has both the fundamental importance for understanding physics of plasmas and practical applications. The latter include (but not limited to) plasma heating, inertial fusion, generation of high-intensity coherent microwave radiation, acceleration of charged particles in plasmas – see, e.g., papers [6.1-3] and references therein.

The latest (though negative) application relates to magnetic fusion and deals with runaway electrons. In some discharges in tokamaks, the plasma current decays and is partly replaced by runaway electrons that reach relativistic energies: this poses danger to the mission of the next generation tokamak ITER – see, e.g., papers [6.4-6] and references therein.

Therefore developing diagnostics of a REB and its interaction with plasmas should be important. In the particular case of tokamaks, the development of a REB should be timely detected to allow the mitigation of the problem.

Diagnostics based on the analysis of spectral line shapes have known advantages over others. They are not intrusive and allow measuring plasma parameters and parameters of various fields in plasmas without perturbing the parameters to be measured – see, e.g., books [6.7-14].

In the current paper we present a theory of the Stark broadening of hydrogen/deuterium spectral lines by a REB. The theory is developed analytically by using an advanced formalism. We discuss the application of these analytical results to magnetic fusion, taking into account also the major outcome of the interaction of a REB with plasmas: the development of strong Langmuir waves.

6.2 Analytical results and applications to magnetic fusion

The presence of a REB introduces anisotropy in the process of the Stark broadening of spectral lines in plasmas. A different kind of anisotropic Stark broadening was first considered by Seidel in 1979 [6.15] for the following situation. If hydrogen atoms radiate from a plasma consisting mostly of much heavier ions, then in the reference frame moving with the velocity v of the radiating hydrogen atom, the latter "perceives" a beam of the much heavier ions moving with the velocity v. Seidel [6.15] treated this situation by applying the so-called standard (or conventional) theory of the impact broadening of hydrogen lines, also known as Griem's theory [6.16]. Therefore, while Seidel [6.15] should be given credit for pioneering the anisotropic Stark broadening, his specific calculations had a weakness that plagues the standard theory: the inherent divergence at small impact parameters causing the need for a cutoff defined only by an order of magnitude.

Later in paper [6.17] the authors considered the same situation as Seidel [6.15], but applied a more advanced theory of the Stark broadening called the generalized theory developed in paper [6.18] and presented also in book [6.9]. (It should be emphasized that in paper [6.17] it was the application of the "core" generalized theory from paper [6.18] without the additional effects that were introduced later and were the subject of discussions in the literature.) The authors of paper [6.17] took into the exact account (in all the orders of the Dyson expansion) the projection of the dynamic, heavy-ion-produced electric field onto the velocity of the radiator exactly. As a result, there was no divergence at small impact parameters and thus no need for the imprecise cutoff.

In the present paper we use the formalism from paper [6.17] to treat the Stark broadening of hydrogen/deuterium spectral lines by a REB in plasmas. There are two major distinctions from

paper [6.17]: 1) the broadening is by a beam of electrons rather than ions; 2) the electrons are relativistic.

Following paper [6.17] we choose the z-axis in the direction of the REB and represent the Hamiltonian H(t) perturbed by the field E(t) of the REB in the form:

$$H(t) = H_1(t) + V(t)\,, H_1(t) = H_o - d_z E_z(t), V(t) = -d_x E_x - d_y E_y\,. \tag{1}$$

The partial time-dependent Hamiltonian H1(t) is diagonalized here in the parabolic quantization and is allowed for exactly. The residual interaction V(t) is taken into account via the Dyson perturbation expansion.

The starting expression for the lineshape I(ω,v) depends on the velocity v of the REB:

$$I(\omega, v) = -\frac{1}{\pi} Re \sum_{\sigma} \sum_{\alpha\alpha'\beta\beta'} \langle\beta|d_\sigma|\alpha\rangle\langle\alpha'|d_\sigma|\beta'\rangle\langle\langle\alpha\beta|G^{-1}|\alpha'\beta'\rangle\rangle\ . \tag{2}$$

Here, α, α' and β, β' label the Stark sublevels of the upper (a) and lower (b) states involved in the radiative transition; d_σ are components of the dipole moment operator; the spectral operator G is

$$G = i\,\Delta\omega + \Phi_{ab}(v) \tag{3}$$

where the impact operator $\Phi_{ab}(v)$ is

$$\Phi_{ab} = N_b v \int_0^\infty 2\,\pi\rho\; d\rho\; \{S_a S_b{}^* - 1\}_{\vec{p}}\ . \tag{4}$$

Here N_b is the electron density of the REB.

The operator $\Phi_{\mathrm{ab}}(\mathrm{v})$ is subdivided into adiabatic $\Phi^{ad}{}_{\mathrm{ab}}(\mathrm{v})$ and non-adiabatic $\Phi^{na}{}_{\mathrm{ab}}(\mathrm{v})$ contributions

$$\Phi_{ab} = \Phi^{ad}{}_{ab}(v) + \Phi^{na}{}_{ab}(v)\ , \tag{5}$$

where $\Phi^{ad}{}_{\mathrm{ab}}(\mathrm{v})$ contains only the following combination of the diagonal matrix elements of the dipole moment operator: $e^2\left(z_{\alpha\alpha} - z_{\beta\beta}\right)^2$. An important feature of the impact Stark broadening by a beam of ions or electrons is that the adiabatic part $\Phi^{ad}{}_{\mathrm{ab}}(\mathrm{v})$ vanishes - in distinction to the impact Stark broadening by randomly moving thermal ions or electrons [6.17].

The scattering matrix S entering Eq. (4) is represented in the form:

$$S = exp\left[\frac{i}{\hbar}\int_{-\infty}^{\infty} dt\; d_z E_z(t)\right]\hat{T}\; exp\left[\frac{i}{\hbar}\int_{-\infty}^{\infty} dt\; Q^*\left(d_x E_x + d_y E_y\right)Q\right],$$
$$Q = \exp\left[-\frac{\mathrm{i}}{\hbar}\left(H_o t - \int_{-\infty}^{t} dt'\; d_z E_z(t')\right)\right]. \tag{6}$$

For Lyman lines the scattering matrix S_b = 1, which simplifies calculations. Then in the second order of the modified Dyson expansion (6), the matrix elements of the nonadiabatic part of the operator $\Phi_{ab}(v)$ are:

$$\Phi_{\alpha\alpha'} = -4\,\pi\,N_b\,\frac{\mathrm{e}^2}{\hbar^2 v}\sum_{\alpha''} d^x_{\alpha\alpha''}\,d^x_{\alpha''\alpha'}\int_0^\infty C_{\pm}(Z)\,\frac{dZ}{Z}\,. \tag{7}$$

Here

$$Z = \frac{2\,m_e v\,\rho}{3\,n\,\hbar}\,, \tag{8}$$

where n is the principal quantum number of the upper level and ρ is the impact parameter. So, physically the quantity Z is the scaled, dimensionless impact parameter and the integration over Z in Eq. (7) corresponds to the integration over impact parameters.

If the electron beam would be a non-relativistic, so that the electric field produced by the beam electron at the location of the radiating atom would be

$$\boldsymbol{E}(t) = e\,\frac{\boldsymbol{r}(t)}{r^3(t)}\,, \tag{9}$$

where **r**(t) is the radius vector from the beam electron to the radiating atom, then the broadening functions C_+ and C_- entering Eq. (7) for non-diagonal and for diagonal matrix elements, respectively, would be the following double integrals:

$$C_{\pm}(Z) = \frac{1}{2}\int_{-\infty}^{\infty}\int_{-\infty}^{x_1} \frac{dx_1 dx_2}{[g(x_1)g(x_2)]^3} \exp\left[\frac{i}{Z}\left(\frac{1}{g(x_1)} \pm \frac{1}{g(x_2)}\right)\right], \qquad (10)$$

$$g(x) \equiv \sqrt{1+x^2}\,.$$

However, for the REB, Eq. (9) has to be modified to (see, e.g., Eq. (38.8) from book [6.19]):

$$\boldsymbol{E}(t) = e\,\boldsymbol{r}(t)\left[r^3(t)\gamma^2\left(\cos^2\theta + \frac{\sin^2\theta}{\gamma^2}\right)^{\frac{3}{2}}\right]^{-1}. \qquad (11)$$

Here

$$\gamma = \left(1 - \frac{v^2}{c^2}\right)^{-\frac{1}{2}} \qquad (12)$$

is the relativistic factor and θ(t) is the angle between the beam velocity v and vector r(t), so that

$$\cos^2\theta = \frac{v^2t^2}{\rho^2 + v^2t^2}\,, \qquad \sin^2\theta = \frac{\rho^2}{\rho^2 + v^2t^2}\,, \qquad (13)$$

the instant t = 0 corresponding to the closest approach of the beam electron to the radiating atom.

The relativistic counterparts C_{r+} and C_{r-} of the broadening functions C_+ and C_- become as follows:

$$C_{\pm}(Z) = \frac{1}{2\,\gamma^4} \int\limits_{-\infty}^{\infty} \int\limits_{-\infty}^{x_1} \frac{dx_1 dx_2}{[g(x_1)g(x_2)]^3} \exp\left[\frac{i}{Z}\left(\frac{1}{g(x_1)} \pm \frac{1}{g(x_2)}\right)\right], \qquad (14)$$

$$g(x) \equiv \sqrt{1/\gamma^2 + x^2}\,.$$

For the real parts $A_{r\pm}$ = Re $C_{r\pm}$, the double integral in Eq. (14) can be calculated analytically. It yields:

$$A_{r-} = \left(\frac{\pi}{2}\right)^2 \left[\boldsymbol{H}_{-1}\left(\frac{1}{s}\right) + J_1\left(\frac{1}{s}\right)\right], \qquad A_{r+} = \left(\frac{\pi}{2}\right)^2 \left[\boldsymbol{H}_{-1}\left(\frac{1}{s}\right) - J_1\left(\frac{1}{s}\right)\right], \qquad s = \frac{Z}{\gamma}, \qquad (15)$$

where $\boldsymbol{H}_{-1}\left(\frac{1}{s}\right)$ and $J_1\left(\frac{1}{s}\right)$ are Struve and Bessel functions, respectively. Below we omit the suffix "r" for brevity.

The width of spectral line components is controlled by the subsequent integral over the scaled impact parameter Z:

$$a_{\pm} = \int\limits_0^{Z_{max}} A_{\pm}(Z)\frac{dZ}{Z} = \int\limits_0^{Z_{max}/\gamma} A_{\pm}(s)\frac{ds}{s}\,, \qquad s = \frac{Z}{\gamma}. \qquad (16)$$

Figure 1 shows the plot of the integrand $A_{-}(s)/s$ versus s. It is seen that the corresponding integral a_{-} does not diverge at small impact parameters.

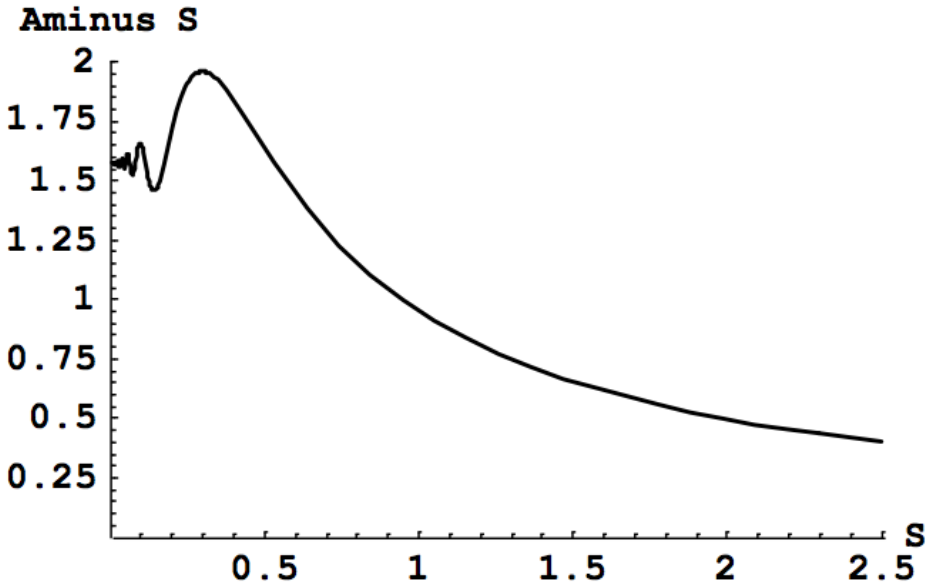

Figure 6.1. The integrand A–(s)/s, corresponding to the widths function a– , versus s = Z/γ, where Z is the scaled impact parameter defined by Eq. (8) and γ is the relativistic factor defined by Eq. (12).

Figure 6.2 presents the plot of the integrand $A_{-}(s)/s$ versus s and Figure 6.3 shows a magnified part of this plot at small impact parameters. It is seen that the corresponding integral a- also does not diverge at small impact parameters.

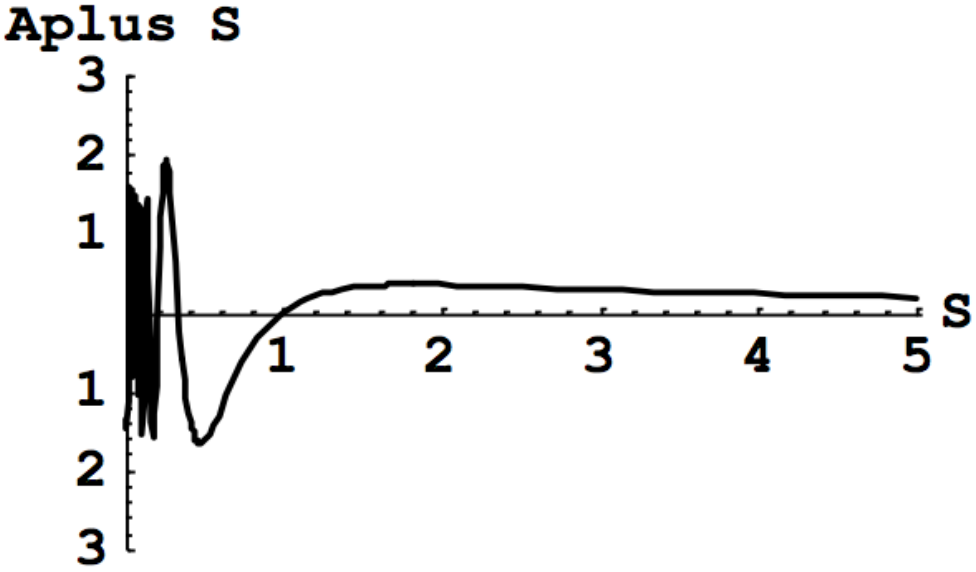

Figure 6.2. The integrand A+(s)/s, corresponding to the widths function a+ , versus s = Z/γ, where Z is the scaled impact parameter defined by Eq. (8) and γ is the relativistic factor defined by Eq. (12).

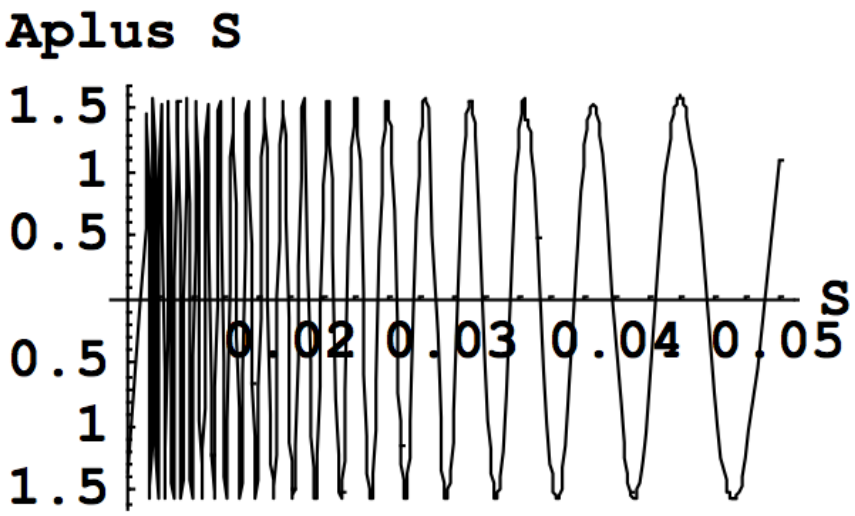

Figure 6.3. Same as in Figure 6.2, but for small impact parameters.

Thus, the integrals over the scale impact parameter Z in Eq. (16) converge at small impact parameters – in distinction to what would have resulted from the standard theory. At large Z the integral diverges (just as what would have resulted from the standard theory), which is physically because of the long-range nature of the Coulomb interaction between the charged particles. However, due to the Debye screening in plasmas, there is a natural upper cutoff Z_{max} :

$$Z_{max} = u\, Z_0\,, \qquad u = \frac{v}{c} = \left(1 - \frac{1}{\gamma^2}\right)^{\frac{1}{2}}, \qquad Z_0 = \frac{2\, m_e c\, \rho_D}{3\, n\, \hbar}\,. \tag{17}$$

Here

$$\rho_D = \left(\frac{T_e}{4\,\pi e^2 N_e}\right)^{\frac{1}{2}} \tag{18}$$

is the Debye radius; T_e and N_e are the temperature and the density of bulk electrons, respectively.

The integration in Eq. (16) can be performed analytically because the integrals in Eq. (16) have the following antiderivatives

$$j_{\pm}(s) = \int A_{\pm}(s)\frac{ds}{s}$$

$$= \frac{\pi^2}{8}\left\{\frac{2}{\pi}\text{MeijerG}\left[\{\{0\},\{1\}\},\left\{\{0,0\},\left\{-\frac{1}{2},\frac{1}{2}\right\}\right\},\frac{1}{4\,s^2}\right] + \boldsymbol{H}_{-1}{}^2\left(\frac{1}{s}\right)\right. \tag{19}$$

$$\left. + \boldsymbol{H}_0{}^2\left(\frac{1}{s}\right) \pm \left[1 - {}_1F_2\left(\frac{1}{2};1,2;-\frac{1}{s^2}\right)\right]\right\},$$

where MeijerG[...] and ${}_1F_2(...)$ are the MeijerG function and the generalized hypergeometric function, respectively. Thus, we obtain analytical results for the width functions:

$$a_{\pm} = j_{\pm}\left(\frac{Z_{max}}{\gamma}\right) - j_{\pm}(0)\,. \tag{20}$$

Below, as an example, we calculate explicitly the shape I(Δω,γ) of the spectral line Ly-alpha broadened by a REB, where Δω is the detuning from the unperturbed frequency of the spectral line. Similarly to paper [6.17], after inverting of the spectral operator, we obtain:

$$I(\Delta\omega,\gamma) = \frac{1}{3\pi}\left(\frac{\Gamma_\pi}{\Delta\omega^2 + \Gamma_\pi{}^2} + \frac{2\,\Gamma_\sigma}{\Delta\omega^2 + \Gamma_\sigma{}^2}\right), \tag{21}$$

where Γ_π and Γ_σ are the half-widths at half-maximum of the π- and σ-components of the Ly-alpha line, respectively. They are expressed as follows:

$$\Gamma_\sigma = \left[\eta_0 \left(1 - \frac{1}{\gamma^2}\right)^{-\frac{1}{2}}\right] \left[j_- \left(\frac{Z_{max}}{\gamma}\right) - j_-(0)\right], \tag{22}$$

$$\Gamma_\pi = \left[\eta_0 \left(1 - \frac{1}{\gamma^2}\right)^{-\frac{1}{2}}\right] \int_0^\infty [A_-(s) - A_+(s)] \, \frac{ds}{s} \, , \tag{23}$$

where

$$\eta_0 = \frac{4\,\pi\,\hbar^2 N_e}{{m_e}^2 c} = 5.618 \times 10^{-10}\, N_e(cm^{-3})\, s^{-1} \, . \tag{24}$$

It is worth noting that in equation (23), the upper limit of the integration is infinity. This is because for the π-component of the Ly-alpha line the width in equation (23) is proportional to the difference of diagonal and non-diagonal matrix elements of the broadening operator, so that the corresponding integral converges not only at small, but also at large impact parameters, yielding the following relatively simple expression for the width:

$$\Gamma_\pi = \frac{\pi^2 \eta_0}{4\left(1 - \frac{1}{\gamma^2}\right)^{\frac{1}{2}}} . \tag{25}$$

Figure 6.4 shows the plot of the scaled width of the σ-component Γ_σ/η_0 (upper curve) and of the scaled width of the π-component Γ_π/η_0 (lower curve) of the Ly-alpha line broadened by a REB versus the relativistic factor γ at $N_e = 10^{15}(cm^{-3})$ and $T_e = 2\ eV$. It is seen that as γ increases from unity, both widths significantly decrease.

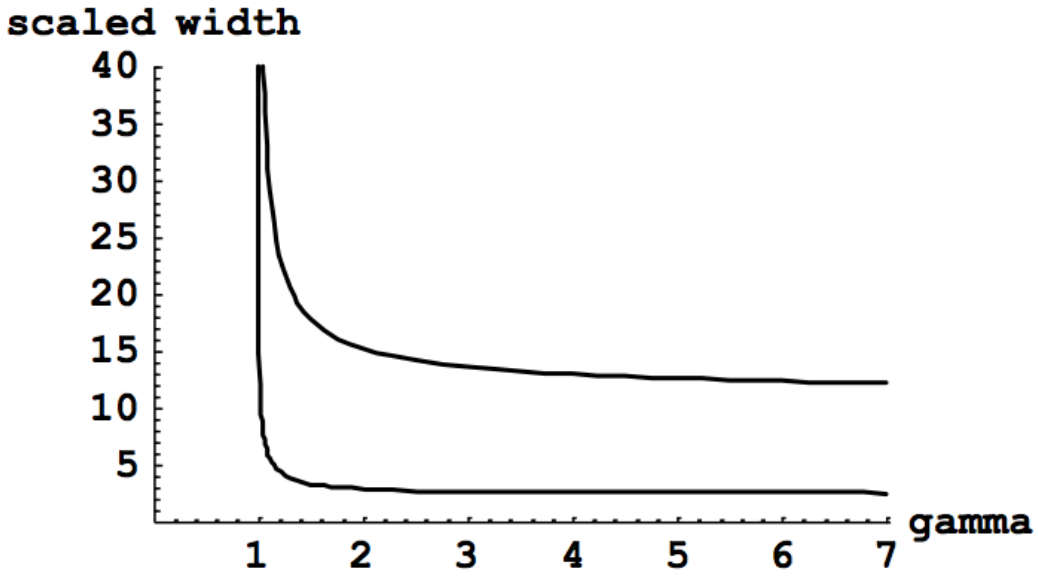

Figure 6.4. The scaled width of the σ-component Γ_σ/η_0 (upper curve) and the scaled width of the π-component Γ_π/η_0 (lower curve) of the Ly-alpha line broadened by a REB versus the relativistic factor γ at $N_e = 10^{15}(cm^{-3})$ and $T_e = 2\ eV$.

Figure 6.5 presents the ratio Γ_σ/Γ_π versus the relativistic factor γ at $N_e = 10^{15}(cm^{-3})$ and $T_e = 2\ eV$. It is seen that as γ increases from unity, this ratio increases, then reaches the maximum, and then decreases. The maximum ratio Γ_σ/Γ_π = 5.39 corresponds to γ = 21/2.

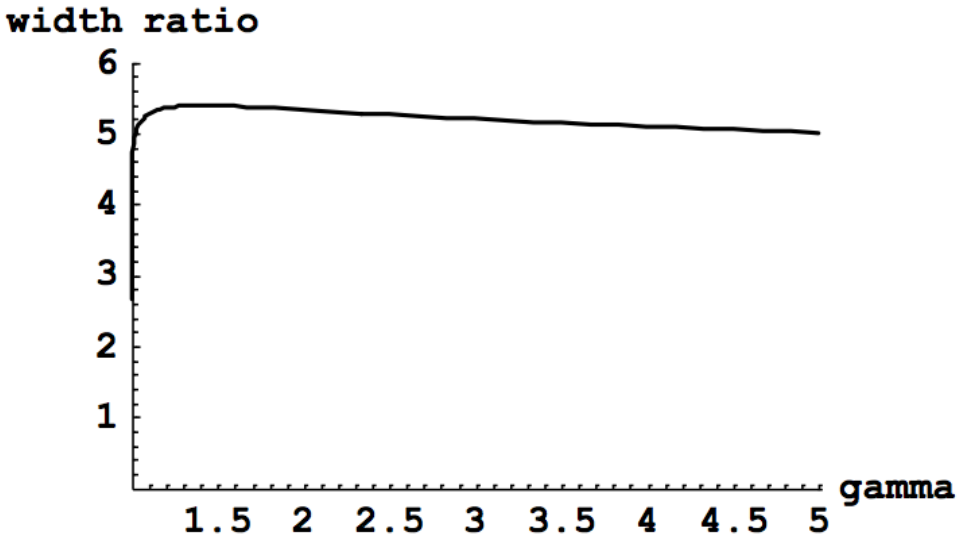

Figure 6.5 Ratio Γ_σ/Γ_π of the widths of the σ- and π-components of the Ly-alpha line versus the relativistic factor γ at $N_e = 10^{15}(cm^{-3})$ and $T_e = 2\ eV$.

Separate measurements of the widths of the σ- and π-components (and thus of the ratio Γ_σ/Γ_π) can be performed for the observation perpendicular to the REB velocity by placing a polarizer into the optical system: when the axis of the polarizer would be perpendicular or parallel to the REB velocity, then one would be able to measure Γ_σ or Γ_π, respectively. By monitoring the dynamics of the ratio Γ_σ/Γ_π, it would be possible, at least in principle, to detect the development of a REB in tokamaks and to engage the mitigation of the problem.

Figure 6.6 shows the theoretical profiles of the entire Ly-alpha line, corresponding to the observation perpendicular to the REB velocity without the polarizer, at $N_e = 10^{15}(cm^{-3})$ and $T_e = 2\ eV$. The profiles were calculated using Eqs. (21) – (24) and presented versus the scaled detuning $\Delta\omega/\Gamma_\pi$ denoted as d. Due to the scaled detuning, the profiles are "universal" in the sense that they are independent of the beam electron density. The solid curve corresponds to $\gamma = 2^{1/2}$, while the dashed curve – to $\gamma = 1$. In the case of $\gamma = 2^{1/2}$, the profile is by 12% narrower than for the case of $\gamma = 1$. Detecting the development of a REB via such relatively small decrease of the width seems to be less advantageous compared to the polarization analysis of the width discussed above, where the widths ratio Γ_σ/Γ_π could increase by an order of magnitude as a REB develops in the plasma.

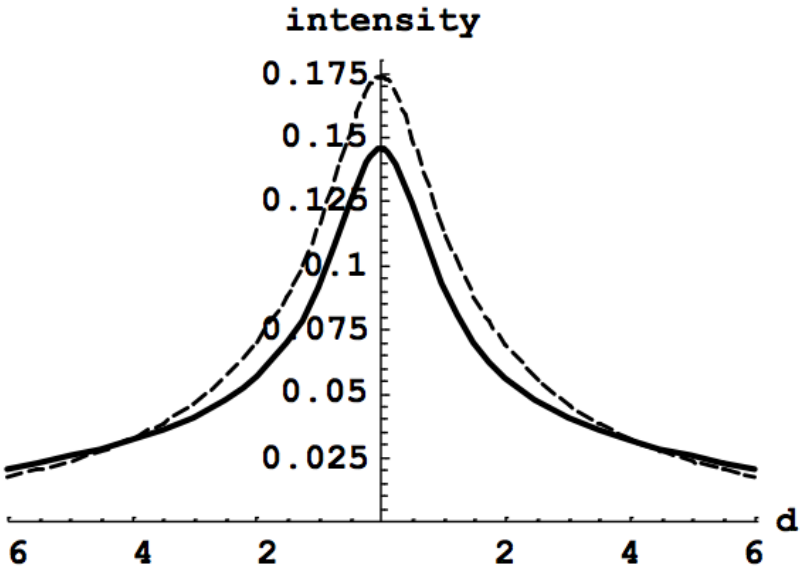

Figure 6.6. Theoretical profiles of the entire Ly-alpha line, corresponding to the observation perpendicular to the REB velocity without the polarizer, at $N_e = 10^{15}(cm^{-3})$ and $T_e = 2\ eV$. The profiles were calculated using Eqs. (21) – (24) and presented versus the scaled detuning $\Delta\omega/\Gamma\pi$ denoted as d. The solid curve corresponds to $\gamma = 2^{1/2}$, while the dashed curve – to $\gamma = 1$.

The above theoretical results represented the Stark broadening of hydrogen/deuterium spectral lines only by a REB without allowing for other factors affecting the lineshapes. This was done for presenting the effect of a REB on the lineshape in the "purest" form. Below we remove this restriction.

The major outcome of the interaction of a REB with plasmas is the development of strong Langmuir waves – see, e.g., book [6.20]. The maximum amplitude E_0 of the Langmuir wave electric field is [6.20]:

$$E_0 = \left[8\,\pi m_e c^2 \gamma^2 N_b^{\frac{4}{3}} / N_e^{\frac{1}{2}}\right]^{\frac{1}{2}}, \qquad \gamma N_b^{\frac{1}{3}} / N_e^{\frac{1}{3}} \ll 1\,. \tag{26}$$

For the case of $N_e = 10^{15}(cm^{-3})$, $N_b = 6\ \times 10^9\ (cm^{-3})$, and $\gamma = 2^{\frac{1}{2}}$, corresponding to an early stage of the development of a REB in tokamaks, Eq. (26) yields $E_0 = 20\ kV/cm$.

The primary manifestation of Langmuir waves in the profiles of hydrogen/deuterium or hydrogenlike spectral lines is the appearance of some local structures (called L-dips) at certain locations of the spectral line profile. This phenomenon arises when radiating atoms/ions are subjected simultaneously to a quasistatic field **F** and to a quasimonochromatic electric field **E**(t) at the characteristic frequency ω, where E < F. In the heart of this phenomenon is the dynamic resonance between the Stark splitting of hydrogenic spectral lines and the frequency ω or its harmonics. There is a rich physics behind the L-dip phenomenon: even when the applied electric field is monochromatic, there occurs a nonlinear dynamic resonance of multifrequency nature involving all harmonics of the applied field – as it was explained in detail in paper [6.21]. Further details on the theory of the ISS can be found in book [6.14].

As for the experimental studies of the L-dips, book [6.14] and later reviews [6.22-24] summarize all such studies with applications to plasma diagnostics. The practical significance of studies of the L-dips is threefold. First, they provide the most accurate passive spectroscopic method for measuring the electron density N_e in plasmas, e.g., more accurate than the measurement from the line broadening. This passive spectroscopic method for measuring N_e does not differ in its high accuracy from the active spectroscopic method – more complicated experimentally – using the Thompson scattering [6.25]. Second, they provide the only one non-perturbative method for measuring the amplitude of Langmuir waves in plasmas [6.14]. Third, in laser-produced plasmas they facilitate revealing physics behind the laser-plasma interaction [6.26-28].

According to the theory [6.14], L-dips originate from a dynamic resonance between the Stark splitting

$$\omega_{stark}\,(F) = \frac{3\,n\,\hbar\,F}{2\,Z_r\,m_e\,e} \tag{27}$$

of hydrogenic energy levels, caused by a quasi-static field **F** in a plasma, and the frequency ω_L of the Langmuir wave, which practically coincides with the plasma electron frequency $\omega_{pe} = (4\,\pi\,e^2 N_e/m_e)^{\frac{1}{2}}$:

$$\omega_{stark}\,(F) = k\,\omega_{pe}(N_e), \qquad s = 1,2,\ldots \tag{28}$$

Here Z_r is the nuclear charge of the radiating hydrogenic atom/ion (radiator), k is the number of quanta (Langmuir plasmons) involved in the resonance.

The resonance condition (28) translates into specific locations of L-dips in spectral line profiles, which depend on Ne since ω_{pe} depends on N_e. In particular, for relatively low density plasmas (like in magnetic fusion machines) or in the situation, where the quasistatic field **F** is dominated by the low-frequency electrostatic turbulence (e.g., the ion acoustic turbulence), for the Ly-lines, the distance of an L-dip from the unperturbed wavelength λ_0 can be expressed as

$$\Delta\lambda_{dip}(qk, N_e) = \left[\frac{{\lambda_0}^2}{2\,\pi\,c}\right] qk\,\omega_{pe}(N_e)\,. \tag{29}$$

Here λ_0 is the unperturbed wavelength of the spectral line and $q = n_1 - n_2$ is the electric quantum number expressed via the parabolic quantum numbers n_1 and n_2 : q = 0, ±1, ±2, ..., ±(n–1). The electric quantum number labels Stark components of Ly-lines. Equation (29) shows that for a given electron density N_e, the locations of L-dips are controlled by the product qk.

It should be emphasized that the abbreviation “L-dip” refers to a local structure consisting of the central minimum and (generally) two adjacent bumps surrounding the central minimum – the latter is called “dip” for brevity. Equation (29) specifies the locations of the central minima (dips) of these structures: it is from the locations of the central minima that the electron density can be determined experimentally. The dip-bump separation is controlled by the Langmuir field amplitude E_0 and thus allows the experimental determination of E_0 [6.14].

For finishing this brief excerpt from the L-dip theory necessary for understanding the next paragraphs, it should be also noted that when a bump-dip-bump structure is superimposed with the inclined part of the spectral line profile, this might lead to the appearance of a secondary minimum of no physical significance. Also, when the L-dip is too close to the unperturbed wavelength, its bump nearest to the unperturbed wavelength might have zero or little visibility. These subtleties were observed numerous times [6.14, 6.22-24] and will also be relevant below.

So, we will use the Ly-delta line of deuterium as an illustrative example of possible diagnostics of the early stage of the development of a REB in tokamaks. The Ly-delta line has four Stark components in each wing, corresponding to q = ±1, ±2, ±3, ±4. Therefore, according to Eq. (29), the L-dip in the profile of the component of q = 1 due to the four-quantum resonance (k = 4) coincides by its location with the L-dip in the profile of the component of q = 2 due to the two-quantum resonance (k = 2) and with the L-dip in the profile of the component of q = 4 due to the one-quantum resonance (k = 1). The superposition of three different L-dips at the same location results in the L-super-dip of the significantly enhanced visibility.

Also, according to Eq. (29), the L-dip in the profile of the component of q = 1 due to the two-quantum resonance (k = 2) coincides by its location with the L-dip in the profile of the

component of q = 2 due to the one-quantum resonance (k = 1). The superposition of two different L-dips at the same location results also enhances the visibility of the resulting structure.

For diagnostic purposes it is important to choose the spectral line where superpositions of several L-dips at the same location in the profile are expected. This is because due to competing broadening mechanisms (such as, e.g., the dynamical broadening by electrons and some ions, as well as the Doppler broadening), a single L-dip could be washed out, but a superposition of two or especially three L-dips at the same location could "survive" the competition.

Figure 6.7 presents the theoretical profile of the Ly-delta line of deuterium, calculated with the allowance for all broadening mechanisms and for the effect of strong Langmuir waves, at the following parameters: $N_e = 10^{15}(cm^{-3})$, $N_b = 6 \times 10^9\ (cm^{-3})$, $\gamma = 2^{1/2}$ (corresponding to the beam kinetic energy of 210 keV), and $T_e = 2\ eV$. The solid curve corresponds to the presence of the strong Langmuir waves of E_0 = 20 kV/cm caused by a REB (according to Eq. (26)), while the dashed curve corresponds to the absence of the REB. The detuning $\Delta\lambda$ (denoted "dlambda" in Figure 6.7) is in Angstrom.

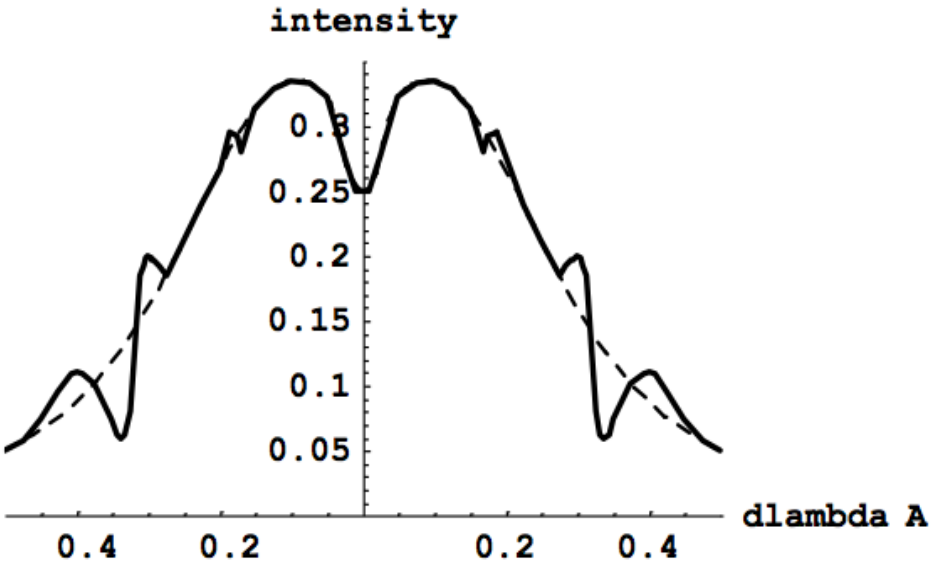

Figure 6.7. Theoretical profile of the Ly-delta line of deuterium, calculated with the allowance for all broadening mechanisms and for the effect of strong Langmuir waves, at the following parameters: Ne = 1015 cm-3, Nb = 6x109 cm-3, $\gamma = 2^{1/2}$ (corresponding to the beam kinetic energy of 210 keV), and Te = 2 eV. The solid curve corresponds to the presence of the strong Langmuir waves of E0 = 20 kV/cm caused by a REB, while the dashed curve corresponds to the absence of the REB. The detuning $\Delta\lambda$ (denoted "dlambda") is in Angstrom.

The theoretical profile shown by the solid curve exhibits two L-dip structures at both the red and blue parts of the profile. The central minimum of the L-super-dips of qk = ±4 is at $\Delta\lambda$ = ±0.338 A. This L-super-dip structure is very pronounced: the central minimum is relatively deep and both of the adjacent bumps are clearly visible. (Being superimposed with the inclined part of the profile, it creates also secondary minima of no physical significance at $\Delta\lambda$ = ±0.275 A.)

The L-dip structure of qk = ±2, whose central minimum is at $\Delta\lambda$ = ±0.169 A, is also visible. However, it is less pronounced (compared with the L-super-dip of qk = ±4) and its bump closest to the unperturbed wavelength has practically zero visibility. This is due to the fact that because of the proximity of this L-dip to the unperturbed wavelength, the ion dynamical broadening is more significant than for the L-super dip at $\Delta\lambda$ = ±0.338 A.

In this example, the ratio of the energy density of the Langmuir waves to the thermal energy density of the plasma (the ratio called sometimes the "degree of the turbulence") is $E_0{}^2/(8\pi N_e T_e)$ ~ 0.06. Since $E_0{}^2/(8\pi N_e T_e)$ >> m_e/M ~ 0.0003 (where M is the mass of deuterium atoms), these Langmuir waves qualify as the strong turbulence.

Thus, the monitoring the shape of deuterium spectral lines (such as, e.g., Ly-delta,or Balmer-beta, or Balmer-delta, or Paschen-beta, or Paschen-delta) and the observation of the formation of the L-dips in the experimental profile would constitute the detection of the early stage of the development of a REB in tokamaks. The detection of the early stage of the development of a REB would allow mitigating the problem in a timely manner.

6.3 Conclusions

We developed an advanced analytical theory of the Stark broadening of hydrogen/deuterium spectral lines by a REB. We showed that the final stage of the development of the REB (where the beam electron density N_b becomes of the same order as the electron density N_e of bulk electrons), would be manifested – and thus could be detected, at least in principle – by a decrease of the width of hydrogen/deuterium spectral lines. We demonstrated that especially sensitive to the final stage of the development of the REB would be the ratio of widths of σ- and π-components, which could be determined by the polarization analysis.

We also showed that the early stage of the development of the REB could be detected by observing the formation of the L-dips in spectral line profiles. The observation of the L-dips, which manifest the development of strong Langmuir waves caused by the REB, could be an important tool for the early detection and the mitigation of the problem of REB in tokamaks.

Chapter 7. Conclusions

This work presents a detailed analysis and improvement of various aspects of the theory of the SB of hydrogen and hydrogen-like ions for a broad range of dense plasma parameters, while looking at both the shape and shift of the spectral line. This was done in an effort to improve the fundamental understanding of Stark shapes and shifts of spectral lines in plasmas (by producing more accurate analytical results than previously existed) and to provide advanced diagnostic methods for determining the electron density.

We introduced an additional source of the shift of hydrogen-like spectral lines arising from the configurations where the nearest perturbing ion is within the radiating atom/ion ("penetrating configurations"). In this way, we eliminated the existing discrepancy of a factor of two between the theory and experiments. We demonstrated, as an example, that for the He II Balmer-α line it is the primary contribution to the total red shift and brings the total theoretical shift in a good agreement with the experimental shift for a measurement of this line, while without the allowance for penetrating configurations the discrepancy between theoretical and experimental shifts was by factors between two and five.

We improved the diagnostic method for measuring the electron density using the asymmetry of spectral lines in dense plasmas by taking into consideration these penetrating configurations, mentioned above. After performing the corresponding analytical calculations we demonstrated that in high density plasmas the allowance for penetrating ions can result in significant corrections to the electron density deduced from the spectral line asymmetry.

We developed a more accurate theory of the broadening of hydrogen-like spectral lines by plasma electrons by using a more accurate description of the electron trajectories. We employed the standard analytical method of separating rapid and slow subsystems by using the fact that the

characteristic frequency of the motion of the bound electron around the nucleus is much higher than the characteristic frequency of the motion of the perturbing electron around the radiating ion. This led to an improvement in the calculation of the width of the spectral line due to the electron broadening, which was not considered before.

For plasmas of magnetic fusion machines, we obtained analytical results for the line shapes under two entangled broadening mechanisms: broadening by the Lorentz field and Doppler broadening – for an arbitrary angle of observation, in distinction to what had previously been done. These two broadening mechanisms intertwine in a complicated way, leading to the evolution of the effect of the suppression of the π-components (compared to the σ-components) as the angle of the observation ψ decreases from 90 degrees. Additionally, the FWHM does not monotonically increase with magnetic field strength due to this complicated relationship between these broadening mechanisms, which is a counterintuitive result.

We developed an advanced analytical theory of the Stark broadening of hydrogen/deuterium spectral lines by a REB and in this way suggested the diagnostic of the development of the REB in a magnetic fusion machine, allowing to timely mitigate such a development, which is disruptive for magnetic fusion machines. We showed that the final stage of the development of the REB (where the beam electron density N_b becomes of the same order as the electron density N_e of bulk electrons), would be manifested – and thus could be detected, at least in principle – by a decrease of the width of hydrogen/deuterium spectral lines. Additionally, we demonstrated that especially sensitive to the final stage of the development of the REB would be the ratio of widths of σ- and π- components, which could be determined by the polarization analysis.

In summary, we improved upon the theory of the SB for HL-lines to aid in diagnostic measurements of a dense plasma, which proves to be very useful in the determination of various important properties of the plasma in question.

References

[1.1] H.R. Griem, *Spectral Line Broadening by Plasmas* (Academic Press, Cambridge) 1974.

[1.2] H.R. Griem, *Principles of Plasma Spectroscopy* (Cambridge University Press, Cambridge) 1997

[1.3] T. Fujimoto, *Plasma Spectroscopy* (Clarendon Press, Oxford, UK) 2004

[1.4] E. Oks, *Stark Broadening of Hydrogen and Hydrogenlike Spectral Lines in Plasmas: The Physical Insight* (Alpha Science International, Oxford, UK) 2006.

[1.5] E. Oks, *Diagnostics of Laboratory and Astrophysical Plasmas Using Spectral Lines of One-, Two-, and Three-Electron Systems* (World Scientific, New Jersey) 2017

[1.6] V.S. Lisitsa, Sov Phys Uspekhi 122 (1977) 603

[2.1] H. Nussbaumer and L. Bieri, *Discovering the Expanding Universe* (Cambridge Univ. Press, Cambridge) 2009.

[2.2] H.R. Griem, *Principles of Plasma Spectroscopy* (Cambridge Univ. Press, Cambridge) 1997, Sect. 4.10.

[2.3] E. Oks, *Stark Broadening of Hydrogen and Hydrogenlike Spectral Lines in Plasmas: The Physical Insight* (Alpha Science International, Oxford) 2006, Sects. 2.6, 6.

[2.4] C.G. Parigger, D.H. Plemmons, and E. Oks, Applied Optics **42** (2003) 5992.

[2.5] T.L. Pittman and C. Fleurier, Phys. Rev. A **33** (1986) 1291.

[2.6] H.R. Griem, Phys. Rev. A**28** (1983) 1596.

[2.7] D.B. Boercker and C.A. Iglesias, Phys. Rev. A **30** (1984) 2771.

[2.8] H.R. Griem, Phys. Rev. A **38** (1988) 2943.

[2.9] D. Salzman, *Atomic Physics in Hot Plasmas* (Oxford Univ. Press, Oxford) 1998.

[2.10] O. Renner et al, J. Phys. B: At. Mol. Opt. Phys. **31** (1998) 1379.

[2.11] H.F. Berg, A.W. Ali, R. Lincke, and H.R. Griem, Phys. Rev. **125** (1962) 199.

[2.12] E. Oks, J. Quant. Spectrosc. Rad. Transfer **58** (1997) 821.

[2.13] A. Könies and S. Günter, J. Quant. Spectrosc. Rad. Transfer **52** (1994) 825.

[2.14] S. Günter and A. Könies, Phys. Rev. E **55** (1977) 907.

[2.15] A.V. Demura, V. Helbig, and D. Nikolic, in *Spectral Line Shapes, 16th ICSLS*, edit. C.A. Back, AIP Conf. Proc. **645** (2002) 318.

[2.16] G.V. Sholin, Opt. Spectosc. **26** (1969) 275.

[2.17] I.V. Komarov, L.I. Ponomarev, and S. Yu. Slavyanov, *Spheroidal and Coulomb Spheroidal Functions* (Nauka, Moscow) 1976, in Russian.

[2.18] B. Held, J. Physique **45** (1984) 1731.

[2.19] B. Held, C. Deutsch, and M.-M. Gombert, Phys. Rev. A **29** (1984) 880.

[2.20] H.R. Griem, *Spectral Line Broadening by Plasmas* (Academic, New York) 1974.

[2.21] D.E. Benredjem, Hoe Nguen, and G. Couland, J. Quant. Spectrosc. Rad. Transfer **43** (1990) 415.

[2.22] M. Blaha and J. Davis, NRL Memorandum Report 5155 (1983).

[2.23] J.P. Marangos, D.D. Burgess, and K.G.H. Baldwin, J. Phys.B: At. Mol. Opt. Phys. **21** (1988) 3357.

[2.24] G.C. Junkel, M.A. Gunderson, C.F. Hooper, and D.A. Haynes, Jr., Phys. Rev. E **62** (2000) 5584.

[2.25] A. Salin, Comp. Phys. Communications **14** (1978) 121.

[2.26] J.D. Power, Phil. Trans. Royal Soc. **A274** (1973) 663.

[2.27] E. Oks, J. Astrophys. & Aerospace Technol. **5** (2017) 143.
[3.1] L.P. Kudrin and G.V. Sholin, Sov. Phys Doklady **7** (1963) 1015.
[3.2] G.V. Sholin, Optics and Spectroscopy **26** (1969) 275.
[3.3] A.V. Demura and G.V. Sholin, J. Quant. Spectrosc. Rad. Transfer **15** (1975) 881.
[3.4] S. Djurovic, M. Ćirišan, A.V. Demura, G.V. Demchenko, D. Nikolić, M.A. Gigosos, and M.A. González, Phys. Rev. E **79** (2009) 046402.
[3.5] A.V. Demura, G.V. Demchenko, and D. Nikolic, Europ. Phys. J. D **46** (2008) 111.
[3.6] N.K. Podder, E.J. Clothiaux, and E. Oks, J. Quant. Spectrosc. Rad. Transfer **65** (2000) 441.
[3.7] C.G. Parigger, L.D. Swafford, A.C. Woods, D.M. Surmick, and M.J. Witte, Spectrochimica Acta Part B **99** (2014) 28.
[3.8] E. Oks, *Diagnostics of Laboratory and Astrophysical Plasmas Using Spectral Lineshapes of One-, Two-, and Three-electron Systems* (World Scientific, New Jersey/Singapore) 2017.
[3.9] E. Oks, J. Quant. Spectrosc. Rad. Transfer **58** (1997) 821.
[3.10] V.P. Gavrilenko, E. Oks, and A.V. Radchik, Optics and Spectroscopy **59** (1985) 411.
[3.11] I.V. Komarov, L.I. Ponomarev, and S. Yu. Slavyanov, *Spheroidal and Coulomb Spheroidal Functions* (Nauka, Moscow) 1976, in Russian.
[3.12] E. Oks and T. Uzer, Europhys. Letters **49** (2000) 5.
[3.13] P. Sanders and E. Oks, J. Phys. B: At. Mol. Opt. Phys. (2017) accepted.
[3.14] J.F. Kielkopf and N.F. Allard, J. Phys. B: At. Mol. Opt. Phys. **47** (2014) 155701.
[3.15] J.P. Marangos, D.D. Burgess, and K.G.H. Baldwin, J. Phys. B: At. Mol. Opt. Phys. **21** (1988) 3357.
[3.16] N. Kryukov and E. Oks, Phys. Rev. A **85** (2012) 054503.
[3.17] L.D. Landau and E.M. Lifshitz, *Quantum Mechanics* (Pergamon, Oxford) 1965.
[4.1] H.R. Griem and K.Y. Shen, Phys. Rev. **122** (1961) 1490.
[4.2] H.R. Griem, *Plasma Spectroscopy* (McGraw-Hill, New York) 1964.
[4.3] H.R. Griem, *Spectral Line Broadening by Plasmas* (Academic Press, Cambridge, MA) 1974.
[4.4] E. Oks, *Stark Broadening of Hydrogen and Hydrogenlike Spectral Lines in Plasmas: The Physical Insight* (Alpha Science International, Oxford, UK) 2006.
[4.5] E. Oks, *Diagnostics of Laboratory and Astrophysical Plasmas Using Spectral Lines of One-, Two-, and Three-Electron Systems* (World Scientific, New Jersey) 2017.
[4.6] V. Galitski, B. Karnakov, V. Kogan, and V. Galitski, Jr., *Exploring Quantum Mechanics* (Oxford University Press, Oxford, UK) 2013, Problem 8.55.
[4.7] G.L. Kotkin and V.G. Serbo, *Collection of Problems in Classical Mechanics* (Pergamon, Oxford) 1971, problem 2.3.
[4.8] F.F. Baryshnikov and V.S. Lisitsa, Sov. Phys. JETP **53** (1981) 471.
[4.9] L.A. Bureyeva and V.S. Lisitsa, *A Perturbed Atom*, Astrophysics and Space Physics Reviews (CRC Press, Boca Raton, FL) 2000.
[4.10] K. Grützmacher and U. Johannsen, in *Spectral Line Shapes*, v. 7, Eds. R. Stamm and B. Talin (Nova Science Publishers, New York) 1993, p. 139.
[4.11] R. Ahmad, Eur. Phys. J. D **7** (1999) 123.
[4.12] Th. Wrubel, S. Büscher, H.-J. Kunze, and S. Ferri, J. Phys. B **34** (2001) 461.

[4.13] V.S. Lisitsa, Sov Phys Uspekhi **122** (1977) 603.
[4.14] M. Baranger, Phys. Rev. **111** (1958) 481, 494; **112** (1958) 855.
[4.15] A.C. Kolb and H.R. Griem, Phys. Rev. **111** (1958) 514.
[4.16] C.R. Vidal, J. Cooper, and E.W. Smith, J. Quant. Spectrosc. Rad. Transfer **10** (1970) 1011; **11** (1971) 263.
[4.17] S. Sahal-Brechot, Astron. & Astrophys. **1** (1969) 91.
[4.18] M.L. Strekalov and A.I. Burshtein, Sov. Phys. JETP **34** (1972) 53.
[5.1] E. Oks, J. Quant. Spectr. Rad. Transfer **156** (2015) 24.
[5.2] B. L. Welch, H.R. Griem, J. Terry, C. Kurz, B. LaBombard, B. Lipschultz, E. Marmar, and J. McCracken, Phys. Plasmas **2** (1995) 4246.
[5.3] N.H. Brooks, S. Lisgo, E. Oks, D. Volodko, M. Groth, A.W. Leonard, and DIII-D Team, Plasma Phys. Reports **35** (2009) 112.
[5.4] E. Oks, in *Atomic Processes in Basic and Applied Physics*, edits. V. Shevelko and H. Tawara, Springer, Heidelberg (2012) Chap. 15.
[5.5] E. Oks, R.D. Bengtson, and J. Touma, Contributions to Plasma Phys. **40** (2000) 158.
[5.6] E. Oks, *Stark Broadening of Hydrogen and Hydrogenlike Spectral Lines in Plasmas: The Physical Insight*, Alpha Science International, Oxford, United Kingdom (2006) Sect. 9.4.
[5.7] U. Feldman and G.A. Doschek, Astrophys. J. **212** (1977) 913.
[5.8] Yu.I. Galushkin, Sov. Astron. **14** (1970) 301.
[5.9] R. Neu, H.P. Summers, and Yu. Ralchenko, J. Phys. B: Atom. Mol. Opt. Phys. **43** (2010) 140201.
[6.1] D. Guenot, D. Gustas, A. Vernier, B. Beaurepaire, F. Böhle, M. Bocoum, M. Losano, A.
Jullien, A. Lopez-Martins, A. Lifschitz, and J. Faure, Nature Photonics **11** (2017) 293.
[6.2] S.A. Kurkin, A.E. Hramov, and A.A. Koronovskii, Appl. Phys. Letters **103** (2013) 043507.
[6.3] P.C. de Jagher, F.W. Sluijter, and H.J. Hopman, Phys. Reports **167** (1988) 177.
[6.4] A.H. Boozer, Nuclear Fusion **57** (2017) 056018.
[6.5] J. Decker, E. Hirvijoki, O. Embreus, Y. Peysson, A. Stahl, I. Pusztai, and T. Fülöp, Plasma Physics and Controlled Fusion **58** (2016) 025016.
[6.6] H. Smith, P. Helander, L.-G. Eriksson, D. Anderson, M. Lisak, and F. Andersson, Physics of Plasmas **13** (2006) 102502.
[6.7] P.V. Minashin, A.B. Kukushkin, and V.I. Poznyak, EPJ Web of Conferences **32** (2012) 01015.
[6.8] B. Kurzan, K.-H. Steuer, and W. Suttrop, Rev. Sci. Instrum. **68** (1997) 423.
[6.9] S. Ide, K. Ogura, H. Tanaka, M. Iida, K. Hanada, T. Itoh, M. Iwamasa, H. Sakakibara, T. Minami, M. Yoshida, T. Maekawa, Y. Terumichi, and S. Tanaka, Nuclear Fusion **29** (1989) 1325.
[6.10] E. Oks, *Diagnostics of Laboratory and Astrophysical Plasmas Using Spectral Lines of One-, Two-, and Three-Electron Systems* (World Scientific, New Jersey) 2017.
[6.11] H.-J. Kunze, *Introduction to Plasma Spectroscopy* (Springer, Berlin) 2009.
[6.12] E. Oks, *Stark Broadening of Hydrogen and Hydrogenlike Spectral Lines in Plasmas: The Physical Insight* (Alpha Science International, Oxford, UK) 2006.
[6.13] T. Fujimoto, *Plasma Spectroscopy* (Clarendon Press, Oxford, UK) 2004.

[6.14] H.R. Griem, *Principles of Plasma Spectroscopy* (Cambridge University Press, Cambridge) 1997.
[6.15] E. Oks, *Plasma Spectroscopy: The Influence of Microwave and Laser Fields*, Springer
Series on Atoms and Plasmas, vol. 9 (Springer, New York) 1995.
[6.16] J. Rosato, S. P. Pandya, Ch. Logeais, M. Meireni, I. Hannachi, R. Reichle, R. Barnsley, Y. Marandet, and R. Stamm, AIP Conf. Proceedings **1811** (2017) 110001.
[6.17] J. Seidel, Z. Naturforsch. **34a** (1979) 1385.
[6.18] H.R. Griem, *Spectral Line Broadening by Plasmas* (Academic, New York) 1974.
[6.19] A. Derevianko and E. Oks, J. Quant. Spectrosc. Rad. Transfer **54** (1995) 137.
[6.20] Ya. Ispolatov and E. Oks, J. Quant. Spectrosc. Rad. Transfer **51** (1994) 129.
[6.21] L.D. Landau and E.M. Lifshitz, *The Classical Theory of Fields* (Pergamon, Oxford) 1971.
[6.22] V.B. Krasovitskiy, *Instabilities of Relativistic Electron Beam in Plasma* (Nova Publishers, New York) 2008.
[6.23] V.P. Gavrilenko and E. Oks, Sov. Phys. JETP **53** (1981) 1122.
[6.24] E. Dalimier, E. Oks, and O. Renner, Atoms **2** (2014) 178.
[6.25] E. Dalimier, A. Ya Faenov, E. Oks, P. Angelo, T.A. Pikuz, Y. Fukuda, A. Andreev, J. Koga, H. Sakaki, H. Kotaki, A. Pirozhkov, Y. Hayashi, I.Yu. Skobelev, S.A. Pikuz, T. Kawachi, M. Kando, K. Kondo, A. Zhidkov, E. Tubman, N.M.H. Butler, R.J. Dance, M.A. Alkhimova, N. Booth, J. Green, C. Gregory, P. McKenna, N. Woolsey, and R. Kodama, J. Phys. Conf. Ser. **810** (2017) 012004.
[6.26] E. Dalimier, E. Oks, and O. Renner, AIP Conference Proceedings **1811** (2017) 190003.
[6.27] E. Oks, St. Böddeker, and H.-J. Kunze, Phys. Rev. A **44** (1991) 8338.
[6.28] O. Renner, E. Dalimier, E. Oks, F. Krasniqi, E. Dufour, R. Schott, and E. Foerster, J. Quant. Spectr. Rad. Transfer **99** (2006) 439.
[6.29] E. Oks, E. Dalimier, A.Ya. Faenov, T. Pikuz, Y. Fukuda, S. Jinno, H. Sakaki, H. Kotaki, A. Pirozhkov, Y. Hayashi, I. Skobelev, T. Kawachi, M. Kando, and K. Kondo, J. Phys. B: At. Mol. Opt. Phys. **47** (2014) 221001.
[6.30] E. Oks, E. Dalimier, A.Ya. Faenov, P. Angelo, S.A. Pikuz, E. Tubman, N.M.H. Butler, R.J. Dance, T.A. Pikuz, I.Yu. Skobelev, M.A. Alkhimova, N. Booth, J. Green, C. Gregory, A. Andreev, A. Zhidkov, R. Kodama, P. McKenna, and N. Woolsey, Optics Express **25** (2017) 1958